ATP-activated currents and calcium signalling in adult murine supporting cells

Piotr Sirko

University College London

Thesis submitted for the degree of Doctor of Philosophy

I, Piotr Sirko, confirm that the work presented in this thesis is my own. Where information has been derived from other sources, I confirm that this has been indicated in the thesis.

Abstract

Purinergic P2 receptors are present in the adult organ of Corti however their role and cellular effects of their stimulation are unclear. To date studies have been hampered by the relative difficulty of accessing intact adult organ of Corti tissue. In this study a novel dissection technique which enabled easy access to the apical turn of the adult mouse organ of Corti was used. The goal of the current study was to determine the distribution of P2 receptors and determine the effect of ATP on membrane conductances in inner sulcus (IS) supporting cells and supporting cells surrounding the IHC afferent synapse in the adult mouse organ of Corti.

Purinergic P2 receptors were localized immunohistochemically and functionally to multiple supporting cells of the organ of Corti. In patch clamp electrophysiology recordings application of extracellular ATP to gap junction coupled IS cells, elicited inward currents and transiently increased resting membrane resistance while making the resting zero current potential more positive. Transmitted brightfield imaging showed that the electrophysiological changes were accompanied by a decrease in cytoplasmic Brownian movement. In IS cells decoupled with gap junction blockers stimulation with ATP elicited monophasically declining membrane currents.

In contrast in decoupled border cells surrounding the IHC afferent synapse ATP activated biphasic currents. The initial component of the currents elicited in border cells desensitized during sustained stimulation and showed high inward rectification, characteristic of some P2X receptor subtypes. In contrast the delayed component was identified as a Ca^{2+}-activated Cl^- channel. It is argued that these conductances could help decrease the potassium concentration around the IHCs during periods of sustained IHC stimulation and thus affect the membrane potential of these sensory cells.

In addition, actively propagating, gap junction-mediated, extracellular ATP-independent Ca^{2+} waves were observed to propagate along the organ of Corti in the IS and Deiters' cell regions. These increases in intracellular Ca^{2+} levels were periodic. Currently the role of the waves is unclear, however increases in intracellular Ca^{2+} of a similar frequency and periodicity have been linked to the regulation of gene expression. Thus the observed waves could be a new mechanism regulating gene expression in the organ of Corti.

Acknowledgements

I would like to thank my supervisor Prof. Jonathan Ashmore for giving me the opportunity to become an independent and impartial scientist. I would also like to thank Dr. Jonathan Gale for discussion and support when designing and conducting experiments.

I would like to thank Miriam for providing invaluable help in the laboratory numerous times, post-docs: Jime, Paromita, Roberta and Zoe as well as fellow students: Assel, Claudia, Elena, Lorcan, Lucile, Sara, and Stephanie for interesting discussions and inspiration.

Finally, I would like to thank Paulina for giving me the energy and confidence necessary to continue throughout the years and my parents for their continued support.

Table of Contents

List of Figures

List of Tables

List of Acronyms

ADP	Adenosine diphosphate
AM	Acetoxymethyl esters
Ano-1	Anoctamin-1
ATP	Adenosine triphosphate
BC	Border cell
BDNF	Brain-derived neurotrophic factor
Ca^{2+}_i	Intracellular Ca^{2+}
CaCC	Ca^{2+}-activated Cl- channel
CaM	Calmodulin
CBX	Carbenoxolone
CC	Claudius cell
CICR	Ca^{2+} induced Ca^{2+} release
C_m	Cell membrane capacitance
CNQX	6-cyano-7-nitroquinoxaline-2,3-dione
DAG	Diacylglycerol
DC	Deiters' cell
ERK	Extracellularly regulated kinase
ES	Extracellular solution
ENaC	Epithelial Na^+ channel
EP	Endocochlear potential
ER	Endoplasmic reticulum
FFA	Flufenamic acid
FW	Full width
GER	Greater epithelial ridge
GFAP	Glial fibrillary acidic protein
GLAST	Glutamate aspartate transporter
HC	Hensen cell
IHC	Inner hair cell
IP_3	Inositol trisphosphate
IP_3R	Inositol trisphosphate receptor
IS	Inner sulcus
JNK	c-Jun N-terminal kinase

KCC	KCl cotransporter
MAPK	Mitogen-activated protein kinase
MET	Mechanotransducer
OHC	Outer hair cell
PC	Pillar cell
PLC	Phospholipase C
PLCδ	Phospholipase C delta
PLP	Myelin proteolipid protein
PPADS	pyridoxalphosphate-6-azophenyl-2',4'-disulfonic acid
PTS	Permanent threshold shift
PVC	Polyvinyl chloride
R_m	Cell membrane resistance
RRP	Readily releasible pool
RyR	Ryanodine receptor
TM	Tectorial membrane
TTS	Temporary threshold shift
UTP	Uridine triphosphate
V_0	Current reversal potential
V_c	Command voltage
V_m	Cell membrane resting potential

1 Introduction

1.1 Structure of the cochlea

1.1.1 Inner ear anatomy

The ear is comprised of the outer, middle and inner ear. The inner ear is encased in an ossified structure, the bony labyrinth. Inside are the inner ear soft tissues which comprise the membranous labyrinth that can be further subdivided into three main structures: the semicircular canals, the vestibule and the cochlea (Dallos et al., 1996). The semicircular canals and vestibules are involved in the detection of rotation and maintenance of balance, while the cochlea is necessary for translating noise-induced vibrations into neuronal signals. The cochlea is a coiled structure and consists of three compartments: the scala vestibuli, scala tympani and in-between them the scala media. The bony pillar forming the central axis of the cochlea is the modiolus (Figure 1.1).

The hearing epithelium the organ of Corti rests on the basilar membrane in the scala media. The basilar membrane varies in width and thickness throughout its length and transmits noise-induced vibrations onto the organ of Corti. The basilar membrane is thickest and narrowest at the base of the cochlea and becomes progressively wider and thinner towards the apex. The differences in the dimensions of the basilar membrane play an important role in the process of hearing as a limited region of the basilar membrane can be induced to vibrate by a particular sound frequency. The scalas of the cochlea are filled with fluid. The scala vestibuli and tympani are filled with perilymph which has a high NaCl content and a composition similar to blood plasma or cerebrospinal fluid. In contrast the scala media is filled with endolymph rich in KCl. Endolymph appears to be unique to the inner ear and can only also be found in the body in the semicircular canals and the vestibule. The different composition of the fluid filling the scala media and tympani and electric isolation between them creates an electric potential, known as the endocochlear potential (EP) between the two compartments. Maintaining the EP is crucial for normal hearing function.

1.1.2 Anatomy of the organ of Corti

The cells of the inner ear can be divided into sensory and non-sensory cells (Dallos et al., 1996). The sensory cells play an active role in the process of hearing. These include one row of inner hair cells (IHCs) and to the outside of them towards the lateral wall of the scala media three rows of outer hair cells (OHCs). At the apical end of hair cells is the cuticular plate a structure which has a high actin content. Embedded in the cuticular

Figure 1.1 A cross section of the cochlea.
Visible are the three cochlear compartments, the scala vestibuli, scala media and scala tympani. The scala vestibuli and tympani are filled with a fluid called perilymph, while the scala media is filled with endolymph. SV – Scala vestibuli, SM – Scala media, ST – Scala tympani, M – Modiolus. (Cochlear section was a gift from Prof. Andrew Forge, Photo: Piotr Sirko).

plate are stereocilia enriched in actin filaments. Synapses with neurons are present at the hair cells basal poles (Flock and Cheung, 1977; Raphael and Altschuler, 2003). IHCs form synapses with afferent neurons, which propagate the neuronal signal from the cochlea to the brain.

OHCs also synapse with afferent neurons, but also form synapses with efferent neurons that propagate neuronal signals from the brain to the cochlea. Supporting cells are the non-sensory cells of the inner ear. Several subtypes have been distinguished based on their morphology (Dallos et al., 1996) (Figure 1.2).

Cuboid epithelial inner sulcus cells are found in a region named the inner sulcus (IS) that stretches from the modiolus towards the IHCs. The specialized IS cells, which

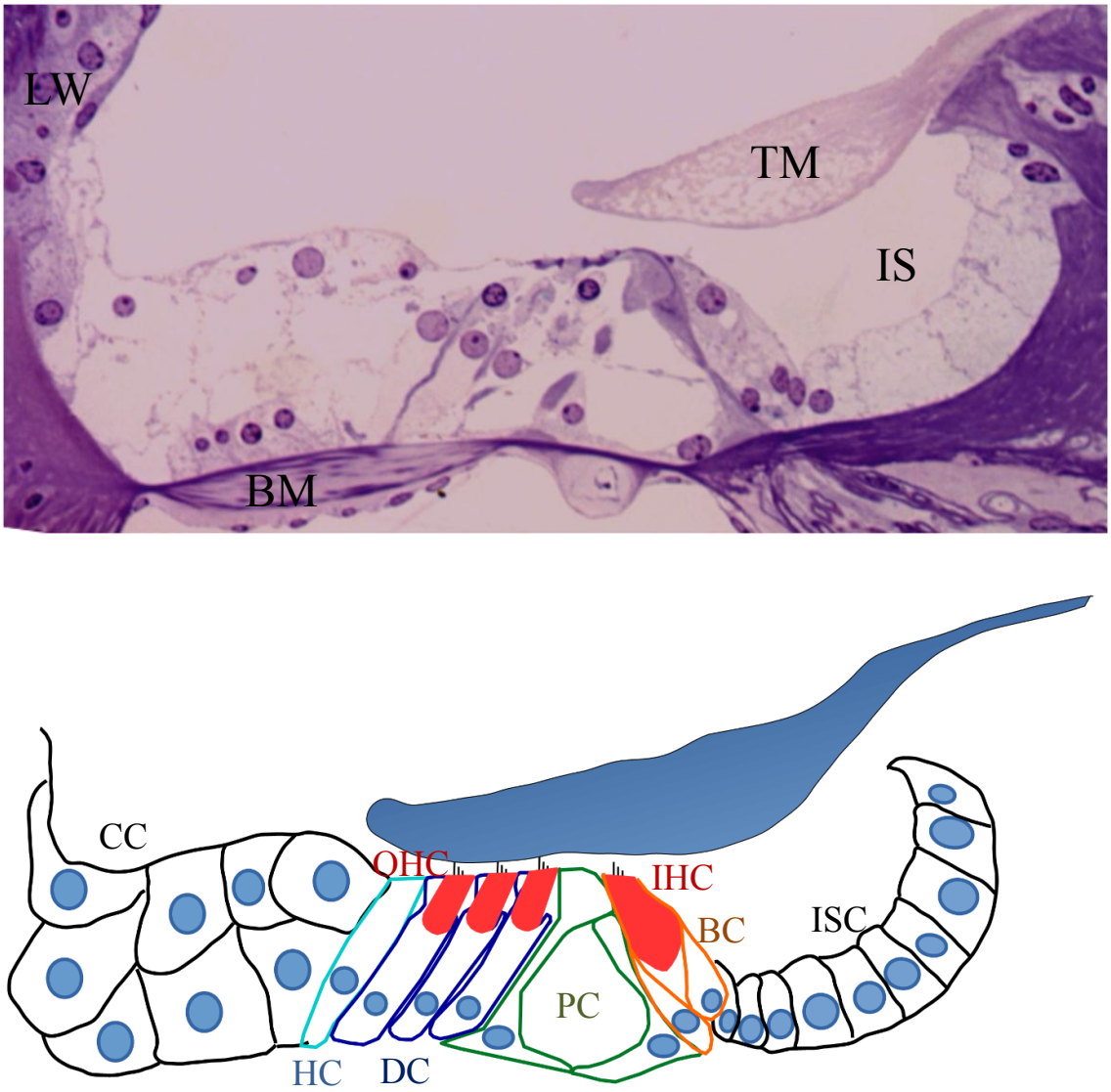

Figure 1.2 A cross section of the organ of Corti and surrounding tissue.
(Top) Labelled from the right clockwise are the TM – Tectorial membrane, IS – Inner sulcus, BM – Basilar membrane, LW – Lateral wall. The organ of Corti rests on the basilar membrane. The tectorial membrane is shrunk and displaced from its normal resting position due to staining procedures. **(Bottom)** A diagram indicating the various organ of Corti and surrounding cells. From the right outlined are: IS cells (ISC, black outline), border and phalangeal cells (BC, orange), inner hair cell (IHC, red), inner and outer pillar cells (PC, green), Deiters' cells (DC, blue), outer hair cells (OHCs, red), Hensen's cell (HC, cyan), Claudius cells (CC, black). Cell nuclei and tectorial membrane are depicted in blue. (Cochlear section was a gift from Prof. Andrew Forge, Photo: Piotr Sirko).

border the hair cell membrane, are called border cells (found on the modiolar side of the IHC) and phalangeal cells (lateral side). These two cell types have a long thin cell projection called a phalange which stretches along the IHC membrane and are considered to be part of the organ of Corti.

To the outside of the phalangeal cells are the inner and outer pillar cells. Pillar cells have a rectangular apical surface which is joined by a rod-like middle portion to the pillar cell footplate resting on the basilar membrane. The cytoplasm of these cells is rich in actin and microtubule filaments. These are mostly present in the pillar cells apical and middle portions (Slepecky and Chamberlain, 1987). The cell membranes of inner and outer pillar cells are in contact with each other only at the pillar cells apical and basal ends. The rest of the pillar cell bodies form the triangular tunnel of Corti. The tunnel of Corti acts as a hinge point for the outer portion of the organ of Corti which oscillates when sound induced vibrations are present.

Outwards from the outer pillar cells, three rows of Deiters' cells are found. The bodies of the Deiters' cells are located beneath the OHCs. Deiters' cells similarly to pillar cells are rich in actin and microtubules (Kuhn and Vater, 1995; Slepecky and Chamberlain, 1987). The apical portion of their cell body is cup shaped and each cell encloses the basal end of one OHC. Deiters' cells similarly to border and phalangeal cells have long thin phalanges. These rise between the OHCs and their apical tips fill the space between the cuticular plates of the OHCs. Each phalange borders with four OHCs in addition to the one enclosed by the Deiters' cell body. Altogether each Deiters' cell borders with five OHCs.

To the outside of the last row of Deiters' cells are Hensen's cells. These cells have a highly elongated shape and in the guinea pig the cytoplasm of Hensen's cells appears to contain large lipid droplets. Some Deiters' and Hensen's cells are innervated by afferent neurons and efferent fibres. However this innervation does not appear to play an active role in hearing (Fechner et al., 2001; Jagger and Housley, 2003). To the outside of the Hensen's cells are Claudius cells. These cells are not part of the organ of Corti. They have a columnar shape and some of them extend onto the lateral wall.

The reticular lamina is the apical part of the organ of Corti, it is in contact with endolymph and acts as a barrier between the endolymph of the scala media and the perilymph of the scala tympani. Excluding the reticular lamina the cell bodies of the organ of Corti cells are in contact with perilymph. Both the sensory and nonsensory cells of the organ of Corti as well as other cells lining the scala media are connected at their apical ends via tight junctions (Gulley and Reese, 1976; Kitajiri et al., 2004). Tight junctions function in epithelia to limit fluid movement (Anderson and Van Itallie,

2009). In the cochlea they limit mixing of the endolymph with perilymph and are crucial for maintaining the EP (Gow et al., 2004).

1.1.3 The development of the organ of Corti

First signs of specialization of the organ of Corti become present at E15 on the dorsal wall of the cochlear duct, which eventually develops into the scala media (Fuchs, 2010; Willott, 2001). At this early stage two regions on the dorsal wall can be differentiated. A modiolar region in which cells proliferate and a striolar region, where cells appear post-mitotic.

The modiolar region eventually forms at E16 the greater epithelial ridge (GER) which accounts for 2/3^{rds} of the dorsal wall of the cochlear duct. The remaining 1/3rd consists of the striolar region, which at this stage is known as the lesser epithelial ridge (LER).

During development and before hearing onset the GER differentiates into the IS and most likely the IHCs, the region occupied by the LER develops into OHCs and other cochlear supporting cells. The IS is fully formed at P12 in the mouse. At P16 the tunnel of Corti reaches is fully formed state. The maturation of the organ of Corti concludes when the separation between OHCs reaches adult levels at P20. The IHCs and OHCs can be first distinguished at E17, but in the mouse only become fully functional around P13-14.

1.1.4 Tectorial membrane, structural role and morphology, contact with hair cells

The tectorial membrane (TM) is an acellular structure located just above the organ of Corti (Figure 1.2). The TM blankets the organ of Corti from base to apex and is connected to the modiolus via a bony ridge called the limbus. The TM is also connected to the top-most row of OHC stereocilia (Lim, 1986). The main components of the TM are collagens and glycoproteins (Richardson et al., 2008; Richardson et al., 1987; Thalmann et al., 1986). The TM plays an important functional role in optimizing and enhancing the IHC response to sound induced vibrations (described in section 1.1.5) (Richardson et al., 2008).

1.1.5 Hearing

Sound induced vibrations induce a traveling wave of oscillations in the basilar membrane. As the dimensions and stiffness of the basilar membrane varies along its length, a particular location on the basilar membrane will only be displaced maximally

by a particular sound frequency. In this way a certain location on the basilar membrane acts as a bandpass filter to a certain sound frequency.

Noise induced vibrations of the basilar membrane stimulate the sensory cells in the organ of Corti by deflecting the hair cell stereocilia. IHCs translate sound induced vibrations into neuronal signals while the (OHCs) in an active process dependent on an OHC membrane protein called prestin, locally amplify the vibrations of the basilar membrane increasing sound sensitivity and frequency selectivity (Ashmore, 2008).

The TM plays a crucial role in translating the sound induced waves traveling laterally along the basilar membrane into forces acting radially on the stereocilia. The hinge point of the TM is more modiolar or closer to the central axis of the cochlea, than the hinge point of the organ of Corti located at the base of outer pillar cells. This causes sound stimulation to create a shearing force between the TM and the basilar membrane which deflects hair cell stereocilia.

At their apical ends stereocilia have mechanically gated ion channels called mechanotransducer (MET) channels. Sound induced deflection of the stereocilia opens the MET channels. In turn the EP allows K^+ from the endolymph to flood into the hair cells through MET channels and depolarize the cells (Raphael and Altschuler, 2003). In IHCs this leads to the opening of L-type voltage-dependent Ca^{2+} channels at the cells base, Ca^{2+}-dependent release of neurotransmitter and transmission of noise-induced neuronal signals further up the auditory pathway via the afferent neuronal fibres. OHC depolarization drives a mechanical prestin dependent process triggering changes in the length of the cell body at the sounds frequency, which amplifies the vibrations of the basilar membrane. K^+ which depolarizes the hair cells is extruded below the reticular lamina into the perilymph of the scala tympani most likely through voltage dependent K^+ channels in hair cells.

1.2 Importance of cochlear supporting cells and gap junctions in the organ of Corti

1.2.1 Gap junctions in the organ of Corti

Cochlear supporting cells are connected via gap junctions, intercellular channels that allow for movement of ions and metabolites between the cytoplasms of the connected cells (reviewed in (Evans and Martin, 2002)). Gap junctions allow the free passage of various molecules of up to 1000 Da and 20 Å in diameter (Flagg-Newton et al., 1979;

Schwarzmann et al., 1981). A single gap junction consists of two hexameric protein assemblies called hemichannels. Each hemichannel spans the membrane of each cell. The subcomponents of the hexamers are called connexins and in mice and humans at least 19 and 20 unique connexin genes are present respectively (Willecke et al., 2002). Connexins can form homomeric or heteromeric assemblies consisting of one or multiple types of connexins.

Hemichannels can pair with hemichannels of a different cell to form gap junctions or remain unpaired and allow for release of substances from the cell into the extracellular environment (Goodenough and Paul, 2003). The different connexins vary in their permeability to different substances and thus the types of connexins forming a hemichannel can fine tune the mass and charge of substances that can permeate them (Evans and Martin, 2002). In the cochlea gap junctions have only been found in nonsensory cells and have not been localized to IHCs or OHCs (Jagger and Forge, 2014).

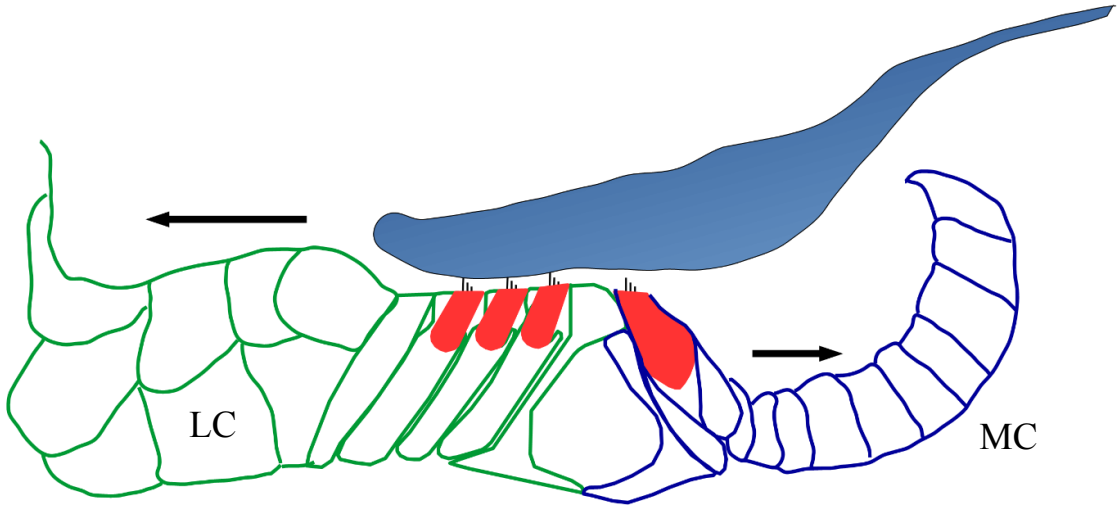

Figure 1.3 Two gap junction connected compartments are present in the organ of Corti of adult mice.
Gap junctions connect supporting cells in the organ of Corti. The gap junction connected cells are thought to form two compartments which are not mutually interconnected (Jagger and Forge, 2006). The medial compartment (MC, outlined in blue) stretches from the IS to the inner pillar cells. The lateral compartment (LC, outlined in green) stretches from the outer pillar cells through Claudius cells towards the lateral wall. Arrows indicate the possible directions of K^+ transport away from the inner and outer hair cells.

Each connexin subtype is named after the inferred kilodalton molecular mass of its human connexin homolog (Mese et al., 2007). In the organ of Corti the two main types of connexins found are connexin 26 and connexin 30 (Forge et al., 2003; Lautermann et

al., 1998). Two distinct connexin connected regions are present in the adult organ of Corti. A medial compartment stretches from the inner pillar cells medially into the IS. A lateral compartment stretches outwards from the outer pillar cells and encompasses the outer pillar cells, Deiters' cells, Hensen's cells and Claudius cells. The two compartments are thought not to be interconnected (Jagger and Forge, 2006) (Figure 1.3).

1.2.2 Role of supporting cells and gap junctions in the organ of Corti

Neurotransmitter release at the IHC afferent synapse depends on Ca^{2+} influx through voltage dependent L-type Ca^{2+} channels. The correct IHC membrane potential is crucial for the correct encoding of sound information. A too low membrane potential and excessive neurotransmitter release can result in afferent bouton swelling and degeneration of both the hair cells and afferent fibres (Puel et al., 1997; Pujol and Puel, 1999; Wang et al., 2002).

To prevent such adverse effects the K^+ extruded from hair cells has to be quickly and efficiently removed from their vicinity. There is circumstantial evidence suggesting that the gap junctions in the organ of Corti play a crucial role in this process. In this model K^+ leaving the OHCs is thought to be transported via the lateral gap junction connected compartment to the lateral wall. There it is transported back into the scala media via specialized marginal cells found in a highly vascularized structure, the stria vascularis (Wangemann, 1995). A similar pathway could be present in the medial gap junction connected compartment (Spicer and Schulte, 1998). In support of the K^+ recycling hypothesis mutations in connexin 26 and 30 have been linked to hearing loss and mice in which either one of these proteins have been knocked out are profoundly deaf (Cohen-Salmon et al., 2002; Erbe et al., 2004; Kenna et al., 2001; Teubner et al., 2003).

KCl cotransporters (KCC) KCC3 and KCC4 necessary for the uptake of K^+ have also been found in phalangeal and Deiters' cells, which surround the hair cells. Hair cells of mice which lack these proteins degenerate shortly after hearing onset (Boettger et al., 2002; Boettger et al., 2003). Gap–junctions found in cochlear supporting cells preferentially allow the diffusion of positively charged molecules (Flagg-Newton et al., 1979). Finally increasing connexin 26 expression levels fully restored normal hearing function in connexin 30 knockout mice (Ahmad et al., 2007).

However other studies indicate that permeability of connexins to other substances than K^+ is also crucial for maintaining normal hearing function. A valine to leucine substitution (V84L) in human connexin 26 which has been identified as causing sensorineural hearing loss does not change the channels unitary conductance or ion specificity (Beltramello et al., 2005; Kenna et al., 2001). It does however decrease the permeability of gap junctions to inositol 1,4,5-trisphosphate (IP_3). This demonstrates that K^+ transport might not be the primary function of cochlear gap junctions. In agreement, lack of gap junctions does not affect endolymphatic K^+ concentration (Cohen-Salmon et al., 2002; Teubner et al., 2003). Gap junction independent pathways of K^+ recycling have also been proposed (Salt and Ohyama, 1993; Zidanic and Brownell, 1990). K^+ after moving into the perilymph could simply be recycled from it, without any need for transport through the gap junction network.

The gap junction system in the organ of Corti could simply be involved in K^+ spatial buffering acting as a K^+ sink and moving K^+ away from high activity regions of the cochlea. A mechanism like this is known to be present in the brain (Jagger and Forge, 2006; Leis et al., 2005). In support of this hypothesis Deiters' cells have been shown to express voltage dependent K^+ channels (Chung et al., 2013; Nenov et al., 1998; Szucs et al., 2006a). These could aid in restoring Deiters' cells membrane potential when depolarized by high extracellular K^+ levels after removal of excess K^+ from the vicinity of the OHCs.

Communication through gap junctions has also been shown to play an important role during epithelial repair in the cochlea (Forge et al., 2013). Apoptotic hair cells are extruded or phagocytosed and the resulting lesion is filled by supporting cells (Gale et al., 2002; Li et al., 1995; Mangiardi et al., 2004). Abnormalities were present during lesion closure in connexin 30 knockout mice (Forge et al., 2013). In mutant animals only one cell was engaged in lesion closure whereas in wild type mice lesion closure was a cooperative process in which multiple supporting cells were engaged. The effects of inhibition of gap junction communication on cochlear epithelial repair were also pronounced in the chick. In *in vitro* cultures of the basilar papilla inhibition of gap junctions blocked cell extrusion and lesion closure (Jagger et al., 2014).

Apart from K^+ regulation supporting cells appear to be also involved in maintaining correct levels of other ions, osmolarity and the optimum pH in the endolymph. Hensen's cells express Ca^{2+}-activated Cl^- channels (CaCCs) (Sugasawa et al., 1996a). This has led

to some speculation that these cells might be involved in regulating transepithelial ion and water transport in the cochlea. Some investigations indicate that Hensen's cells also provide support for the TM and might modulate the transmission of mechanical energy from the basilar membrane onto the organ of Corti (Merchan et al., 1980). Studies have determined that Claudius cells express epithelial Na^+ channels (ENaC) implicating these cells in removal of excess Na^+ from the endolymph of the scala media (Yoo et al., 2012).

A Cl^- / HCO_3^- exchanger has been detected in Deiters' cells (Wangemann et al., 2007). It is thought that maintaining the correct pH could be crucial for efficient Ca^{2+} removal from the endolymph. Mice in which the expression of the Cl^- / HCO_3^- exchanger pendrin (Slc26a4) was disrupted had elevated endolymph Ca^{2+} levels and did not acquire hearing (Wangemann et al., 2007). In the same study the acid sensitive epithelial Ca^{2+} channels TRPV5 and TRPV6 were immunohistochemically localized to the scala media. TRPV5 was mainly localized to the stria vascularis, however high TRPV6 expression levels were found in the IS and Claudius cells. These Ca^{2+} channels are known to be inhibited by low pH (Wangemann et al., 2007). A decrease from optimum endolymphatic pH levels could adversely impact their function. The resulting increased endolymphatic Ca^{2+} levels might result in Ca^{2+} overload of hair cells precipitating their death (Fridberger et al., 1998; Vicente-Torres and Schacht, 2006).

1.2.3 Role of supporting cells at the afferent synapse

Supporting cells also play a very important role in sound information transmission at the glutamatergic IHC afferent synapse (Glowatzki et al., 2006). To accurately encode auditory stimuli the IHC must be able to release neurotransmitter rapidly and for sustained time periods. Several adaptations have evolved, which enable this. Each IHC is contacted at 10-30 specialized structures named synaptic ribbons, by afferent neurons. Each of these boutons belongs to a different spiral ganglion cell. Multiple glutamate containing vesicles are released at each synaptic ribbon. Within the first few milliseconds after the onset of sound stimulation a large readily releasable pool (RRP) of vesicles estimated at 280 per ribbon fuses with the IHC membrane to release their content into the synaptic cleft. The release rate eventually decreases to a sustainable constant level which does not decrease for at least 1 second (Moser and Beutner, 2000).

The high rate of release and number of synapses present necessitates efficient means of removing excess or spill-over glutamate from the vicinity of the synaptic cleft to

prevent swelling of the synaptic terminals and glutamate excitotoxicity (Puel et al., 1997; Pujol and Puel, 1999; Pujol et al., 1990). Studies have uncovered that in the organ of Corti the sole glutamate transporter is the glutamate aspartate transporter GLAST (Furness and Lawton, 2003; Glowatzki et al., 2006). GLAST has been found in border and phalangeal cells surrounding the IHC afferent synapse. Low expression levels have also been observed in Deiters' cells near the afferent synapses of OHCs. To date there is no evidence for the presence of GLAST in hair cells or afferent and efferent neuronal terminals which synapse with them. Thus the supporting cells play a crucial and very important role in sound encoding as no other organ of Corti cells can remove excess extracellular glutamate. This also implicates the border, phalangeal and Deiters' cells in synaptic maintenance a role prescribed to glial cells (Henn and Hamberger, 1971; Kirischuk et al., 2007). Indeed border, phalangeal and Deiters' cells also express the glial cell marker GFAP (Rio et al., 2002). Border and phalangeal cells have also been found to express both the myelinated oligodendrocyte marker myelin proteolipid protein (PLP) and brain derived neurotrophic factor (BDNF) (Mallon et al., 2002; Mellado Lagarde et al., 2014). Selective ablation of border and phalangeal cells at P10 was found to severely limit IHC survival after hearing onset (Mellado Lagarde et al., 2014). Adult mice lacking BDNF expression in border, phalangeal cells and afferent fibres showed reduced IHC exocytosis in the basal region of the cochlea and reduced ribbon count (Zuccotti et al., 2012). These effects were mediated most likely by BDNF release from the supporting cells as deletion of BDNF from supporting cells in the vestibular system correlated with a reduction in the number of ribbons in vestibular hair cells (Gomez-Casati et al., 2010). The above observations indicate that the supporting cells surrounding the IHC afferent synapse play a critical role in its normal function. Finally cochlear supporting cells are known to express P2 receptors which are considered to play a role in regulating hearing sensitivity (described in detail below).

1.2.4 Purinergic receptors

ATP in addition to acting as an energy storage molecule in the cell has been shown to be a paracrine extracellular messenger (Lipmann, 1941). Adenine compounds were first described to have physiological effects in 1929, when injected into the bloodstream they were found to slow down the action of the heart (Drury and Szent-Gyorgyi, 1929). The existence of purinergic signalling and purinergic receptors was first postulated by Burnstock in the 1970s (Burnstock, 1972; Burnstock, 1976). Eventually two classes of

receptors were defined: P1 receptors sensitive to adenosine and P2 receptors sensitive to ADP/ATP (Straub and Bolis, 1978). Studies have localized purinergic receptors to most tissues in the body among them: the respiratory system, gut, urinary system, immune system, cardiovascular system, exocrine and endocrine glands, musculoskeletal system, connective tissue, the nervous system and the senses (including the inner ear) (Burnstock and Knight, 2004). Correspondingly, P2 receptors have been found to play important roles in processes as diverse as neurotransmission and vascular dilation among other (reviewed in (Burnstock, 2006)).

Based on their pharmacological profile and transduction P2 receptors can be further subdivided into two main classes (Abbracchio and Burnstock, 1994) (Figure 1.4). Ionotropic P2X receptors and metabotropic P2Y receptors (reviewed in (Burnstock, 2007)).

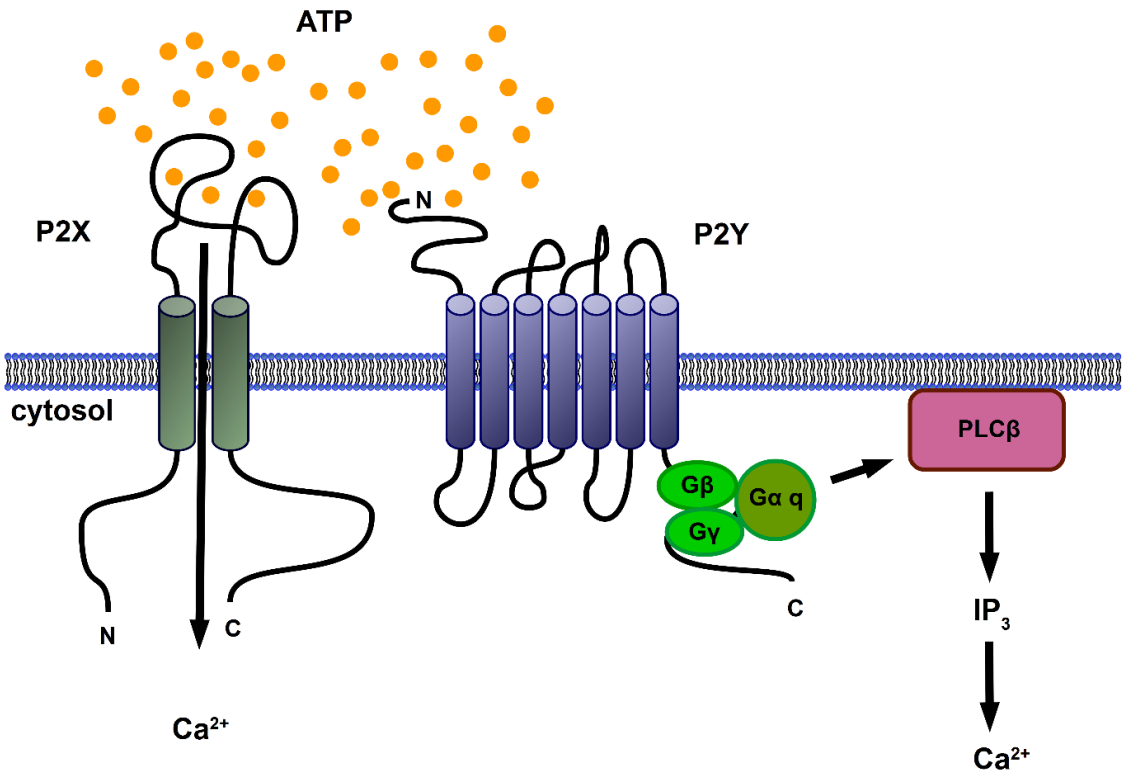

Figure 1.4 Two types of P2 receptors.
P2X receptors are ligand gated ion channels while P2Y receptors are G-protein coupled receptors. Stimulation of both leads to an increase in intracellular Ca^{2+} levels albeit via distinct mechanisms (details in text).

P2X receptors are nonselective, ATP-gated cationic trimer ion channels. Each subunit has two transmembrane domains. So far 7 unique genes which code for these receptors have been identified in humans (Burnstock, 2007). The majority of the discovered P2X

subunits can combine with other P2X subunit types to form heteromultimers, which have unique conductance and desensitization properties compared to receptor homomultimers. P2X receptors are permeable to monovalent and divalent cations. The permeability of P2X receptors to Ca^{2+} is especially important for regulating multiple cellular processes. The EC_{50} for ATP of P2X receptors varies and is between 1-300 µM (Burnstock and Williams, 2000). For the $P2X_2$ receptor, which has been shown to be present in the adult cochlea the EC_{50} for ATP is ~10 µM.

Based on the effects of prolonged agonist exposure P2X receptors can be classified as desensitizing and non-desensitizing. The ability of P2X receptors to desensitize appears to be controlled by C-terminal residues as their removal or mutation can affect desensitization rates (Smith et al., 1999). Indeed, studies have found that the propensity of P2X channels to desensitize is controlled by only several negatively charged electrostatic side chains located near the receptors proximal end (Koshimizu et al., 1999). Additionally truncation of the C-terminal domain can impair receptor permeability (Surprenant et al., 1996; Virginio et al., 1999b) and a single amino acid mutation in the C-terminal can lead to loss of function (Gu et al., 2001). Multiple transcripts for each receptor gene have also been detected and a single P2X gene can code for both desensitizing and non-desensitizing receptor subtypes (Koshimizu et al., 2006).

As an example the product of the $P2X_{2b}$ transcript which lacks part of the C-terminal domain desensitizes rapidly in contrast to the product of the full $P2X_{2a}$ transcript. Removal of the rest of the C-terminal of $P2X_{2b}$ increases desensitization even more (Koshimizu et al., 2006). In addition the N-terminal also plays a role in controlling the $P2X_2$ channel desensitization rates (Koshimizu et al., 2006). Altogether N-terminal splicing together with alternative C-terminal splicing has been shown to have an additive effect on P2X channel desensitization.

The P2X channel pore of some subtypes of P2X receptors has been found to increase in diameter or dilate upon prolonged agonist exposure (Khakh et al., 1999; Virginio et al., 1999b). The ability of receptors to dilate has been found to be mediated by the C-terminal domain similarly to desensitization (Eickhorst et al., 2002). For example in contrast to rat, mice $P2X_2$ receptors do not dilate even though they differ in only 14 of 472 amino acids. 7 of these differences map to the C-terminal domain. In rats the ability of $P2X_2$ receptors to dilate has been found to depend on the presence of two C-terminal

amino acids: I432 and G444. In mice these differ and are S432 and D444. When the rat amino acids are substituted with the mice ones the $P2X_2$ receptor loses the ability to dilate (Eickhorst et al., 2002).

The second type of purinergic receptors found in the cochlea are the metabotropic P2Y receptors. P2Y receptors belong to the G-protein receptor family and can function as single receptors or dimers. Currently 8 P2Y receptor genes are known (Burnstock, 2007). A single P2Y subunit has 7 transmembrane domains an extracellular N-terminal and an intracellular C-terminal. Stimulation of P2Y receptors can lead via the dissociated Gαq protein to an increase in intracellular IP_3 and Ca^{2+} levels. The EC_{50} for ATP in P2Y receptors varies and is usually in the hundred nanomolar to single digit micromolar range (Abbracchio et al., 2006; Bogdanov et al., 1998; Burnstock, 2007; Godecke et al., 1996).

Other nucleoside tri and diphosphates such as UTP and ADP can activate P2Y receptors as well with equal or higher potency than ATP depending on receptor subtype. For example $P2Y_2$ and $P2Y_4$ which have been localized to the cochlea are equally sensitive to ATP and UTP in mice (Abbracchio et al., 2006; Bogdanov et al., 1998; Godecke et al., 1996).

1.2.5 Purinergic signalling in the cochlea

Extracellular ATP was first described to affect hearing in 1978 by Bobbin and Thompson when screening for potential cochlear neurotransmitters (Bobbin and Thompson, 1978). The investigators observed a decrease in the compound action potential of the cochlear nerve after perfusing ATP into the guinea pig scala tympani. These observations were confirmed later as in further studies in the guinea pig it was shown that perfusion of ATP into the scala media decreased both the cochlear microphonic and EP (Munoz et al., 1995). To date the expression of P2 purinergic receptors has been immunohistochemically and functionally shown in the cochlea in hair cells, afferent neurons and supporting cells (Ashmore and Ohmori, 1990; Housley et al., 1999; Jagger and Housley, 2003; Sugasawa et al., 1996a; Sugasawa et al., 1996b).

In isolated adult guinea pig OHCs ATP activated a cationic conductance and increased intracellular Ca^{2+} (Ca^{2+}_i) levels. The expression of P2X receptors in OHCs was limited to the apex of the cell or its stereocilia (Ashmore and Ohmori, 1990; Housley et al., 1992). ATP also increased Ca^{2+}_i levels and elicited a cationic conductance in adult

guinea pig IHCs (Dulon et al., 1991; Sugasawa et al., 1996b). Species specific differences in hair cell P2X receptor expression might be present as in at least one study IHC ATP-activated currents were only observed during a limited time window during rat development and were nearly gone by hearing onset (Tritsch and Bergles, 2010).

Apart from the hair cells P2X and P2Y receptors have also been localized to cochlear supporting cells via multiple techniques. An mRNA hybridization screen localized $P2X_2$ receptor mRNA in multiple cell types lining the endocochlear compartment (Housley et al., 1998). Indeed, $Ca^{2+}{}_i$ levels have been shown to increase after ATP stimulation in both the supporting cells of the organ of Corti as well as the lateral wall and Reissner's membrane (Ikeda et al., 1995; Suzuki et al., 1995). P2X ATP-dependent currents have been recorded in most of the nonsensory cells found in the scala media. In the mature organ of Corti ATP-activated cationic conductances have been documented in Pillar, Deiters' and Hensen's cells (Lagostena et al., 2001; Lagostena and Mammano, 2001). ATP-activated currents were also recorded in rat IS supporting cells (Tritsch and Bergles, 2010). In contrast to currents in IHCs IS currents did not subside up to P16. ATP-activated currents have also been recorded using whole-cell voltage-clamp from Reissner's membrane cells (King et al., 1998).

1.3 Importance of ATP signalling in the cochlea

1.3.1 Protective role of cochlear ATP signalling

It has been hypothesized based on EP measurements that one of the roles of P2 purinergic receptors in the cochlea is the modulation of cochlear function (Munoz et al., 1995). Scala media ATP levels have been observed to increase following exposure to moderate noise levels in the guinea pig (Munoz et al., 2001). P2X receptor expression has also been shown to increase following exposure to noise (Wang et al., 2003b). Activated P2X receptors could allow K^+ to leave the scala media providing a K^+ shunt conductance. The resulting quick decrease in EP would help prevent noise-induced damage to hair cells and neurons. Recent studies appear to support this hypothesis and implicate $P2X_2$ receptors in the development of a temporary hearing loss called a temporary threshold shift (TTS). Mutant mice lacking cochlear $P2X_2$ receptors lacked a TTS after moderate noise overexposure (85 dB, 8-16 kHz for 30 minutes) and are more susceptible to permanent hearing loss (permanent threshold shift (PTS)) after exposure to damaging noise levels (100 dB, 8-16 kHz, 2 hours) (Housley et al., 2013). Indeed mutations in $P2X_2$ receptors are associated with progressive hearing loss in humans and

mice (Yan et al., 2013). Deiters' cells have been shown to express voltage dependent K^+ channels, these could potentially aid in moving K^+ from the scala media and help restore the membrane potential after activation of ATP receptors (see section 1.2.2). Supporting cells are connected by gap junctions (section 1.2.1) and thus have a low resting electrical membrane resistance. Treatment with ATP was observed to transiently increase the membrane resistance in guinea pig Deiters' and Hensen's cells (Lagostena et al., 2001; Lagostena and Mammano, 2001). This effect has been attributed to the ATP elicited increase in $Ca^{2+}{}_i$ levels and subsequent Ca^{2+}-dependent hemichannel closure (Lagostena et al., 2001; Rose et al., 1977). Gap junction closure might inhibit the K^+ recycling pathway and thus be advantageous during exposure to high sound levels.

1.3.2 Purinergic cotransmission in the cochlea

ATP was considered to be a co-transmitter at the IHC afferent synapse as afferent neurons show high levels of P2X receptor expression (Housley et al., 1999; Jagger et al., 2000; Jarlebark et al., 2002). However in recordings from afferent boutons the AMPA receptor antagonist 6-cyano-7-nitroquinoxaline-2,3-dione (CNQX) fully blocked all excitatory post-synaptic potentials bringing the validity of this hypothesis in doubt (Glowatzki and Fuchs, 2002).

1.3.3 Effects of extracellular ATP-dependent intracellular Ca^{2+} regulation on cochlear supporting cells

Stimulation of P2 receptors can increase $Ca^{2+}{}_i$ levels via two distinct mechanisms.

1. Permeation through activated P2X receptors.
2. Release from intracellular stores following P2Y stimulation, activation of phospholipase C (PLC) and cleavage of IP_3 from the membrane bound fraction of phosphatidylinositol 4,5-bisphosphate (PIP_2) (Burnstock, 2007).

Ca^{2+} plays an important role in the cell and an increase in $Ca^{2+}{}_i$ concentration can regulate numerous processes relating to cell physiology and biochemistry (Clapham, 2007).

In the cochlea addition of 100 µM ATP to the extracellular solution was shown to affect the shape of Deiters' cells phalanges and increase the stiffness of the outer sulcus. These changes depended on an increase in $Ca^{2+}{}_i$ levels (Bobbin, 2001; Dulon et al., 1994). Such shape changes could potentially affect the geometry of the organ of Corti and thus sound wave propagation along the basilar membrane. In support after exposure to

intense noise, which could increase scala media ATP levels, the Deiters' and Hensen's cell region of the organ of Corti was observed to be displaced, possibly due to Deiters' cell movement (Flock et al., 1999; Munoz et al., 2001). A model predicting that a change in stiffness of the Deiters' cells would affect the motion of the basilar membrane has also been proposed (Kolston and Ashmore, 1996).

In Hensen's cells stimulation with ATP in addition to activating a P2X type conductance, activated a Ca^{2+}-dependent Cl conductance. The role of it is unclear but it might participate in the regulation of the composition of endolymph or participate in the regulation of osmolarity within the scala media (Lagostena et al., 2001; Sugasawa et al., 1996a).

In the neonatal cochlea extracellular ATP-dependent signalling was found to mediate intercellular Ca^{2+} waves. Intercellular Ca^{2+} waves are changes in $Ca^{2+}{}_i$ levels which propagate from cell to cell (Cornell-Bell et al., 1990; Gale et al., 2004). Such events have also been described in glia and multiple other cell types (Boitano et al., 1992; Cornell-Bell et al., 1990; Demer et al., 1993; Enomoto et al., 1992; Nathanson et al., 1995).

1.3.4 Mechanism of propagation of ATP-mediated Ca^{2+} waves

Propagation of most intercellular Ca^{2+} waves requires diffusion of intracellular factors through gap junctions or release of mediators through hemichannels into the extracellular space. (Scemes and Giaume, 2006). Organ of Corti Ca^{2+} waves were initially shown to arise in a neonatal organotypic culture after inducing mechanical or laser damage to single cochlear hair cells (Gale et al., 2004). Damage evokes a $Ca^{2+}{}_i$ rise, which triggers ATP release through hemichannels. ATP triggers a $Ca^{2+}{}_i$ rise in the neighbouring cell and thus propagation of an intercellular wave. (Gale et al., 2004).

The $Ca^{2+}{}_i$ increase of the passing wave was found to increase ERK dependent MAPK phosphorylation in the supporting cells surrounding the site of damage, perhaps acting as a damage sensing mechanism.

Further studies have determined that extracellular ATP mediated Ca^{2+} waves also occur spontaneously before the onset of hearing in a region of the immature organ of Corti called the greater epithelial ridge (GER) (Tritsch et al., 2007). There in a structure called Köllikers organ, spontaneous increases in $Ca^{2+}{}_i$ have been shown to propagate in

an extracellular ATP and hemichannel dependent manner (Tritsch and Bergles, 2010; Tritsch et al., 2007).

The molecular mechanisms of ATP release are not yet clear. Research on glial cells indicates that the Ca^{2+}_i increase is crucial for opening unpaired hemichannels (De Vuyst et al., 2006). Studies indicate that Ca^{2+}_i does not act directly on the connexins (De Vuyst et al., 2009). Instead it is thought that Ca^{2+}-activated intracellular proteins such as calmodulin (CaM), CaM-dependent kinase, p38 mitogen activated kinase and a range of other factors might be involved in regulating connexin channel state and ATP release.

How ATP activates cochlear supporting cells is much better understood (Anselmi et al., 2008; Majumder et al., 2010). ATP activates P2Y receptors leading to the activation of phospholipase C (PLC). PLC in turn breaks down membrane bound phosphotidylinositol 4,5-bisphosphate (PIP_2) into diacylglycerol (DAG) and IP_3. DAG remains membrane bound while IP_3 diffuses through the cytoplasm and acts on inositol triphosphate receptors (IP_3Rs) on the endoplasmic reticulum (ER). This leads to Ca^{2+} release from the ER. The released Ca^{2+} further potentiates the action of IP_3 in a process called Ca^{2+}-induced Ca^{2+} release (CICR) (Endo et al., 1970; Ford and Podolsky, 1970). Eventually, homeostatic mechanisms bring down the Ca^{2+}_i concentration to resting levels.

1.3.5 Significance of spontaneous ATP-mediated Ca^{2+} waves in the neonatal cochlea

It is thought that ATP released during intercellular Ca^{2+} waves in Kölliker's organ acts on P2X receptors on the IHCs. The depolarized IHCs initiate bursts of action potentials in the afferent neurons (Tritsch et al., 2010a; Tritsch et al., 2007). These action potential bursts might be important for the development and maturation of brain regions involved in processing auditory information. The importance of ATP for generation of spontaneous bursting events has subsequently been however disputed. A study on intact immature organ of Corti tissue has found that even though millimolar ATP levels can increase bursting frequency nanomolar ATP levels can have an opposite effect and hyperpolarize the IHCs reducing bursting frequency (Johnson et al., 2011). The most likely mechanism is through P2X and Ca^{2+}-dependent activation of SK channels, which are present in the immature IHCs and when activated hyperpolarize the cells. The study's authors found that the resting IHC membrane potential is depolarized enough even without ATP stimulation that it allows for spontaneous Ca^{2+} action potentials. In

addition to nanomolar ATP levels, the study's investigators found that the IHC membrane potential can be further hyperpolarized by acetylcholine which is released from efferent terminals still present at this stage of development at the IHCs base.

The frequency of both Ca^{2+} waves and bursting declines during maturation and these events are no longer present at the time of hearing onset (Beutner and Moser, 2001; Kros et al., 1998). Köllikers organ is also superseded by IS cells at this time. Spontaneous ATP-dependent Ca^{2+} waves are only present in Kölliker's organ. Ca^{2+} waves can however be induced in different regions of the immature cochlea by damage (as described above), or by rapid uncaging of caged IP_3 compounds (Anselmi et al., 2008; Gale et al., 2004; Majumder et al., 2010). Ca^{2+} waves can also be elicited in the immature organ of Corti by damaged hair cells after aminoglycoside treatment. Waves are most likely triggered by release of ATP from damaged hair cells (Gale personal communication).

Stimulation of both P2X and P2Y receptors in Köllikers organ elicited inward currents (Tritsch and Bergles, 2010). The onset of currents elicited by the specific P2Y agonist UTP was delayed when compared to the ATP evoked currents consistent with them depending on second messenger generation. In agreement application of ATP produced an initial fast P2X dependent response followed by a delayed component, which might at least partially be the result of P2Y receptor stimulation.

The identity of the slow onset ATP-activated conductance in Köllikers organ cells is not yet elucidated. There is circumstantial evidence that it could be a CaCC (Tritsch et al., 2010b). An immunohistochemical investigation has found the CaCC Ano-1 staining specifically in Köllikers organ at developmental stages corresponding to those during which spontaneous activity was observed (Yi et al., 2013). Bright-field observations of Köllikers organ indicate that the spontaneous Ca^{2+} waves happen concurrently with shrinkage or "crenation" of Köllikers organ cells (Tritsch et al., 2007).

These observations are consistent with the presence of CaCCs. Rapid loss of Cl^- from the cell might lead to an osmotic imbalance, resulting in water movement and cell shrinkage. In agreement with this hypothesis Ano-1 staining could no longer be detected in Köllikers organ by P16, similarly to spontaneous Ca^{2+} waves and morphological changes.

The importance of the morphological changes and the CaCCs in Köllikers organ remain unclear however. In addition to its role in hearing maturation the spontaneous activity could also be important for the regulation of endolymph composition or the detachment of the TM from the IS (Tritsch et al., 2007). Why the spontaneous activity ceases and if IS cells from the mature organ of Corti lack any CaCCs is not clear. It also remains to be determined why similar morphological changes have not been observed in other epithelial cells expressing CaCCs such as Hensen's cells (Sugasawa et al., 1996a). Finally if and to what extent Ca^{2+} waves are present in the mature organ of Corti remains to be determined. Hampering studies on P2 receptor signalling in the adult cochlea is the relative difficulty of accessing the intact organ of Corti in adult animals. Thus the effects of P2 receptor activation in various cochlear cells and the physiological role of P2 receptors in hearing mammals remain unclear and is the main topic of this thesis.

2 Materials and Methods

2.1 General reagents

All reagents were obtained from Sigma-Aldrich, USA unless stated otherwise. All Ca^{2+} indicators were obtained from Molecular Probes (Invitrogen, UK).

2.2 Ex vivo preparation

2.2.1 Obtaining and dissecting adult mouse cochlear tissue

Cochleas isolated from adult C57/BL6 mice days (P30 and older) were used. To obtain cochleas mice were killed in accordance with Schedule One Procedures of the UK Home Office guidelines, and then decapitated. The temporal bone with an intact cochlea was removed and transferred into freshly prepared extracellular solution (ES) composed of (in mM): 140 NaCl, 5.4 KCl, 1.3 $CaCl_2$, 1 $MgCl_2$, 10 HEPES, pH 7.4 osmolarity was adjusted to 320 milliosmoles with glucose. In some cases Ca^{2+} was omitted from ES to make a low Ca^{2+} extracellular solution. Additionally in some instances 2 mM or 10 mM EGTA was added to the low extracellular Ca^{2+} solution to bind any remaining free Ca^{2+} ions. Solutions were maintained at room temperature thereafter. All procedures were conducted in ES containing 1.3 mM Ca^{2+} unless specified otherwise. The organ of Corti was accessed by diligently removing the bone on top of the apical cochlear coil. The stria vascularis and TM in some instances were gently peeled off and the organ of Corti was left intact to mimic as closely as possible the *in vivo* cellular organization. For experimentation cochleas were mounted using superglue onto glass coverslips or 35 millimetre cell culture dishes.

2.3 Electrophysiology

2.3.1 Solutions

The intracellular solution contained in mM: 130 KCl, 0.5 EGTA, 2 $MgCl_2$, and 10 HEPES, pH 7.3. Osmolarity was adjusted to 320 milliosmoles with glucose. In some recordings KSCN was substituted for KCl and EGTA was replaced by 10 mM BAPTA or 5 mM EGTA.

2.3.2 Recording electrodes and puff pipettes

For single cell patch clamp electrophysiology, recording electrodes were made from borosilicate glass capillaries with a fibre inside (dimensions: outer Ø = 1.2 mm, inner Ø = 0.94 mm, length = 75 mm, Harvard Apparatus, UK) with a pipette puller (Narishige, Japan). Electrodes were back filled with intracellular solution and the pulling temperature was adjusted to obtain electrodes with a resistance of 3 – 4 MOhms

as measured after filling with intracellular solution and placing the electrode in ES. For local drug application, glass pipettes were pulled using the same borosilicate glass and procedure as detailed for recording electrodes. The pulling temperature was adjusted so that the tip opening had an approximate diameter of 2 µm. Some experiments necessitated the use of two puff pipettes each containing solution with a different P2 agonist. In those cases two glass pipettes (outer Ø = 1.0 mm, inner Ø = 0.78 mm, length 75 mm, Harvard Apparatus, UK) were joined together along their shafts. The joined shafts were heated up at their middle with a Bunsen burner and carefully twisted together. The joined and twisted at the middle pipettes were then inserted into a pipette puller and the pulling temperature was adjusted so that that the joint tip of the conjoined pipettes was no wider than 4 µm.

2.3.3 Recording equipment

An Olympus BX50WI upright microscope (Olympus, Japan) equipped with Hoffman modulation contrast optics (objectives and condensers) was used for all electrophysiology experiments. The microscope was equipped with a 10x/0.3w and a 60x/0.9w objective. A perfusion closed loop system consisting of two Gilson Minipuls 3 peristaltic pumps (Gilson, USA) and polyvinyl chloride (PVC) tubing was set-up to provide constant perfusion of experimental samples at a rate of 2.5 ml/min. One pump was responsible for pumping solution into the bath and the second for removing solution from the bath and back into the main solution reservoir. The solution was heated prior to entering the bath by winding tubing around a custom made heating coil. The coils temperature was controlled via a custom built control module, so that temperature of the solution in the bath was maintained at 30ºC.

An Axopatch 200B capacitor feedback patch clamp amplifier (Molecular Devices, USA) was used to obtain recordings and data was filtered at 10 kHz while recording. Subsequently data was amplified and digitized via a 1322A analog to digital converter (Molecular Devices, USA) and recorded using the pClamp 9.0 (Molecular Devices, USA) software suite on a PC computer running Windows 2000 (Microsoft, USA). Depending on the applied protocols recordings were digitized and sampled every 10 - 100 µs.

2.3.4 Cell identification

Electrophysiological recordings were conducted on cochlear IS cells, border supporting cells and IHCs. Cells were initially identified visually. To aid in the identification of

supporting cells, the recording pipette was filled with an intracellular solution containing 0.1 mM of 10,000 MW dextran conjugated fluorescein. The fluorescent signal was collected using a long pass (> 510 nm) filter and a cooled CCD camera (PCO Sensicam, Pulse Photonics, UK) and images were recorded at 320 x 256 (8 x 8 binning) or 640 x 512 (4 x 4 binning) pixel resolution. Upon completion of electrophysiological recordings cochleas were fixed in 4% PFA for 30 minutes and stored in PBS containing 0.05% NaN_3 for further imaging. The fixed cochleas were imaged using confocal microscopy and fluorescence was elicited at 488 nm and collected by the microscope through a 510-540 nm band pass filter.

2.3.5 Application of P2 agonists

A glass pipette with a 2 µm tip was made using a pipette puller (section: 2.3.2) and filled with extracellular solution containing 100 µM ATP or 100 µM UTP. The pipette was mounted in a holder and placed in the bath solution and the pipette's tip was carefully positioned above the organ of Corti in the dissected mounted cochlea. The back of the pipette was connected by PVC tubing to the outlet port of a Cornerstone PMI-100 microinjector (Dagan, USA). The microinjector is a device that enables precise temporal control of air pressure delivered to its outlet port and thus enabled temporarily precise delivery of agonist containing solution onto the organ of Corti. In cases, where two drugs were applied to the same cell a double puff pipette was used as detailed in section 2.3.2. Each pipette was backfilled with ES containing a different agonist. The pipettes were connected to the microinjector via PVC tubing. A plastic tap was used to regulate the flow of air into the appropriate puff pipette.

2.3.6 Blocking gap junctional coupling

Cochlear supporting cells are connected by gap junctions. To obtain recordings from single cells gap junction blockers are required. 1-octanol (1 mM), flufenamic acid (FFA) (100 µM) and carbenoxolone (100 µM) were added to the extracellular solution where appropriate to reduce gap junction coupling. To limit exposure of the tissue to gap junction blockers the ES was substituted for solution containing gap junction blockers only upon attaining whole cell recording conditions.

2.3.7 Electrophysiological patch clamp recordings

Upon lowering the patch pipette into the bath and bringing the tip to within 50 µm of the cells to be recorded from the pipette offset was adjusted to 0 pA and pipette

capacitive transients were cancelled via the Axopatch 200B amplifier. The pipettes tip resistance was monitored in pClamp and calculated online from 10 mV test pulses.

Backpressure was applied to the patch pipette during this time. The pipette was brought in towards the cell chosen for recordings until the back pressure created a dimple on the cells membrane. At this point back pressure was released and if the electrical resistance between the pipette tip and the cellular membrane did not increase above 1 GOhm immediately gentle suction was administered to the back of the pipette to raise the electrical resistance. Once at least 1 GOhm resistance was reached the membrane was broken through by an additional brief jolt of suction. After obtaining whole cell recording conditions and if not explicitly stated otherwise cells were voltage clamped at the command potential of V_c = -55 mV, a potential found to maximize the possible length of recording from the cell, or current clamped at 0 A and subjected to further experimental electrophysiological protocols. Series resistance were left uncompensated. Liquid junction potentials were corrected offline (Sakmann and Neher, 2009).

2.3.8 Correction of liquid junction potentials

Liquid junction potentials were measured using the patch clamp amplifier. The patch clamp amplifier was placed in current clamp mode and the 'meter' set to the 'Vm' position. The ground electrode was inserted into a glass pipette (made as described in section 2.3.2) and filled with 3 M KCl. The pipettes tip was then broken off. A 35 mm tissue culture dish was filled with intracellular solution and a glass electrode filled with ES was inserted into the intracellular solution. The ground electrode was also inserted into the intracellular solution. The value of the liquid junction potential could be read off the patch clamp amplifier. Values obtained for KCl based intracellular solution were 2.2 mV (average of 4 independent measurements), whereas the values of a KSCN based solution were on average 3.3 mV (average of 4 independent measurements). The obtained values were later subtracted from the values of V_c to obtain the value of the membrane potential corrected for the liquid junction potential (e.g. when a KCl based intracellular solution was used a V_c -75 mV became -77.2 mV).

2.3.9 Recording protocols used

Current – voltage (I – V) protocols

To obtain current – voltage plots and obtain information about the voltage dependence of any channels present in the cell and any elicited currents, a protocol consisting of multiple traces was utilized. For each trace the V_c was first changed for 350 ms to -75

mV to obtain a capacitive transient which could be used during offline analysis to obtain the cells capacitance. From this level in each trace the potential was changed in 5 mV increments to values between -100 and +25 mV for 100 ms for each trace, upon which it was returned back to -75 mV and after a further delay of 350 ms back to a V_c of -55 mV.

Voltage ramps

For voltage ramps V_c was initially lowered to -75 mV for 350 ms similarly as this was done in current – voltage protocols described above. Voltage ramps were applied by steadily increasing V_c from -90 to +45 mV over a period of 500 ms. Applying ramps instead of I – V protocols was found to increase the amount of time available for recordings before whole cell recording conditions were lost, and was used to determine cells membrane resistance and voltage activated conductances when decoupling supporting cells with 1-octanol. In some recordings 500 ms (-90 to +45 mV) voltage ramps were also applied before, at different time-point during agonist application (1.5 – 7.5 s post application onset), and after agonist application to measure the reversal potential of agonist activated currents and probe if currents returned to baseline levels. When intracellular Cl^- was replaced with SCN^- in some cases a 1 s -90 to +90 mV voltage ramp was applied instead of the 500 ms ramp described above. For analysis and plotting current traces obtained for voltage ramps during agonist application were subtracted from current traces obtained for the same voltage ramps applied before agonist application.

Local application of P2 receptor agonists

The effects of P2 receptor agonists were probed by applying agonists for varying amounts of time (150 – 15000 ms) whilst clamping the cell at V_c = -55 mV. The tip of the puff pipette was placed approximately 50 µm away from the cell recorded from. The microinjector was controlled through the pClamp software suite so that precise control of the duration of agonist application could be achieved. In some instances voltage ramps (as described above) were applied during agonist application to determine current reversal potential (V_0). In addition membrane potential (V_m) was observed during microinjector activation in select recordings.

Peak current responses (I_{max}) to agonist application were measured by subtracting the value of the maximum elicited current during agonist application from the resting

current level. The resting current was measured as the average of the first 500 ms at the beginning of the recording.

2.3.10 Data analysis

All data was analysed offline in MATLAB 2011-2013 (Mathworks, USA), Clampfit (Molecular Devices, USA) and OriginPro (OriginLab, USA). For offline electrophysiology data analysis data recorded in .abf files (Molecular Devices, USA) was transferred to a computer running MATLAB software. Data was extracted from the .abf files using the 'abfload' script made freely available by Harald Hentschke at: http://www.mathworks.com/matlabcentral/fileexchange/6190-abfload and subjected to further offline analysis in MATLAB.

To establish basic properties of the cell during recording, a voltage step to 20 mV below the holding potential (described in section 2.3.9) was applied at the beginning of select experimental protocols. This step was used to establish the values of:

R_s – Series resistance

R_m – Cell membrane resistance

which (as described in (Sakmann and Neher, 2009)) were calculated from the values of:

I_{in} – Instantaneous current just after the voltage change

I_{SS} – Steady state current

Upon establishing whole cell recording conditions the cells membrane acts as a capacitor and the cells capacitance can be used as a measure of cell size. After changing the holding potential of the cell a sharp peak in current passing through the membrane is visible, this current declines with a time constant which can be fit by single or multiple exponentials and corresponds to the charging phase of a capacitor.

Capacitance was calculated by integrating in MATLAB the area underneath the capacitive transient evoked by the 20 mV voltage step described above.

2.4 Immunohistochemistry

2.4.1 Fixation

Cochleas were fixed for 30 minutes in 4% PFA and stored in PBS containing 0.05% NaN_3 pending immunostaining. For P2 receptor immuno-labelling cochleas were fixed immediately following dissection, while cochleas in which cochlear IS or border cells

were fluorescently labelled were fixed pending completion of experimental manipulations.

2.4.2 Immuno-labelling

Cochleas were stained using primary antibodies against P2X and P2Y receptor subunits (Alomone, Israel) and Myosin VIIA (Developmental Studies Hybridoma Bank, USA). The final concentrations of the primary anti-P2 receptor and anti-myosin antibodies used during this study are summarized in Table 2.1. Secondary anti-rabbit and anti-mouse antibodies conjugated with Alexa fluorophores (488, 550 and 568) were used to visualize P2 receptors and MyosinVIIA.

Primary antibody	**Anti-P2X2**	**Anti-P2Y2**	**Anti-P2Y4**	**Anti-Myosin VIIA**
Dilution	1:500	1:500	1:500	1:250
Stock concentration	0.8 µg/µl	0.8 µg/µl	0.8 µg/µl	0.4 µg/µl
Species	rabbit	rabbit	rabbit	mouse

Table 2.1: Showing the dilution and type of primary antibodies.

For all procedures related to immuno-labelling, cochleas were gently rocked on a laboratory rocking table. Fixed cochleas were incubated in blocking solution (containing: 0.1 mM PBS, 10% Goat Serum, 0.1% Triton X-100) for 1 hour at 21ºC. Primary antibodies were added and cochleas were incubated overnight at 4ºC. Subsequently cochleas were washed three times, each time for 5 minutes in PBS and incubated with secondary antibodies for 3 hours at 21ºC in blocking solution. After secondary antibody incubation cochleas were washed a final time. For convenience these steps are summarized in Table 2.2.

No	**Step**	**Solution**	**Time**
1.	Blocking	Blocking solution	1 hour, 21ºC
2.	Primary antibody	Blocking solution	Overnight, 4ºC
3.	Wash	PBS	5 minutes, 3 times
4.	Secondary antibodies	Blocking solution	3 hours, 21ºC
5.	Wash	PBS	5 minutes, 3 times

Table 2.2: Showing the duration of and steps applied to immune-labelled tissue.

After staining cochleas were either stored in PBS containing 0.05% NaN_3 pending confocal imaging or imaged directly.

2.4.3 Confocal imaging

Confocal images were taken using a Zeiss LSM 510 confocal microscope equipped with a 488, 543 and a Ti – Sapphire laser. Fluorescence was collected using 500-550 nm and 565-615 nm band pass filters, and a 40x/0.8 water immersion objective. Images were recorded in 12 bits and further processed in ImageJ (http://imagej.nih.gov/ij/).

2.5 Brightfield imaging

2.5.1 Brightfield imaging and analysis

To detect any cytoplasmic or morphological changes in cells treated with ATP, cells were observed using an optical microscope as detailed in section 2.3.3. Images were captured using the 60x/0.9w objective and a cooled CCD camera (PCO Sensicam Pulse Photonics, UK) at a sampling rate of 500 to 1500 ms and a resolution of 1280 x 1024 pixels. To quantify cytoplasmic changes brightfield images were subjected to further processing in MATLAB. A differential image was obtained by subtracting subsequent frames from each other. Subtracting every sixth frame was found to give the best results.

Frames were subtracted according to the formula:

$$F_{diff(1)} = (F_{(7)} - F_{(1)})$$
$$F_{diff(2)} = (F_{(8)} - F_{(2)})$$
$$\vdots$$
$$F_{diff(n)} = (F_{(n)} - F_{(n-6)})$$

$F_{diff(n)}$ – is the differentially subtracted frame

$F_{(n)}$ – bright field frame number ‘n’

After obtaining the differential images, the standard deviation (SD) of all the pixel values in 10 x 10 µm or 30 x 30 µm regions of interest (ROIs) placed over the IS or IHCs was determined for each frame. SD values of the frames from the first 6 seconds of the recording (before agonist application) and the last 6 seconds of the recording (after agonist effects subsided) were averaged. Values for frames between these points were linearly interpolated. The interpolated values were subtracted from the measured SD values to determine the change in SD from background SD for each frame. Traces

were synchronized to the frame in which agonist was puff applied and averaged. In some cases traces were normalized before averaging.

2.6 Calcium Imaging

2.6.1 Calcium indicator loading and intracellular Ca^{2+} imaging

Dissected cochleas were incubated for 45 minutes at 37ºC in ES with a 20 µM concentration of the acetoxymethylesters (AM-esters) of Fluo-4 or Oregon Green 488 BAPTA-1 (OGB-1) (Molecular Probes, USA). Pluronic acid was added to a concentration of 0.04% *v/v*. After incubation loaded cochleas were briefly washed in ES and mounted on 35 mm tissue culture plates for further imaging. Images were captured using an upright microscope fitted with a 60x/0.9 water objective. Fluorescence was excited at 470 nm using a monochromator (Kinetic Imaging, UK). The fluorescent signal was collected using a > 510 nm long pass filter using a cooled CCD camera (PCO Sensicam Pulse Photonics, UK) and images were recorded at 320 x 256 (8 x 8 binning) or 640 x 512 (4 x 4 binning) pixel resolution. For imaging using a confocal microscope fluorescence was elicited at 488 nm and collected using a > 505 nm long pass filter, with the pinhole fully open. Imaging was conducted using either a 10x/0.3 or 40x/0.8 water immersion objective. Fluorescence collected using a confocal microscope was monitored every 6 or 12 seconds for up to 600 frames in a 560 x 430 pixel size region in which each square pixel had a side length 0.24 or 1.5 µm. In some instances after collecting images were digitally stabilized to correct for any movement during imaging using the free ImageJ (imagej.nih.gov/ij/) plugin 'Image stabilizer' by Kang Li and Steven Kang. After capturing images were subjected to further experimental manipulations.

2.6.2 Measuring the duration of intracellular Ca^{2+} increase

After loading tissue with Ca^{2+} indicator dyes fluorescence was measured for each frame as the average pixel fluorescence in ROIs placed over various cell types. If an increase in signal was detected trace background fluorescence was subtracted (measured as described in section 2.6.3). The resulting fluorescence traces were normalized to their maximum value. The duration for which fluorescent signal remained elevated above various fractions of the maximum signal was measured.

2.6.3 Measuring the percentage change of Ca^{2+} indicator signal

The percentage of signal increase was measured in 5 x 5 µm ROIs overlaid over captured images (section 2.6.1). Fluorescence increase was measured according to the formula:

$F_{\%increase} = ((F_{(n)} - F_{(0)}) / F_{(0)})*100\%$

$F_{\%increase}$ – Fluorescence increase in percent from baseline

$F_{(0)}$ – Baseline fluorescence value

$F_{(n)}$ – Fluorescence value of the measured frame in the image stack

Baseline fluorescence was measured as the median fluorescence of approximately 5 minutes spanning a time period before, during and after the measured $Ca^{2+}{}_i$ increase.

2.6.4 Subtracting background fluorescence

In some instances to increase the signal to noise ratio fluorescence values of each frame were subtracted from the average value of all captured frames according to the formula:

$F_{sub(n)} = F_{(n)} - F_{avg}$

$F_{sub(n)}$ – The nth frame with subtracted fluorescence

$F_{(n)}$ – The nth frame in the image stack

F_{avg} – The average value of fluorescence for all the captured frames in the current series

2.6.5 Comparing the intracellular Ca^{2+} increase evoked by different P2 receptor agonists

A single double barrel puff pipette (section 2.3.2) was used to eliminate the need for any manipulation to the experimental setup in-between applying agonists specific for different receptor groups. Each barrel of the puff pipette was filled by a different P2 receptor agonist or filled with ES with a different Ca^{2+} concentration. If the Ca^{2+} concentration varied between both pipette barrels, dissected organs of Corti were kept in-between puff applications of the P2 receptor agonist in the ES with the smaller Ca^{2+} concentration. The pipette was placed at the mid-point of the organ of Corti region accessible to experimental manipulations. Percentage of Ca^{2+} indicator fluorescence increase was calculated.

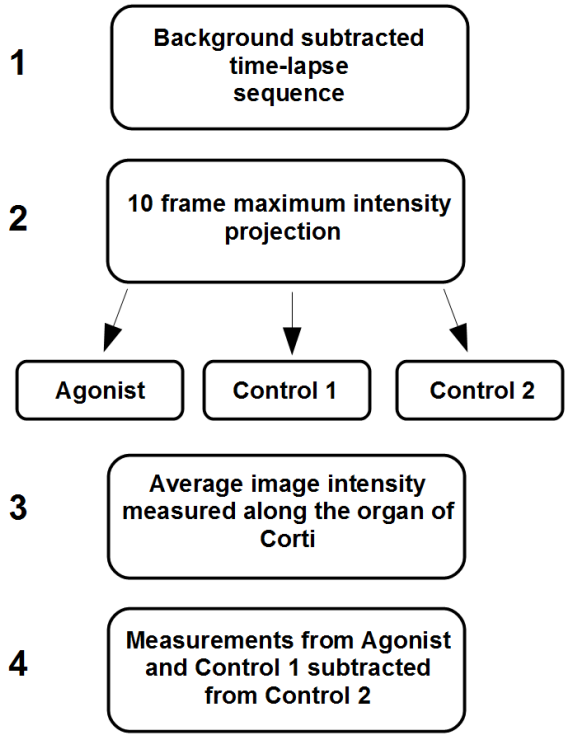

Figure 2.1 Diagram showing sequence of image processing to obtain plots relating the distance from the source of ATP to fluorescent signal intensity.
The steps undertaken during analysis are indicated by numbers on the left.

To relate the ATP evoked increase in fluorescent signal to the distance from the source of ATP a maximum intensity projection of 10 frames (60 seconds) starting immediately after the onset of agonist application was obtained for the background subtracted (detailed in section 2.6.4) observed organ of Corti region (Figure 2.1, step 1 and 2). Fluorescence was measured along a 75 µm wide curved line plotted along the IHCs on the background subtracted maximum intensity projection (Figure 2.1, step 3). Due to incomplete background subtraction, the measured values (Agonist) were further subtracted from values measured in the same region taken in-between agonist applications (Control 2). An additional 10 frame maximum intensity projection of the same region taken in-between agonist applications, was used as control (Control 1) and subtracted from Control 2.

2.6.6 Treatment with P2 receptor antagonists and apyrase

In some experiments the P2 receptor antagonists PPADS (pyridoxalphosphate-6-azophenyl-2',4'-disulfonic acid) (50 µM) and suramin (150 µM) were added to the ES to inhibit P2 receptors and stop any possible extracellular ATP signalling. In independent experiments potato apyrase, an enzyme which removes phosphate groups from ATP and

ADP was dissolved in the ES to a concentration of 40 units (U) to inhibit possible extracellular ATP signalling.

2.6.7 Laser ablation of hair cells

The 720 nm output from a Ti-Sapphire laser was used to selectively ablate hair cells in Ca^{2+} indicator loaded organs of Corti. The laser was used to cause damage in a 2 by 2 or 10 by 10 pixel region which corresponded to an area of approximately 3 by 3 µm when using 10x and 40x objectives respectively. The pixel dwell time was 100 µs. Following laser ablation fluorescence was monitored.

2.6.8 Measurement of Ca^{2+} wave properties

Confocal microscope captured time lapse images (section 2.6.1) were subjected to further analysis to detect and measure properties of Ca^{2+} waves. Where appropriate background fluorescence was subtracted as detailed in section 2.6.4. ROIs where placed at fixed distances along the observed waves travel path to visualize and measure wave propagation speed and distance.

For automated MATLAB analysis to remove artefacts caused by preparation movement during imaging a different background subtraction method was used. Subsequent frames were subtracted from a moving average of 35 frames taken between 17 frames preceding and following the subtracted frame. This procedure was found to give ample signal to noise amplification whilst minimizing the number of frames unavailable for analysis due to moving average subtraction.

To automatically determine the frequency of the observed spontaneous Ca^{2+} waves average pixel value was monitored in a 5 x 10 µm ROI placed over Deiters' or IS cells using ImageJ. The raw data was imported into MATLAB. To determine if increases in fluorescence were present the frame with the highest fluorescence signal was compared to the mean fluorescence value. If it was found to be at least 2 standard deviations above the mean, data was subjected to further analysis.

Traces were normalized to the highest fluorescence present and all detected points in which fluorescence increased to 0.4 of the maximum were treated as an increase in Ca^{2+}_i in the observed ROI. The time intervals between detected Ca^{2+}_i increases were used to determine the inter-wave interval or the duration between rises in Ca^{2+}_i levels if measured in single cells. Frequency was extrapolated from the inter-wave interval and

the standard deviation (SD) of the inter-wave intervals was measured as the average SD of inter-wave intervals from individual ROIs.

2.6.9 Measurement of Ca^{2+} wave parameters from kymographs

To visualize and further analyse Ca^{2+} waves a line was plotted through the region occupied by the Deiters' or IS cells. Pixel values at each point of this line were monitored in every frame. The pixel values found along the line at each frame were re-plotted as a straight line. Values from subsequent frames were plotted below each other to make a kymograph. Kymographs were used to manually measure wave propagation distance and duration.

For automated analysis, kymographs were first thresholded using ImageJ to reduce background noise and improve the signal to noise ratio of fluorescent signal. The resulting kymographs had only two colour values, black and white. These simplified kymographs were used for further automated wave detection and analysis. Individual areas of contiguous white pixel values from the thresholded kymographs were detected using a custom MATLAB protocol. Information on the height and width of each of the detected areas was obtained and the length of each area computed using Pythagorean theorem. To remove signal which was not the result of Ca^{2+} wave signalling the pixel ratio of each of the detected white areas thickness to length was determined. If the ratio was above 0.1, the area was assumed to not be a Ca^{2+} wave and omitted from further analysis.

The remaining white areas were fit with a regression function. The areas in which the R value of the fitted line was below 0.7 were discarded and not analysed further. An additional F-test was performed on the regression lines fitted to the remaining white areas. If the F-test value was above 0.05, the white areas were omitted from further analysis. The remaining detected kymograph white areas were assumed to show Ca^{2+} waves and analysed to find wave propagation distance and propagation time. In some instances pixel values were measured along a vertical line on the kymograph. These values were used to determine Ca^{2+} wave frequency and the inter-wave interval as described in section 2.6.8.

2.7 Data presentation and statistical analysis

Images are in some instances accompanied by a scale displaying the range of 16bit pixel values present in the image. All mean values are shown with the standard error of the

result unless indicated otherwise. Error bars in figures denote the standard error. If not indicated otherwise the following procedure was used to compare data: Prior to analysing data was tested for normality using the Kolmogorov-Smirnov test. If a normal distribution could not be discounted unpaired two sample t-tests were used to compare groups, unless indicated otherwise. The significance of the difference between groups was determined assuming unequal variance (Welch correction). If data was found to not have a normal distribution Kruskal-Wallis ANOVA was used in addition to determine the significance of the difference between groups. Statistical significance in figures is denoted with stars where: * indicates a probability the data being obtained from the same population of less than 0.05, ** a probability of less than 0.01 and *** a probability of less than 0.001. N.S. – denotes a difference which was not significant ($P > 0.05$).

3 Results

3.1 ATP receptors are present in supporting cells of the adult mouse organ of Corti

3.1.1 Introduction

To date Ca^{2+} signalling events have been extensively studied in organotypic cochlear cultures from prehearing animals. In these preparations spontaneous extracellular ATP-dependent Ca^{2+} waves have been observed in a region occupied later by the IS called Köllikers organ (Tritsch and Bergles, 2010; Tritsch et al., 2007). The Ca^{2+} signalling events in Köllikers organ are thought to play an important role in the maturation of the organ of Corti and are present between P0 and P10. These spontaneous Ca^{2+} signalling events are thought to subside around hearing onset post P11 in the rat.

At this time the cochlea undergoes a major developmental shift. The morphology of the organ of Corti changes as Köllikers organ cells undergo programmed cell death and are replaced by the IS (Kamiya et al., 2001; Knipper et al., 1999). The expression profile of ion channels in hair cells changes and IHCs no longer evoke spontaneous action potentials in the afferent neurons (Kros et al., 1998; Marcotti et al., 2003a; Marcotti et al., 2003b). During maturation there is also a shift in the expression profile of connexins which mediate the extracellular ATP-dependent waves in the immature organ of Corti (Jagger and Forge, 2006). Medial and lateral connexin connected compartments are established in the organ of Corti. Unfortunately to date no major studies of Ca^{2+} signalling have been undertaken in the adult organ of Corti and it is unclear how the developmental changes in the organ of Corti affect Ca^{2+} signalling in the IS and other cochlear supporting cells.

The aim of this investigation was to determine the extent of P2 receptor expression in the IS and organ of Corti of the hearing mouse. To achieve this a combination of immunohistochemical staining and cytoplasmic $Ca^{2+}{}_i$ was used.

3.1.2 ATP receptor immunohistochemistry

To determine whether ATP receptors are present in the adult mouse organ of Corti, an immunohistochemical examination was conducted. This involved the main types of receptors found previously to be present in the cochlea, the ionotropic $P2X_2$ and metabotropic $P2Y_2$, and $P2Y_4$. Staining was repeated on 3 cochleas for each receptor subtype and representative stainings are shown below. (Figure 3.1, Figure 3.2, Figure

3.3) (Housley et al., 1999; Housley et al., 1998; Huang et al., 2010). $P2X_2$ receptor staining was observed in all cochlear supporting cells. In addition staining was visible also in OHC stereocilia (98 of 112 or 88 % of observed OHCs). Weak staining was also present in the stereocilia of 19 of 35 observed IHCs (54 %) (Figure 3.1, Figure 3.2, Figure 3.3). Strong $P2X_2$ receptor staining was found in the IS cells, border and phalangeal cells, inner and outer pillar cells, Deiters' cells and Hensen's cells. The strongest signal was found to be in the pillar cells. In the IS and cells surrounding the IHC afferent synapse staining was visible at the cuticular plate as well as in the perilymph exposed membrane below (Figure 3.1, Figure 3.2). $P2Y_2$ staining was also broadly distributed however a strong signal was associated with the OHC membrane (Figure 3.1, Figure 3.3). $P2Y_4$ staining was found broadly distributed among sensory and nonsensory cell types in the organ of Corti. A strong $P2Y_4$ signal was visible in the membranes of the heads of pillar cells (Figure 3.1). Overall the $P2X_2$ receptor staining appeared mostly confined to supporting cells, whereas P2Y receptor staining quality was poor and appeared mostly unspecific, therefore was not quantified. To further verify the distribution of P2 receptors cytoplasmic Ca^{2+} levels were visualized using Ca^{2+} indicators and monitored whilst applying P2 receptor agonists.

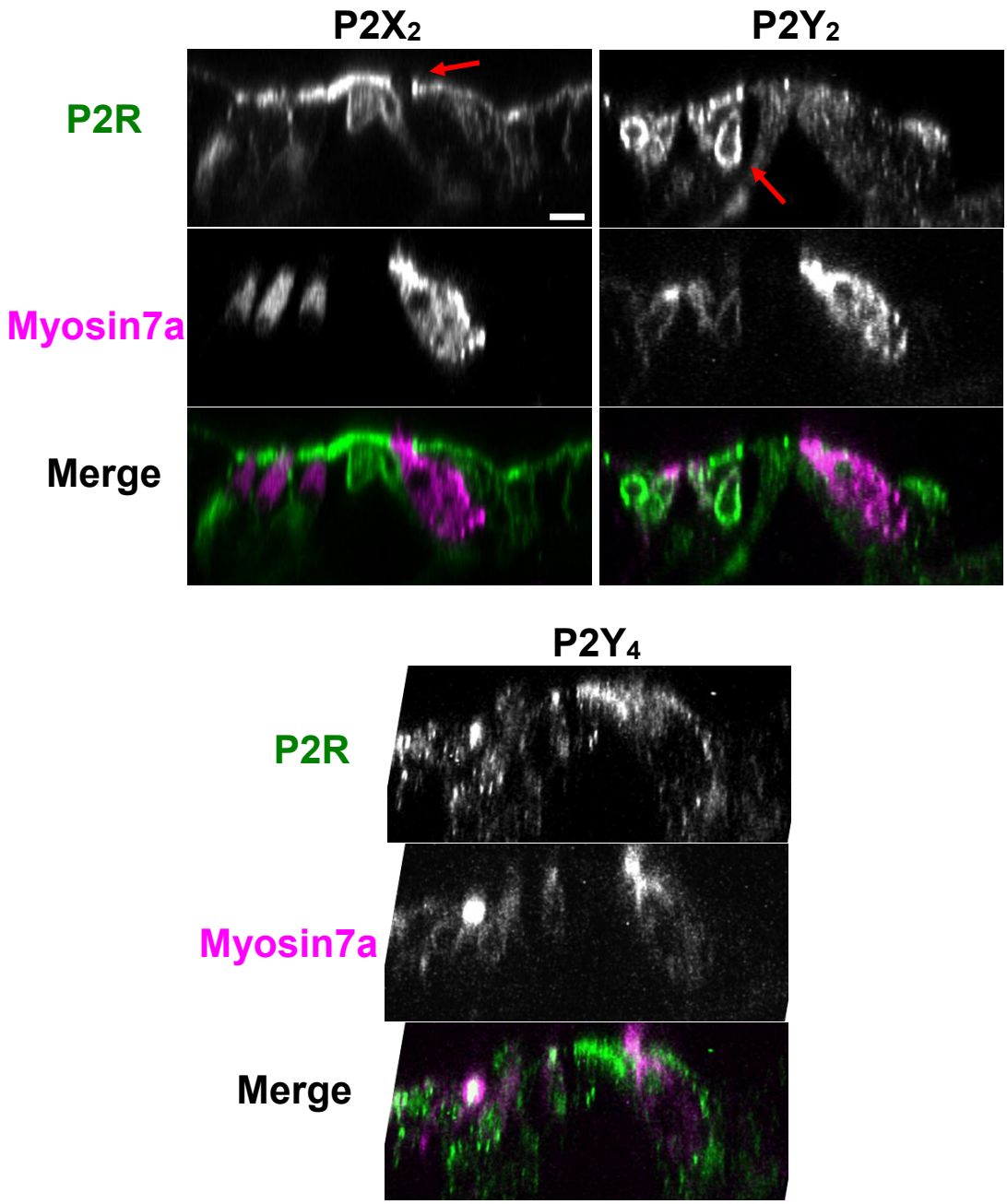

Figure 3.1 P2X and P2Y receptor immunohistochemistry, cross-section through the organ of Corti.
$P2X_2$, $P2Y_2$ and $P2Y_4$ receptor staining (green), myosin 7a (pink) and merge. Hair cells membranes are visible as they are enriched in myosin 7a. Red arrows point to high level staining in the apical membrane of pillar cells in the $P2X_2$ group and show membrane staining in the OHCs in the $P2Y_2$ group. Scale bar is 10 µm.

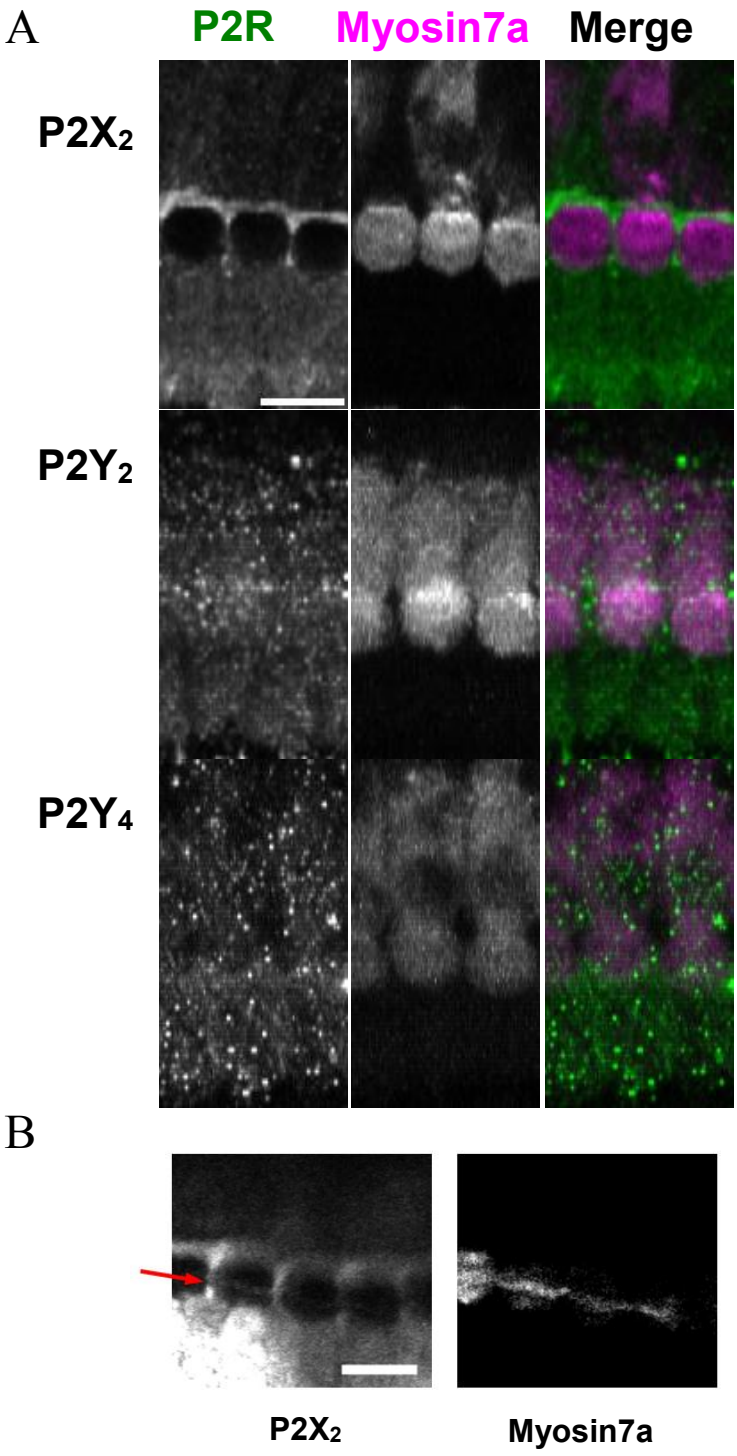

Figure 3.2 P2X and P2Y receptor immunohistochemistry in the IHC region of the adult mouse organ of Corti.
(A) $P2X_2$, $P2Y_2$ and $P2Y_4$ receptor staining (green), myosin 7a (pink) and merge, 9 µm thick maximum intensity projections. **(B)** In some instances faint staining was visible in the stereocilia of $P2X_2$ receptor stained IHCs. Red arrow points to stereocilia, brightness has been enhanced to emphasize stereocilia staining, slice is 1.3 µm thick, Scale bar is 10 µm in both (A) and (B).

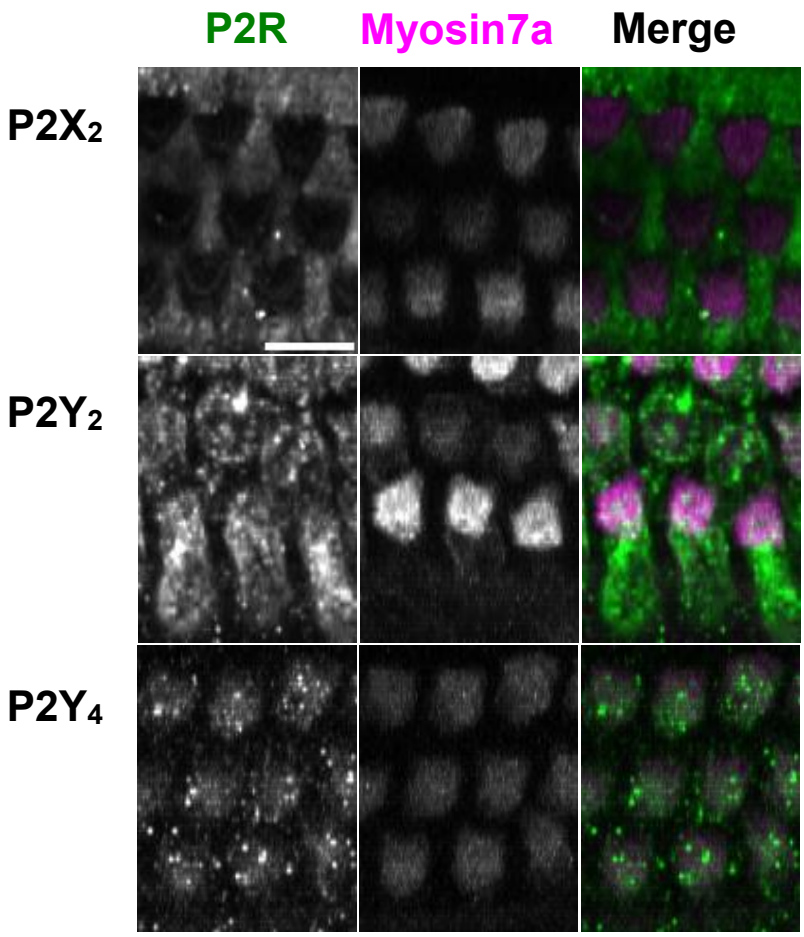

Figure 3.3 P2X and P2Y receptor staining in the Deiters' cell region.

$P2X_2$, $P2Y_2$ and $P2Y_4$ receptor staining (green), myosin 7a (pink) and merge, 9 µm thick maximum intensity projections. Scale bar is 10 µm.

3.1.3 Exposure to extracellular ATP increases intracellular Ca^{2+} in supporting cells of the organ of Corti

It has been shown that P2 receptor stimulation can increase Ca^{2+}_i levels via at least two distinct mechanisms. Ca^{2+} can enter the cell via ionotropic P2X receptors or can be

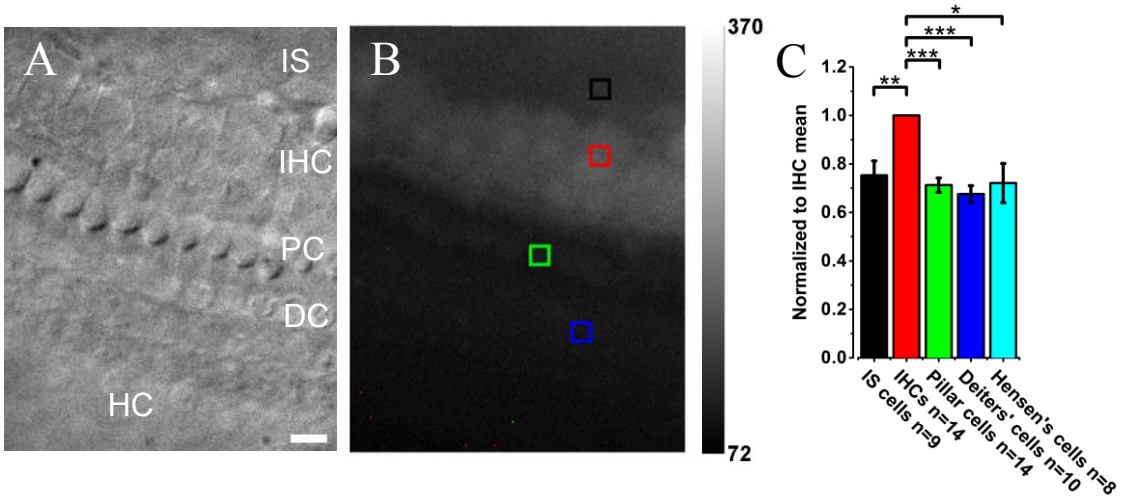

Figure 3.4 Nominal fluorescence in supporting cells normalized to nominal IHC fluorescence levels after incubating cells with the Ca^{2+} indicator OGB1-AM.
(A) Bright field view of the dissected organ of Corti. **(B)** Same view as in (A) but while evoking fluorescence at 488 nm. **(C)** After loading with OGB1-AM nominal fluorescence levels were measured in 5 x 5 µm ROIs at the level of the cell body (shown in B) of **(IS) cells (black)**, IHCs (red), heads of outer pillar cells (PC, green), Deiters' cells (DC, blue) and Hensen's cells (HC,cyan). Nominal fluorescence levels were found to be significantly higher in IHCs when compared to outer pillar, Deiters' and Hensen's cells. Data was collected from the following numbers of cochleas for the different cell types: 6 IS, 8 IHCs, 8 pillar, 7 Deiters' and 5 Hensen's. Number of cells is indicated as 'n' in the graph. $*P < 0.05$, $**P < 0.001$, $***P < 0.001$. Scale bar is 10 µm.

released from intracellular stores via a P2Y G – protein, phospholipase C (PLC) and IP_3 dependent pathway (Burnstock, 2007). To determine if ATP application can increase Ca^{2+}_i levels in the adult organ of Corti dissected organs were loaded with the AM forms of the Ca^{2+} dyes Fluo4 and OGB1. Fluorescence was monitored subsequently using epifluorescence microscopy. IHCs appeared to show higher nominal fluorescence levels then surrounding supporting cells. To compare nominal fluorescence levels, fluorescence was averaged in 5 x 5 µm ROIs placed at the level of the nucleus or pillar head (for outer pillar cells) of various organ of Corti cells and normalized to the level found in IHCs for each recording. Nominal fluorescence levels in cochlear supporting cells were found to be at the following fractions of IHC levels and the significance of this difference was

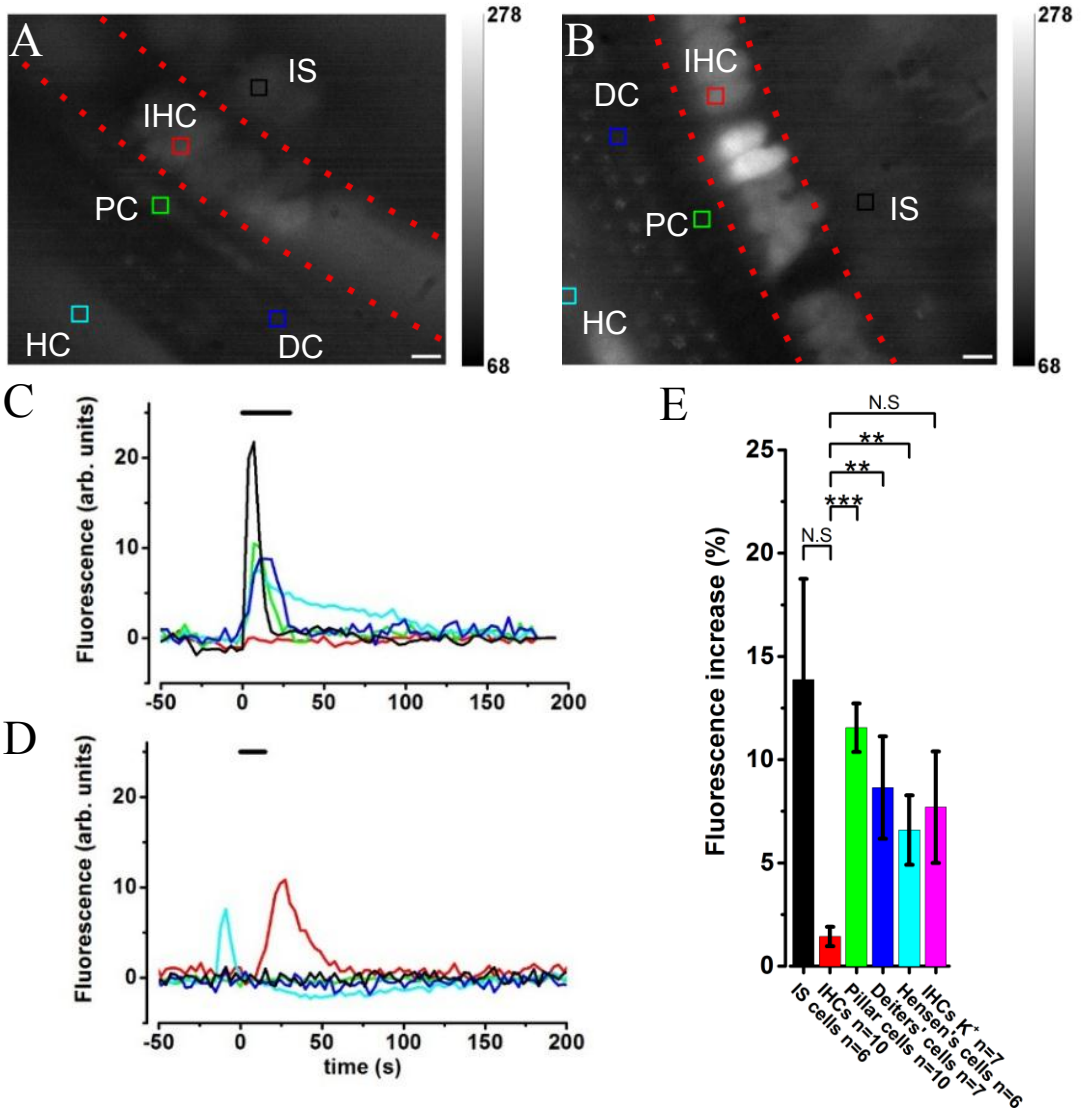

Figure 3.5 Puff application of 100 µM ATP increases fluorescence in Ca^{2+} indicator loaded organ of Corti supporting cells.

(A) and **(B)**, view of the OBG1-AM loaded organ of Corti whilst evoking fluorescence at 488 nm. 5 x 5 µm ROIs were placed over various types of supporting cells (color coded as in Figure 3.4), **(C)** 100µM ATP was puff applied for 29 s while monitoring fluorescence in the ROIs indicated in (A), black bar shows duration of ATP application. **(D)** An extracellular solution in which 100 mM NaCl was substituted for 100 mM KCl was puff applied for 15 s to organ of Corti supporting cells (black bar). Fluorescence was monitored in a 5 x 5 µm ROIs shown in (B). Note the spontaneous $Ca^{2+}{}_i$ increase in Hensen's cells in (D). Cell types are color-coded as in Figure 3.4. **(E)** The increase in fluorescence in different supporting cell types after a 5 s 100 µM ATP and in IHCs after a 15 s 100 mM KCl ES application (labelled: IHCs K^+). The difference in fluorescence increases between IHCs and outer pillar cells, Deiters' cells and Hensen's cells were found to be statistically significant. The difference between IS cells and IHCs to which 100 mM KCl containing ES was applied tended to be increased but didi not reach significant levels. **P*<0.05; ***P*<0.01; ****P*<0.001, N.S – not significant. Data was obtained from the following number of cochleas for the indicated cell types: 4 IS, 6 IHCs, 6 pillar, 5 Deiters', 5 Hensen's, 2 IHC K^+. 'n' number indicates the number of observed cells. Scale bar is 10 µm.

determined using two sample t-tests: 0.75 ± 0.06 IS cells n = 9 observations (*P* = 0.0032), 0.71 ± 0.03 (*P* = 2.1E-7) for outer pillar cells, n = 14, 0.68 ± 0.03 for Deiters' cells, n = 10 (*P* = 6.2E-6) and 0.72 ± 0.08 (*P* = 0.011) for Hensen's cells, n = 8 (Figure 3.4). Application of ATP (100 µM) elicited a strong increase in signal in the IS, outer pillar cells, Deiters' cells, and Hensen's cells. No substantial increase in $Ca^{2+}{}_i$ upon ATP stimulation could be detected in IHCs (Figure 3.5 A,C and Figure 3.6 A).

As base fluorescence levels were high in OGB1-AM loaded IHCs an extracellular solution in which 100 mM of NaCl was replaced with an equivalent amount of KCl was puff applied to determine if $Ca^{2+}{}_i$ levels could also be increased in IHCs. The KCl should depolarize IHCs, and open L-type voltage gated Ca^{2+} channels resulting in an increase in IHC $Ca^{2+}{}_i$ levels. Indeed a 15 s puff application of this KCl enriched extracellular solution increased the fluorescence in IHCs, but not supporting cells (Figure 3.5 B and D, Figure 3.6 B).

Puff application of ATP increased the fluorescence levels by (percent) 13.9 ± 4.9 in IS cells, 1.4 ± 0.5 in IHCs, 11.6 ± 1.2 in outer pillar cells, 8.6 ± 2.5 in Deiters' cells and 6.6 ± 1.7 in Hensen's cells. Fluorescence increased by 7.7 ± 2.7 percent in IHCs treated with ES in which 100 mM Na^+ was replaced with K^+. The difference in fluorescence increase between ATP treated IHCs and ATP treated IS cells tended to be increased but was not significant (*P* = 0.051). The difference between outer pillar cells (*P* = 4.19e-6), Deiters' cells (*P* = 0.027), and Hensen's cells (*P* = 0.027) was significant. IHCs exposed to 100 mM KCl containing extracellular solution were found to increase their fluorescence and the difference tended to be higher than in ATP exposed IHCs (*P* = 0.060) but was not statistically significant (Figure 3.5 E).

Following ATP application $Ca^{2+}{}_i$ was found to return more slowly to baseline levels in Hensen's cells (Figure 3.7 A). To better determine the dynamics of this difference the values of the full width at half maximum (FW 0.5) of the extracellular ATP induced $Ca^{2+}{}_i$ increase were determined for each of the observed supporting cell types (Figure 3.7 B). These were found to be (in seconds) 15.2 ± 2.4 for IS cells, 30.7 ± 3.3 for pillar cells, 28.6 ± 4.3 for Deiters' cells and 63.0 ± 14.2 for Hensen's cells. The differences in the response between IS cells (*P* = 0.019) and Hensen's cells were found to be significant. The difference between Hensen's cells and outer pillar cells (*P* = 0.072) and Deiters' cells (*P* = 0.060) tended towards being significant. In addition the value of the FW 0.5 significantly differed between IS cells and both

outer pillar ($P = 0.0017$) and Deiters' cells ($P = 0.022$). The difference between outer pillar and Deiters' cells was not significant ($P = 0.71$).

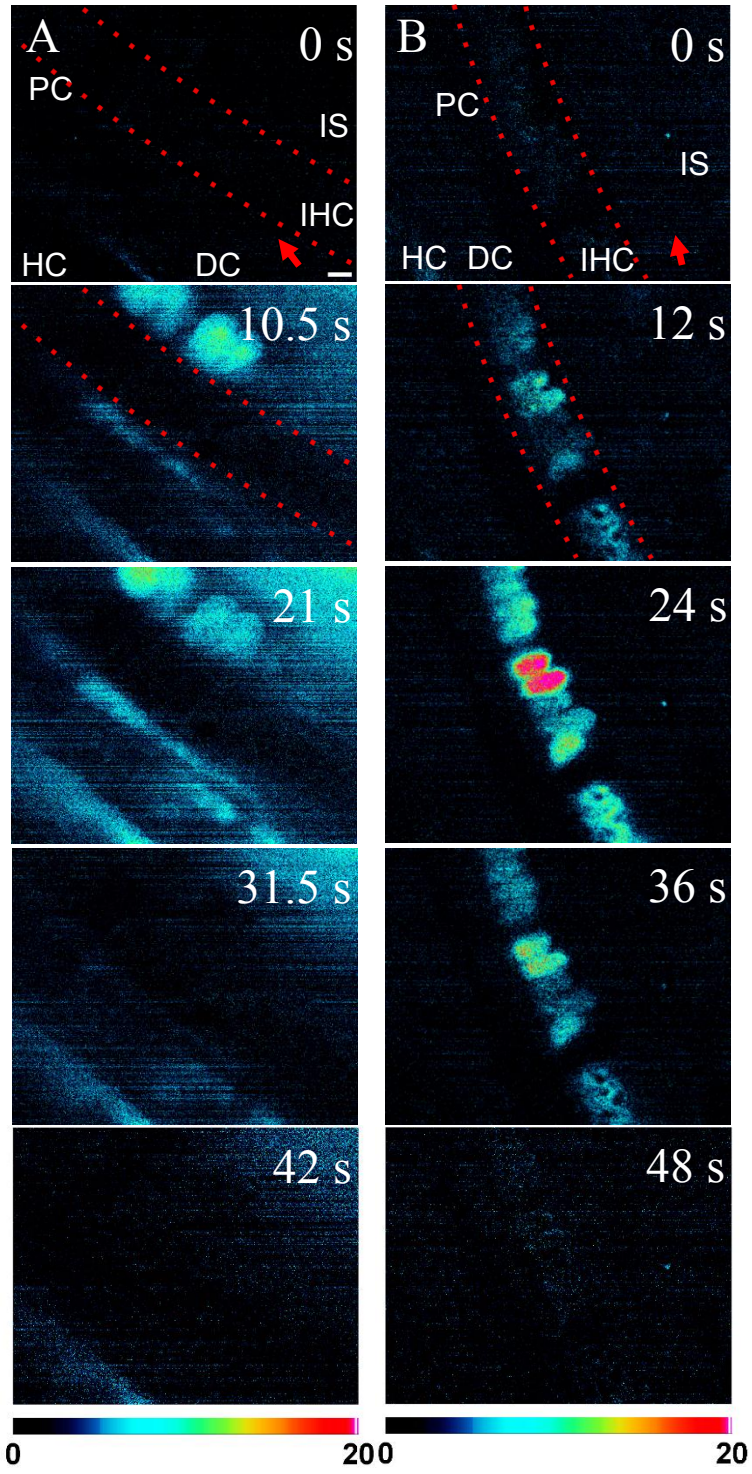

Figure 3.6 Puff application of ATP increases Ca^{2+}_i in supporting cells but not IHCs.
(A) When 100 µM ATP was puff applied Ca^{2+}_i levels increased in organ of Corti supporting cells but not IHCs.

(B) An extracellular solution containing 100 mM KCl was puff applied to determine if Ca^{2+}_i levels can increase in IHCs.

(A) and (B) are the same organ of Corti fragments shown in Figure 3.5 A and B respectively. Scale bar is 10 µm. Red arrows indicate the approximate direction the puff pipette was facing.

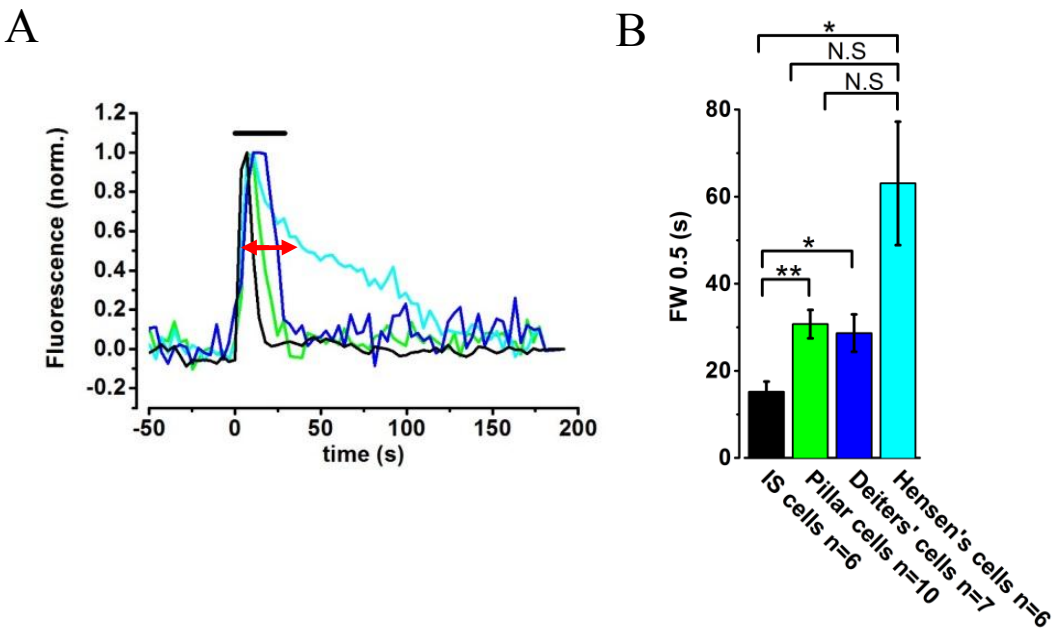

Figure 3.7 The full-width at half-maximum (FW 0.5) response of different supporting cell types to puff application of 100 µM ATP.
(A) The normalized responses to a 29 s puff application of a 100 uM ATP solution shown in Figure 3.5 C. **IS (black)**, outer pillar heads (green), Deiters' cells (blue) and Hensen's cells (cyan). Red arrow denotes the duration of the FW 0.5 of the Ca^{2+} increase in a Hensen's cells.

(B) The FW 0.5 values of the fluorescence increase after 5 s ATP application. Fluorescence was measured in a 5 x 5 µm ROIs placed over the indicated cell types. The FW 0.5 duration of the response in Hensen's cells was significantly longer than the FW 0.5 value found IS cells. The duration of FW 0.5 in outer pillar and Deiters' cells was found to be significantly longer than the response elicited from IS cells. **P*<0.05; ***P*<0.01, N.S – not significant.

3.1.4 Both P2X and P2Y receptor stimulation contributes to the ATP mediated intracellular Ca^{2+} increase in supporting cells

Since both P2X and P2Y receptors could contribute to the observed extracellular ATP elicited Ca^{2+}_i increase, P2Y receptors were selectively stimulated to determine their contribution (Burnstock, 2007). Fluorescence at 488 nm in OGB1-AM loaded cochleas was observed using a confocal microscope, while stimulating P2Y receptors or both P2X and P2Y receptors. To confirm the presence of P2Y receptors Ca^{2+} was omitted from the external solution and 2 mM EGTA was added to reduce the concentration of any remaining Ca^{2+} in the ES.

Under these conditions puff application of 100 µM ATP elicited an increase in Ca^{2+}_i levels of 0.50 ± 0.04 (*P* = 3.1e-4) in IS cells, 0.51 ± 0.05 (*P* = 7.3e-6) outer pillar cells, 0.63 ± 0.09 Deiters' (*P* = 0.011), 0.90 ± 0.19 (*P* = 0.76) Hensen's cells and 0.57 ± 0.07

(P = 0.0036) in the border cell region of the $Ca^{2+}{}_i$ increase elicited in the same cochleas, cell types and ROIs by puff application of 100 μM ATP under high (1.3 mM) extracellular Ca^{2+} conditions (Figure 3.8 A-D, Figure 3.9 A, C). Application of 100 μM UTP a selective agonist of P2Y receptors elicited an increase in $Ca^{2+}{}_i$ levels which was found to be at: 0.67 ± 0.04 (P = 0.0032) in IS cells, 0.70 ± 0.03 (P = 8.6e-5) in outer pillar cells, 0.80 ± 0.10 (P = 0.22) in Deiters', 0.88 ± 0.07 (P = 0.31) in Hensen's cells and 0.64 ± 0.07 (P = 0.0052) in the border cell region of the signal intensity in the same ROI elicited by 100 μM ATP. This observation was consistent with UTP acting only on a subset of the P2 receptor population (Figure 3.8 E, Figure 3.9 B, D). These experiments were repeated in 3 cochleas from different mice.

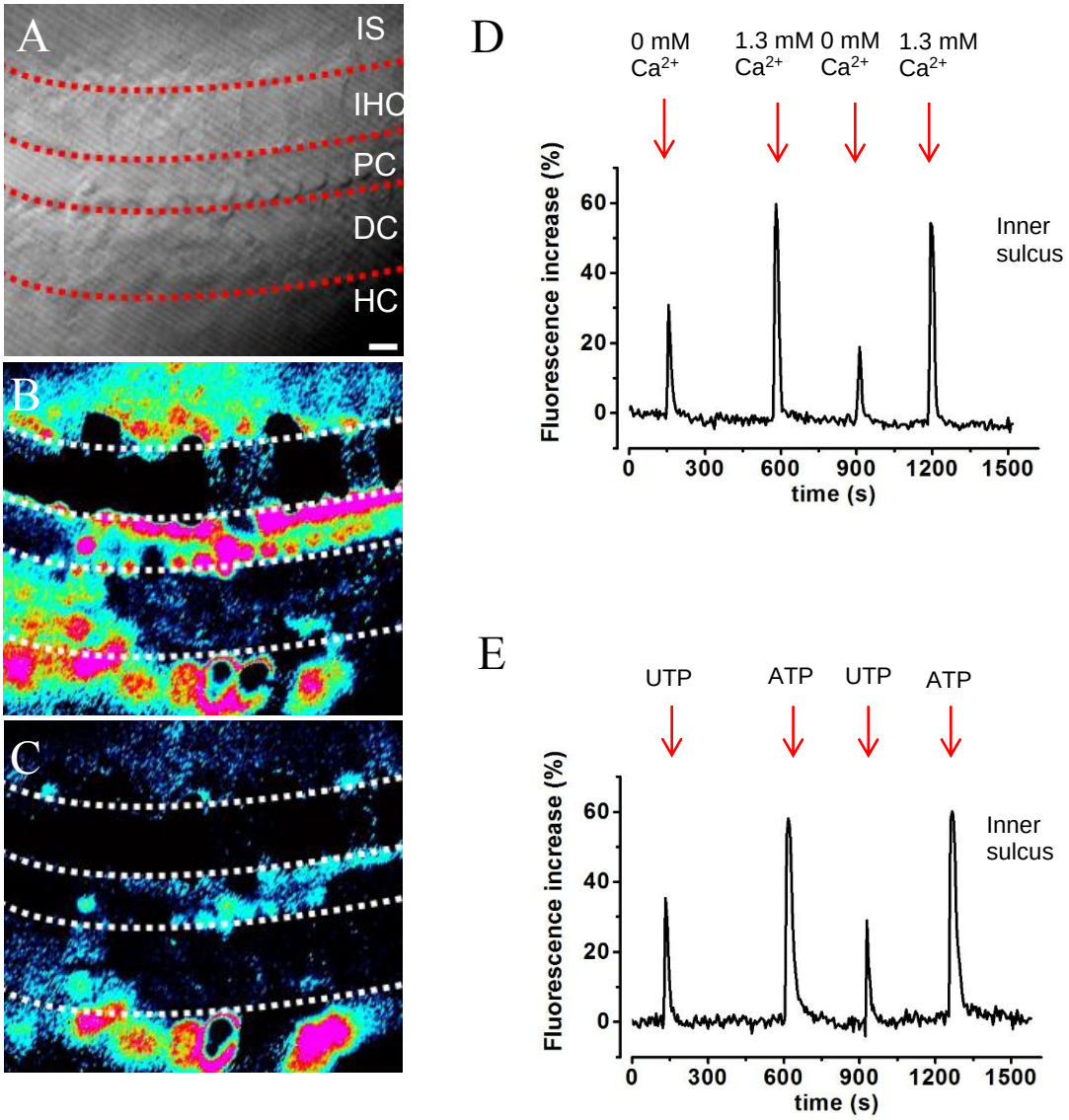

Figure 3.8 100 µM ATP stimulation increases Ca^{2+}_i levels under low extracellular Ca^{2+} conditions.
(A) A transmitted light image of the dissected organ of Corti, **(B)** Same fragment as in (A) background subtracted and false coloured at the peak of response to 100 µM ATP with 1.3 mM Ca^{2+} in the ES and **(C)** with no additional Ca^{2+} and 2 mM EGTA. **(D)** A 5 x 5 µm ROI was placed over the IS and fluorescence was monitored. Arrows indicate the application of ATP under low and 1.3 mM extracellular Ca^{2+} conditions. **(E)** (100 µM) UTP and ATP were puff applied in an ES containing 1.3 mM Ca^{2+}. The experiment was repeated in 3 cochleas for each set of conditions, and the results from individual agonist puffs are quantified in Figure 3.9. Scale bar is 10 µm.

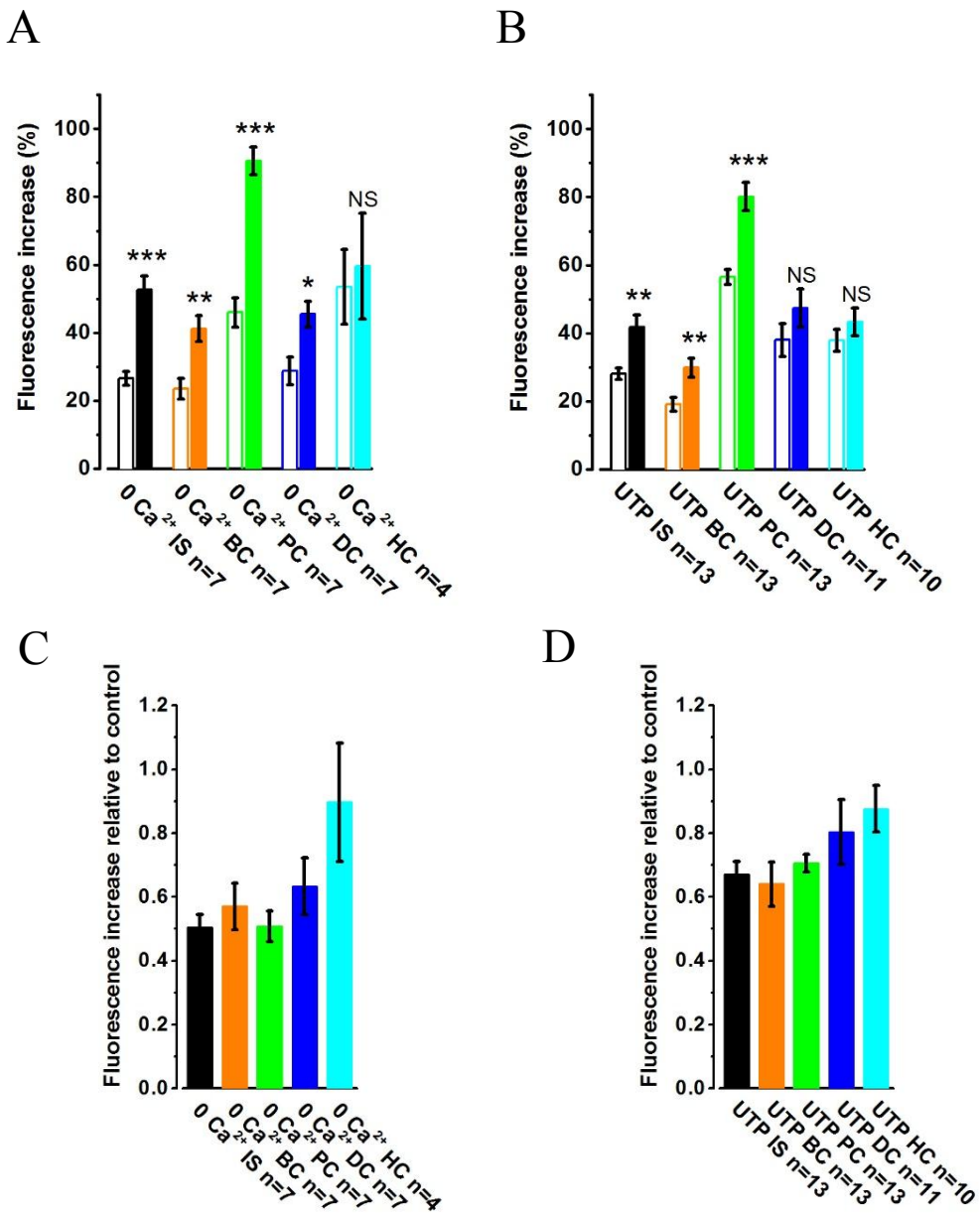

Figure 3.9 Stimulation of P2X and P2Y receptors increases Ca^{2+}_i levels more than stimulation of P2Y receptors only.
The fluorescence increase in different cell types (as shown in Figure 3.8) was quantified. 100 µM ATP was dissolved in either low Ca^{2+} (no additional Ca^{2+}, 2 mM EGTA, open bars) or high Ca^{2+} (1.3 mM Ca^{2+}, coloured bars) ES and applied from a double-barrel puff pipette. Fluorescence was evoked at 488 nm and monitored with the help of a confocal microscope in 5 x 5 µm ROIs placed over various organ of Corti cell types. **(A)** Percent of fluorescence increase when compared to base fluorescence levels.

(B) 100 µM UTP (open bars) and ATP (coloured bars) were dissolved in ES with 1.3 mM Ca^{2+} and puff applied. Fluorescence was monitored similarly as in (A). **(C)** The response to extracellular ATP in low Ca^{2+} shown in (A) was quantified as the ratio of the one evoked in high Ca^{2+}. **(D)** The UTP evoked responses from (B) shown as percent of the ATP response. **P*<0.05; ***P*<0.01; ****P*<0.001; N.S., not statistically significant (*P* > 0.05). IS – Inner Sulcus, BC – border cells, PC – outer pillar cells, DC – Deiters' cells, HC – Hensen's cells. 'n' numbers correspond to the number of quantified agonist applications. Experiments were done using 3 cochleas for each of the compared groups.

The value of the full width (FW) at 0.25, 0.3, 0.4 and 0.5 (FW 0.5) of the maximum Ca^{2+}_i increase elicited by stimulation of the various receptor populations was obtained. The Ca^{2+}_i levels in Hensen's cells were found to return to baseline significantly slower than in other cell types confirming the observations conducted using epifluorescence microscopy (Figure 3.7 Figure 3.10).

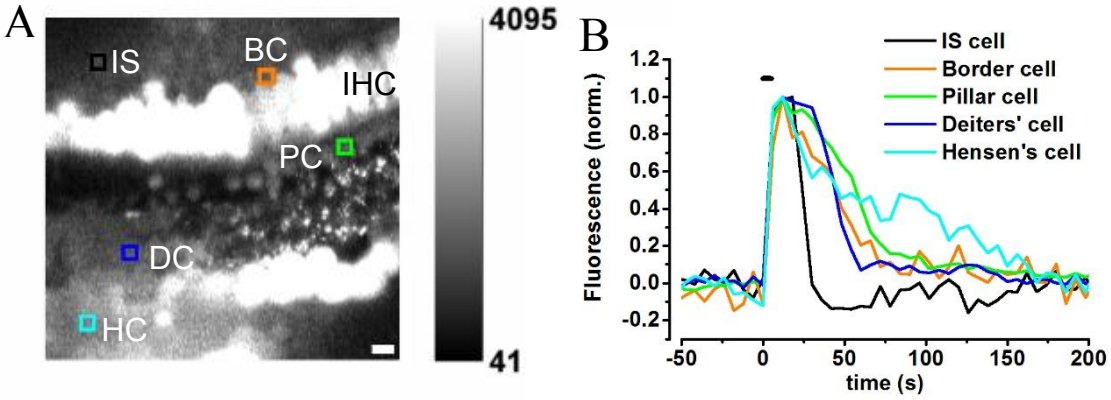

Figure 3.10 The FW of the Ca^{2+}_i increase after exposure to extracellular ATP when monitored using confocal microscopy was consistent with the data obtained using epifluorescence microscopy.
(A) Fluorescence was measured in 5 x 5 µm ROIs placed over the cell bodies of various supporting cell types. **(B)** Normalized fluorescence as detected in the ROIs shown in (A). Scale bar is 10 µm.

However when using confocal microscopy these differences became statistically significant only when the FW was measured at 0.4 and below of the maximum response. The values of the FW in seconds of the Ca^{2+}_i increase at different values of the maximum response and for different conditions and cell types have been plotted in (Figure 3.11 and Figure 3.12) for recordings obtained using confocal microscopy.

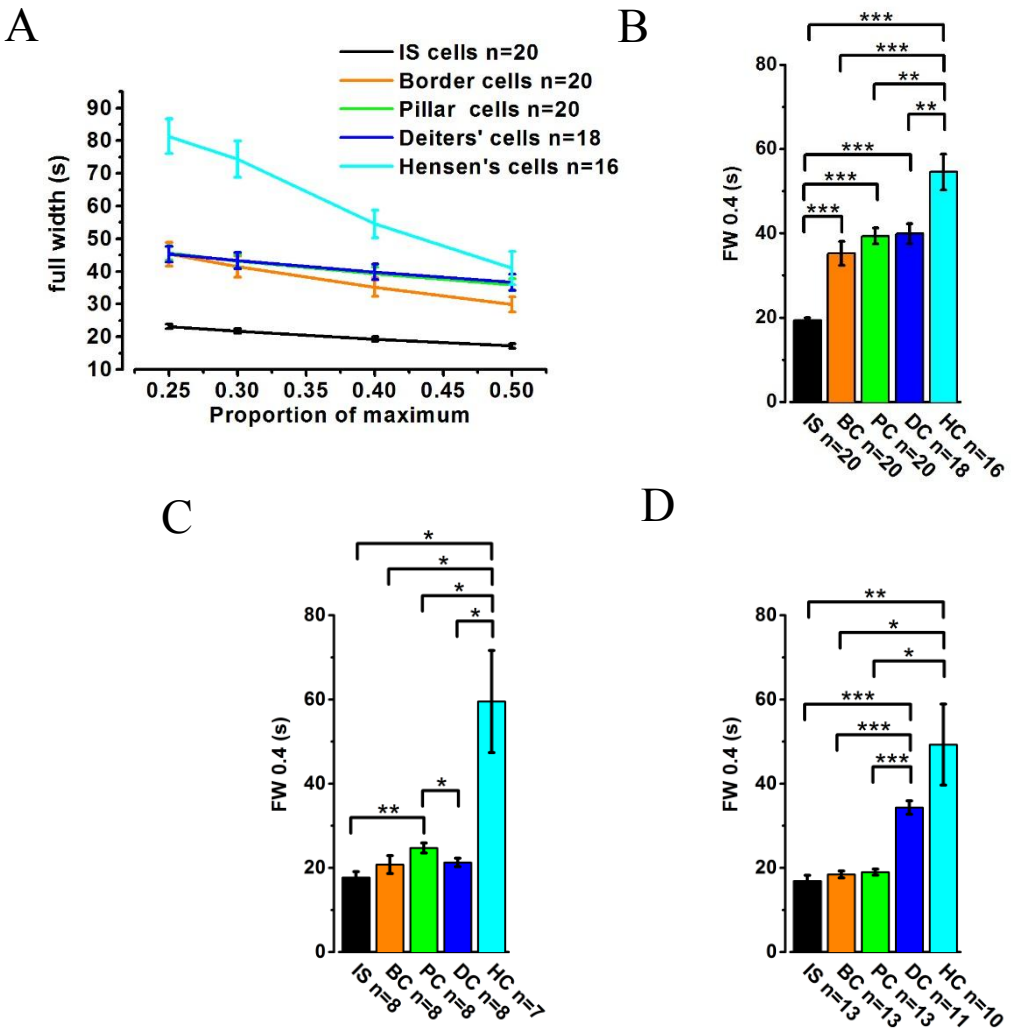

Figure 3.11 The duration of the FW of the Ca^{2+}_i increase at different proportions of the maximum response to puff application of extracellular ATP varies in different organ of Corti supporting cell types.
(A) The average FW values at 0.5, 0.4, 0.3 and 0.25 of the maximum of the response to a 5 s puff application of 100 µM ATP with 1.3 mM Ca^{2+} in the ES in IS, border, outer pillar, Deiters' and Hensen's cells when measured using confocal microscopy.
FW values at 0.4 of the maximum response were compared between the different cell types when ATP was puff applied: in ES with 1.3 mM Ca^{2+} **(B),** in ES with no additional Ca^{2+} and 2 mM EGTA **(C)**, and when puff applying UTP in ES with 1.3 mM Ca^{2+} **(D)**. **P*<0.05; ***P*<0.01; ****P*<0.001. Each group in (A-C) shows data from 3 cochleas, 'n' number indicates number of ROIs and cells used for measurements. IS – Inner Sulcus, BC - border cells, PC – outer pillar cells, DC – Deiters' cells, HC – Hensen's cells.

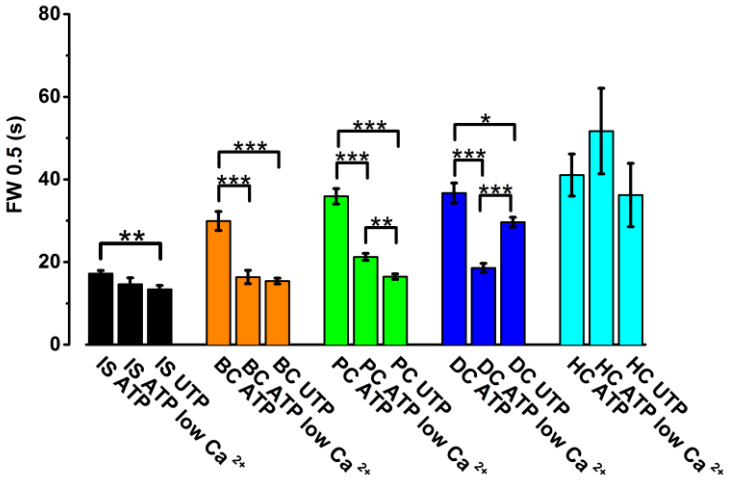

Figure 3.12 The Ca^{2+}_i increase was briefer when only P2Y receptors could be stimulated compared to conditions in which P2X receptors could also be stimulated.

Indicated is the agonist used ATP or UTP. Ca^{2+} was omitted from the ES and 2 mM EGTA added to obtain low Ca^{2+} conditions. IS – Inner Sulcus, BC – border cells, PC - outer pillar cells, DC – Deiters' cells, HC – Hensen's cells. **P*<0.05; ***P*<0.01; ****P*<0.001. Data obtained from 3 cochleas, same 'n' numbers as in Figure 3.11.

3.1.5 At least two populations of P2 receptors with different agonist sensitivities are present in the organ of Corti

P2X and P2Y receptors are known to differ in their sensitivity to ATP. The half-activation concentration of ATP at P2X receptors has been found to be at the μM level, whereas P2Y receptors can still be stimulated at low nM levels of extracellular ATP (Piazza et al., 2007). When applying ATP from a puff pipette the concentration of ATP is expected to decrease with increasing distance from its source as the ATP diffuses into the ES and eventually should fall to levels insufficient to activate P2X receptors but still sufficient to stimulate P2Y. If extracellular Ca^{2+} is removed then ATP will stimulate only the P2Y receptor population. Thus above a certain distance from the puff pipette the Ca^{2+}_i increase elicited by puff application of ATP in high and low extracellular Ca^{2+} conditions should be similar since only P2Y receptors can be stimulated at that distance. Stimulation of P2Y receptors releases Ca^{2+} from intracellular stores and the amount released should be independent of extracellular Ca^{2+} levels. The rate of the decrease in fluorescence signal intensity from the source of ATP should also be different when stimulating one and both receptor populations.

To stimulate both P2X and P2Y receptors 100 µM ATP was puff applied for 5 s in ES containing 1.3 mM Ca^{2+}. To selectively stimulate the P2Y receptor population 100 µM

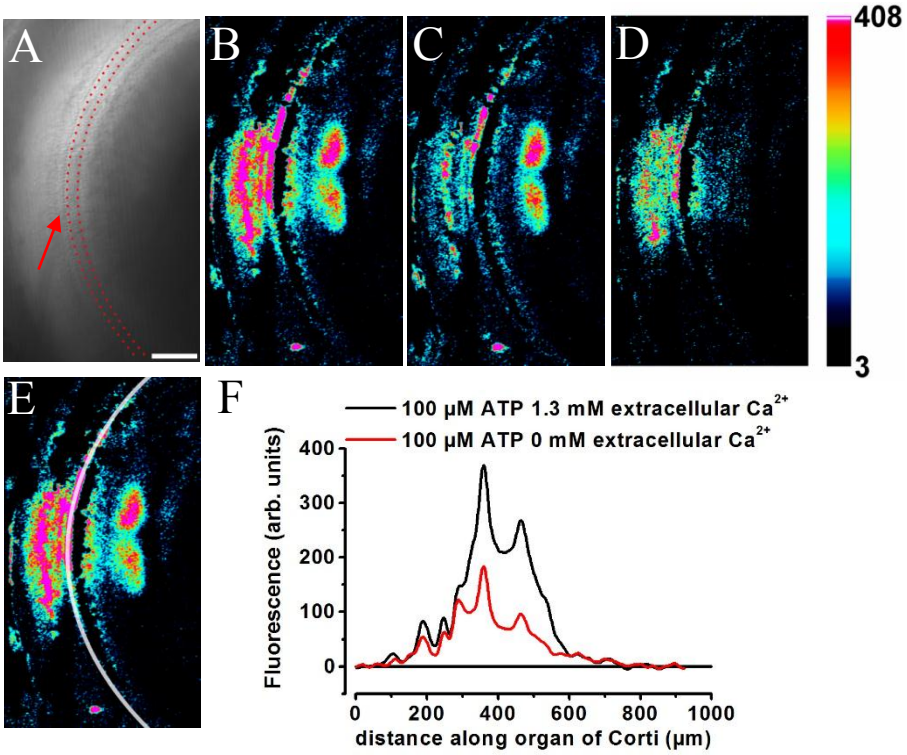

Figure 3.13 The difference in the magnitude of the Ca^{2+}_i increase evoked by puff application of 100 µM ATP under high and low extracellular Ca^{2+} conditions decreased with the distance from the source of ATP.
(A) Transmitted light view of the dissected organ of Corti. **(B)** Background subtracted, maximum intensity projection of 10 frames (60 s) after the start of a 5 s puff of 100 µM ATP in ES with 1.3 mM Ca^{2+}, **(C)** after the start of a 5 s puff of 100 µM ATP in ES containing no additional Ca^{2+} and 2 mM EGTA and **(D)** the difference of the two images. The images are false coloured to indicate the increase in Ca^{2+}_i levels. **(E)** Fluorescence was measured and averaged for each point along a 50 µm wide line the centre of which is indicated by the white line, measured values are plotted in **(F)** for ES containing 1.3 Ca^{2+} (black) and no additional Ca^{2+} with 2 mM EGTA. Red arrow indicates the direction the puff pipette was facing. Scale bar: 100 µm.

ATP in Ca^{2+} free solution containing 2 mM EGTA was applied for 5 s (Figure 3.13).

100 µM UTP in high Ca^{2+} solution was also puff applied to selectively stimulate P2Y receptors in a separate set of experiments. A 50 µm wide curved line stretching into the IS and Deiters' cells region was plotted along the IHCs on the background subtracted maximum intensity projection and the average fluorescence value along the length of this line was measured after puff application of the P2 receptor agonists (Methods 2.6.4) (Figure 3.13). To compare and average these observations the point at which the fluorescence started to decrease was used as the initial point for each set of observations shown in Figure 3.14. The Ca^{2+} signal was found to be significantly higher up to

approximately 100 µm away from the initial point when stimulating both P2X and P2Y receptors compared to selective P2Y receptor stimulation. At further distances the signal remained significantly above background fluorescence levels, however no significant differences were found between groups. When responses in the compared groups were normalized to their respective maxima, the response elicited by P2Y stimulation alone was found to return to baseline at a slower rate than when both receptor groups were stimulated (Figure 3.14 E, F).

3.1.6 Summary of results

The results obtained with the help of immunohistochemistry and Ca^{2+}_i imaging indicate that both P2Y and P2X receptors are present in the organ of Corti, and that these are present chiefly in the supporting cells and not the IHCs. In addition to the Ca^{2+}_i increases elicited by stimulation with extracellular ATP, 'spontaneous' changes in Ca^{2+}_i levels were observed in the Deiters' cell region. These changes were further investigated and are described in section 3.3.

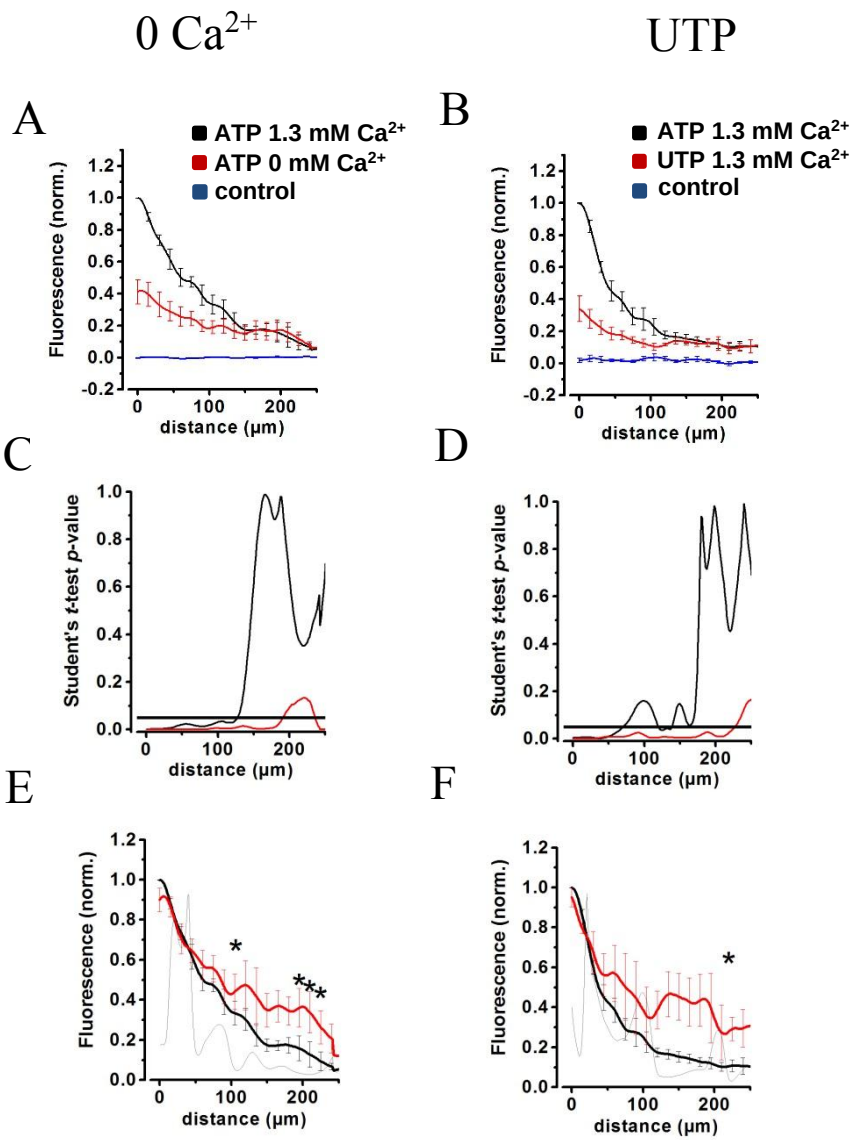

Figure 3.14 The difference in the magnitude of the Ca^{2+}_i increase evoked by puff application of 100 µM ATP under high and low extracellular Ca^{2+} conditions decreased with the distance from the source of ATP.
Increases in fluorescence evoked by ATP or UTP were averaged and plotted from the point of their initial decrease (as shown in Figure 3.13). **(A)** Plotted and compared are changes evoked by 100 µM ATP (black) in ES containing 1.3 mM Ca^{2+} and changes evoked when Ca^{2+} was omitted from the ES and 2 mM EGTA was present (red). Background negative control (blue) **(B)**. Similar to (A), the compared fluorescence increase was evoked by 100 µM ATP (black) and 100 µM UTP in ES containing 1.3 mM Ca^{2+} (red) **(C-D)**: Paired student t-test *P* values obtained by comparing both agonist groups (black) and comparing the fluorescence increase evoked by 100 µM ATP in 1.3 mM extracellular Ca^{2+} to background fluorescence values (red). **(E-F)** P2 agonist groups from (A-B) normalized to the maximum elicited signal in each group. Thin black line indicates student t-test *P* value after comparing both groups. n = 5 measurements, 3 cochleas for (A), (C) and (E) and n = 4 measurements, 2 cochleas for (B), (D) and (F). $*P < 0.05$.

3.2 The effects of extracellular ATP signalling on supporting cell membrane conductances and inner sulcus cell cytoplasmic state

3.2.1 Introduction

Köllikers organ cells found in pre-hearing animals have been found to have ATP and UTP-activated currents and are thought to express both P2X ionotropic receptors as well as other ion channels such as CaCCs (Tritsch and Bergles, 2010). No major studies have to date been undertaken to determine what sort of currents are present in the IS which replaces Köllikers organ in hearing animals. The effect of ATP signalling on border and phalangeal cells which show analogies to glia and surround the IHC afferent synapse are also currently unclear. The aim of this part of the investigation was to characterize ATP-elicited currents of the IS and border cells surrounding the IHC afferent synapse. To achieve this goal ATP-activated currents were recorded using single cell patch clamp electrophysiology.

3.2.2 ATP application transiently decreases gap junctional coupling

Patch clamp electrophysiological recordings were made from IS cells. After attaining whole cell recording conditions, cells were found to have on average membrane resistance (R_m) of 221 ± 43 MOhms n = 22 cells and a negative zero current potential (V_0) of -46.5 ± 4.1 mV. ATP activated an inward current of 556 ± 68 pA from a base

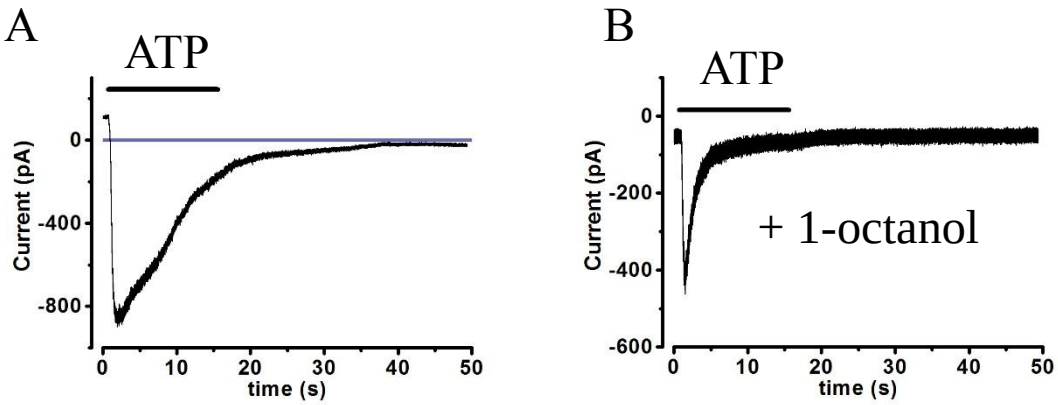

Figure 3.15 Extracellular ATP changes the resting current of coupled IS cells. Whole cell patch clamp electrophysiological recordings were made from IS cells in the adult mouse cochlea. The cells membrane potential was held at -55 mV while applying 100 µM ATP for 15 s (black bar). A change of the cells resting current was visible after ATP application in coupled cells **(A)** blue line indicates 0 pA. In contrast in cells decoupled with the gap junction inhibitor 1-octanol (1 mM) the resting current returned to pre-ATP application levels **(B).** Maximum elicited current was measured at -556 ± 68 pA in coupled and -472 ± 166 in 1-octanol decoupled IS cells.

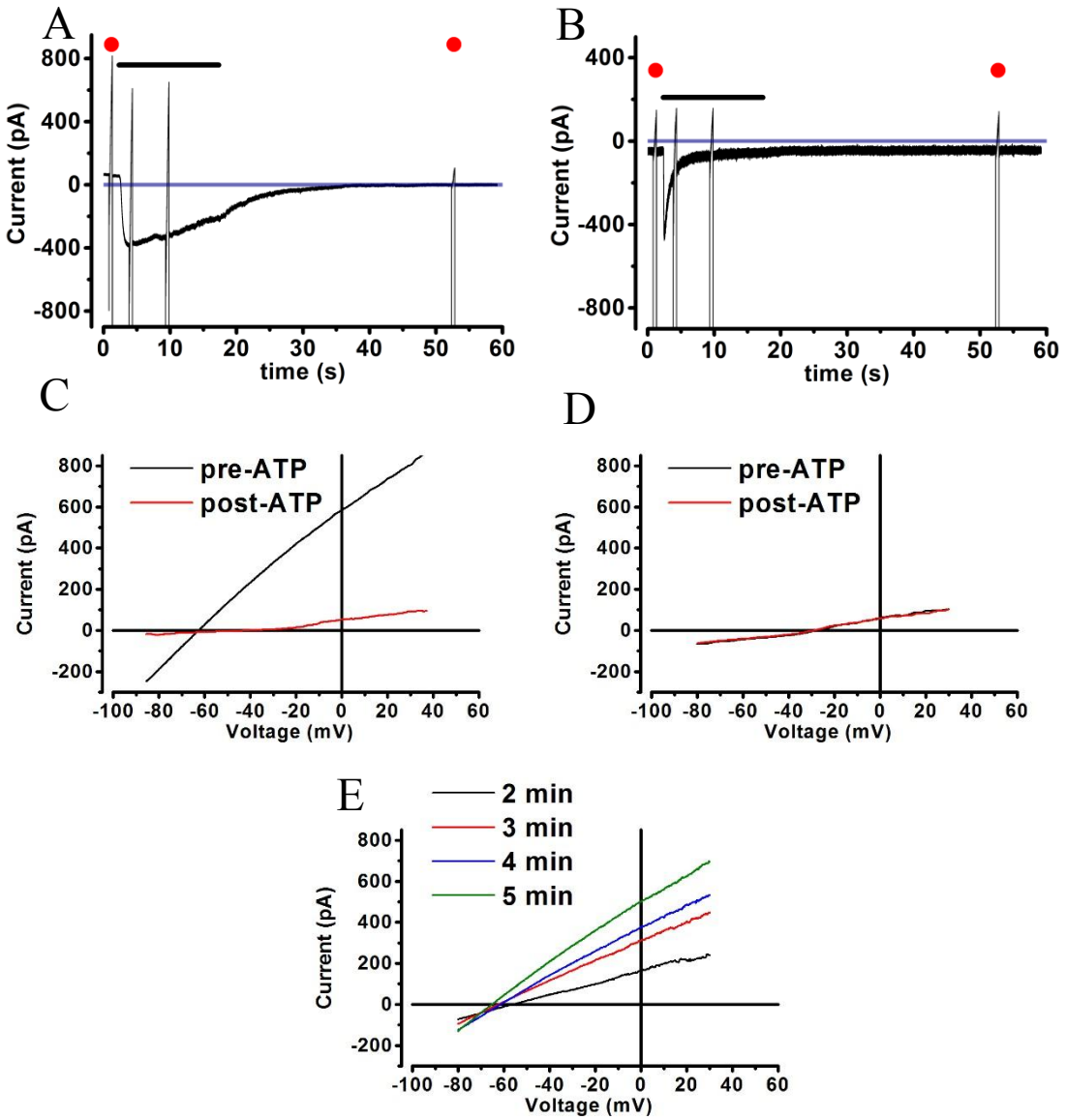

Figure 3.16 Extracellular ATP decreased the leak conductance in gap junction coupled IS cells.
Voltage ramps were applied before during and 55 s after the onset of ATP application in coupled IS cells **(A)** and after decoupling with the gap junction blocker 1-octanol **(B)**. In coupled cells the resting membrane current did not immediately return to pre-ATP application levels. Red dots indicate ramps shown in (C) and (D).
(C) and **(D)** The first (black, before ATP application) and last (red, 55 s after the onset of ATP application.) current traces resulting from voltage ramps indicated by red dots respectively in (A) and (B). The leak conductance decreased post-ATP application in coupled cells but not in cells decoupled from the surrounding syncytium with gap junction blockers.
(E) Same cell shown in (A) and (C). Voltage ramps were applied every minute from 2 to 5 min post ATP application. The cells leak current gradually increased towards pre-ATP application levels.

resting current of -100 ± 69 pA (Figure 3.15). The cell capacitance was estimated at 7.1 ± 0.6 pF. Estimation of cell capacitances in gap junction connected cells is known to be unreliable as membrane voltage can only be reliably clamped at limited distances from the patch clamp electrode (Armstrong and Gilly, 1992; de Roos et al., 1996).

After puff application of 100 µM ATP resting current did not recover immediately to pre-ATP exposure levels (Figure 3.15 A, Figure 3.16). Measurements on average at 79.5 ± 7.0 seconds after the start of ATP application yielded an R_m value of 2060 ± 735 MOhms n = 22 cells, which was significantly higher than the R_m of coupled cells (P = 0.021) and V_0 of -41.3 ± 4.5 mV (P = 0.40), which did not differ significantly. As considerable variability existed in the V_0 of coupled cells, the change in V_0 from initial pre-ATP application values was measured instead. The change in V_0 was normalized to the highest positive value for each cell and the normalized values averaged, before plotting (Figure 3.17 B). R_m values before and after application of ATP were also compared using the nonparametric Kruskal-Wallis ANOVA and were again found to be significantly different (P = 4.4e-5).

There was a significant positive change in V_0 values after puff application of ATP (measured on average at 79.5 ± 7.0 after the start of ATP application) and V_0 recovered completely over a time course of 320 seconds. Recovery was incomplete in the case of R_m which after 320 seconds was still 1.5 ± 0.1 times higher than the initial value (Figure 3.16, Figure 3.17 A). Similar changes in V_0 and R_m following extracellular ATP application have been described in Deiters' and Hensen's cells of the organ of Corti by other investigators and are thought to most likely be the result of a Ca^{2+}-dependent closure of gap junctions. Once Ca^{2+}_i is brought down to resting levels by homeostatic mechanisms gap junctions re-open and R_m and V_0 should return to resting levels. Indeed the values of R_m and V_0 after adding the gap junction blocker 1-octanol (1 mM) and puff applying ATP returned to pre-ATP application levels (Figure 3.16 B). Puff application of extracellular ATP also transiently significantly increased the cells capacitance (C_m) from 7.1 ± 0.6 pF to 11.5 ± 0.7 pF (P = 1.3e-5) 79.5 ± 7.0 seconds after the end of ATP application. Capacitance recovered to pre-ATP application levels within 320 s post-ATP application.

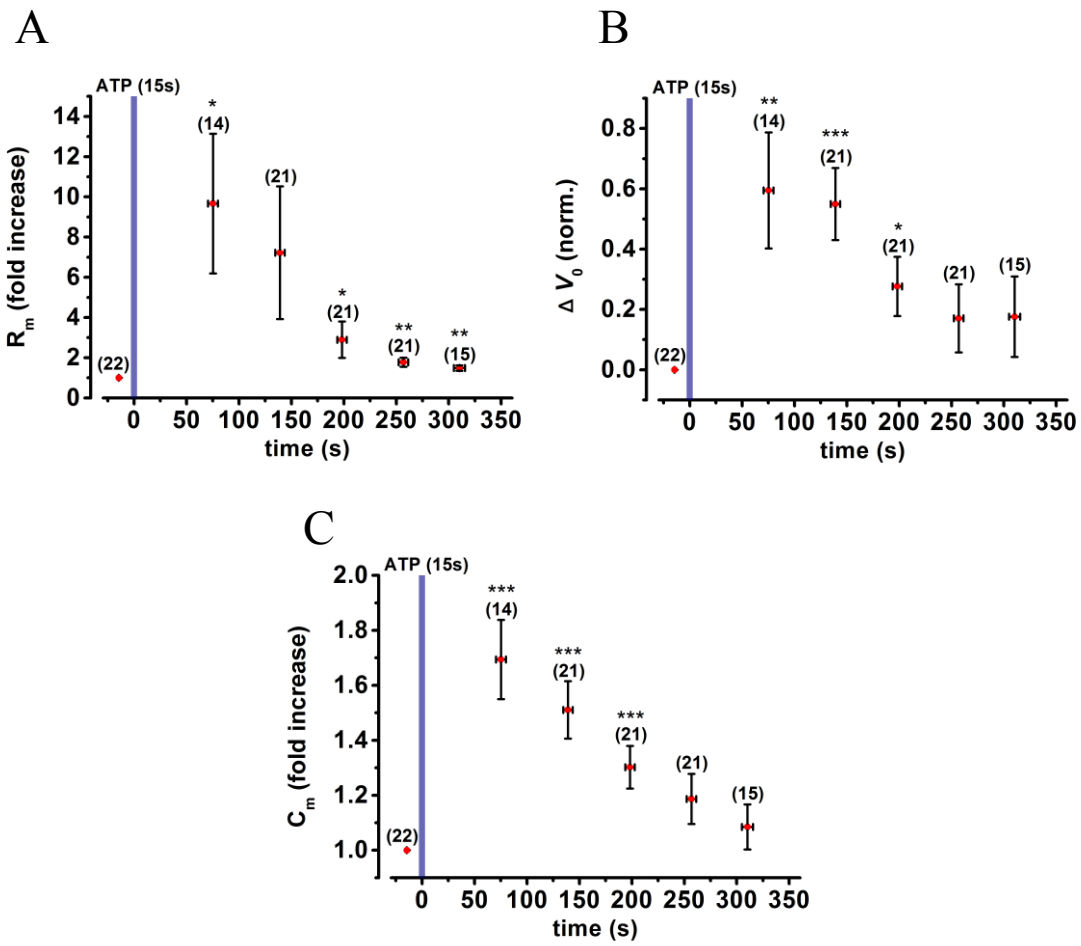

Figure 3.17 ATP changes membrane resistance, current reversal potential and capacitance of IS cells.
The change in membrane resistance **(A)**, current reversal potential **(B)** and the cells capacitance **(C)** were measured during whole cell electrophysiological recordings before and at different time points post-ATP application in coupled IS cells (red points, black bars SEM, number of cells indicated above in parentheses. Stars indicate the significance of the change when compared to initial values using two sample t-tests). The pre-ATP parameter values were respectively: 221 ± 43 MOhms, -46.5 ± 4.1 mV, 7.1 ± 0.6 pF. These values at on average 79.5 s after the start of ATP application were found to be: 2060 ± 735 MOhms, -41.3 ± 4.5 mV and 11.5 ± 0.7 pF.

3.2.3 ATP elicits cytoplasmic changes in border and inner sulcus supporting cells but not inner hair cells

Extracellular ATP elicits morphological changes in a transient structure called Köllikers organ in the immature organ of Corti (Tritsch et al., 2007). Cells of this structure have been shown to spontaneously release extracellular ATP initiating spontaneous Ca^{2+} waves. Such Ca^{2+} waves are accompanied by shrinkage of the cells through which these waves pass. These changes are most likely the result of the opening of CaCCs (Tritsch and Bergles, 2010; Tritsch et al., 2007). In this model movement of Cl^- out of the cell leads to an osmotic water loss eventually resulting in the cell shrinking or 'crenating'.

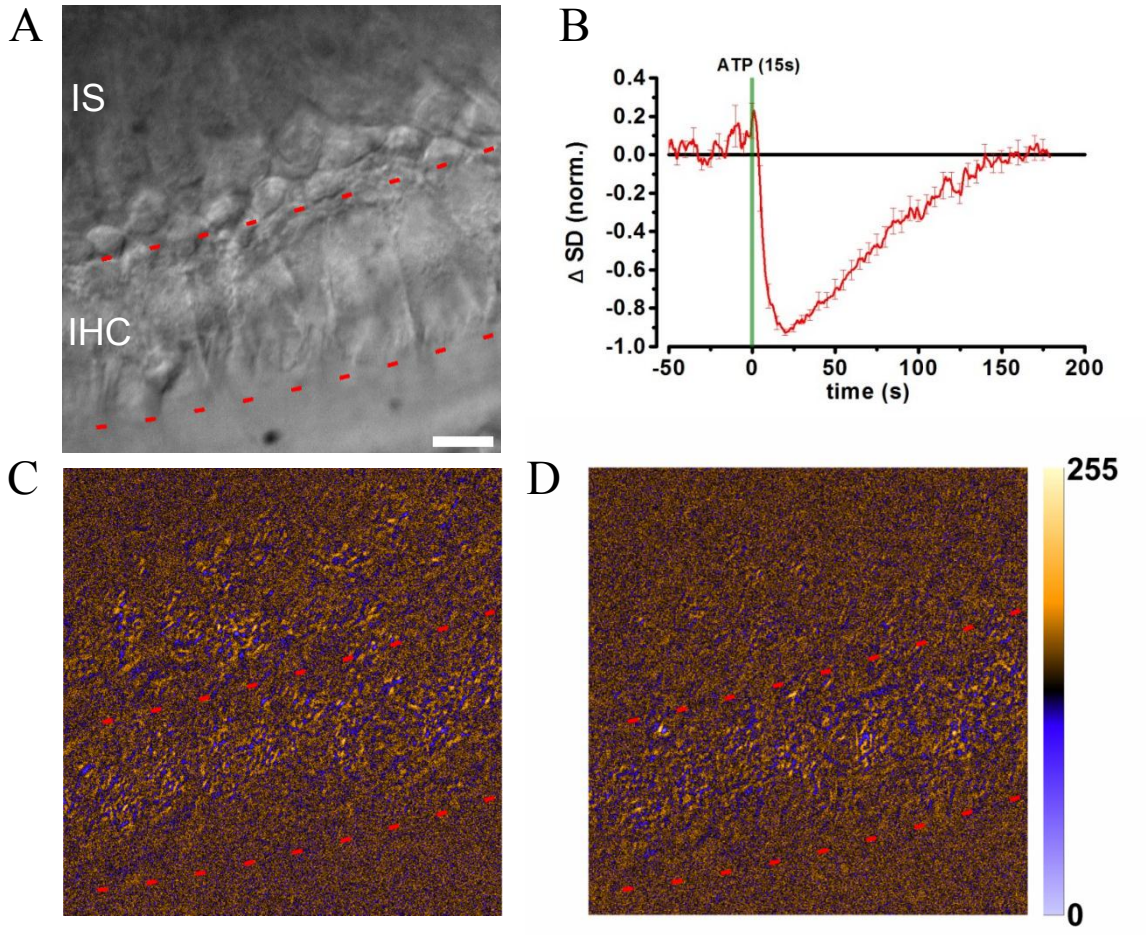

Figure 3.18 Stimulation of P2X receptors but not P2Y decreases Brownian motion in the cytoplasm of IS cells but not IHCs.
(A) Time-lapse bright-field images of the organ of Corti were captured and further processed to make differential images. **(B)** ATP was applied for 15 s (application onset indicated by the green line at t = 0). SD of pixel values in the differential image was measured in a 30 x 30 µm ROI and the change in SD from background SD determined for each frame (for further explanation see section 2.5.1). SD changes in the IS region were monitored for 179 s post-ATP application, normalized and averaged (red, n = 17 ATP applications, 5 cochleas).
Differential and false coloured image of the organ of Corti fragment shown in (A), **(C)** before ATP application and **(D)** 12 s after the onset of ATP application. IHCs are found between the red lines. The range of SD values after ATP application is smaller in the IS but not in IHCs. Scale bar is 10 µm.

The role of these spontaneous waves is currently unknown however they might be important for maintaining spontaneous spiking in the immature organ of Corti or the detachment of the TM. Köllikers organ is replaced by the IS prior to the onset of

hearing and it is not clear if extracellular ATP can still elicit similar morphological changes in IS supporting cells. To determine if ATP can cause crenation in the IS of hearing animals, bright field images of the organ of Corti were captured, while applying 100 µM ATP. Puff application of ATP did not cause cells to shrink. Instead a decrease in the Brownian motion in the cytoplasm of the IS cells was observed. To help quantify the changes in cytoplasmic Brownian movement time-lapse images captured using bright-field microscopy were subtracted from each other to make a differential

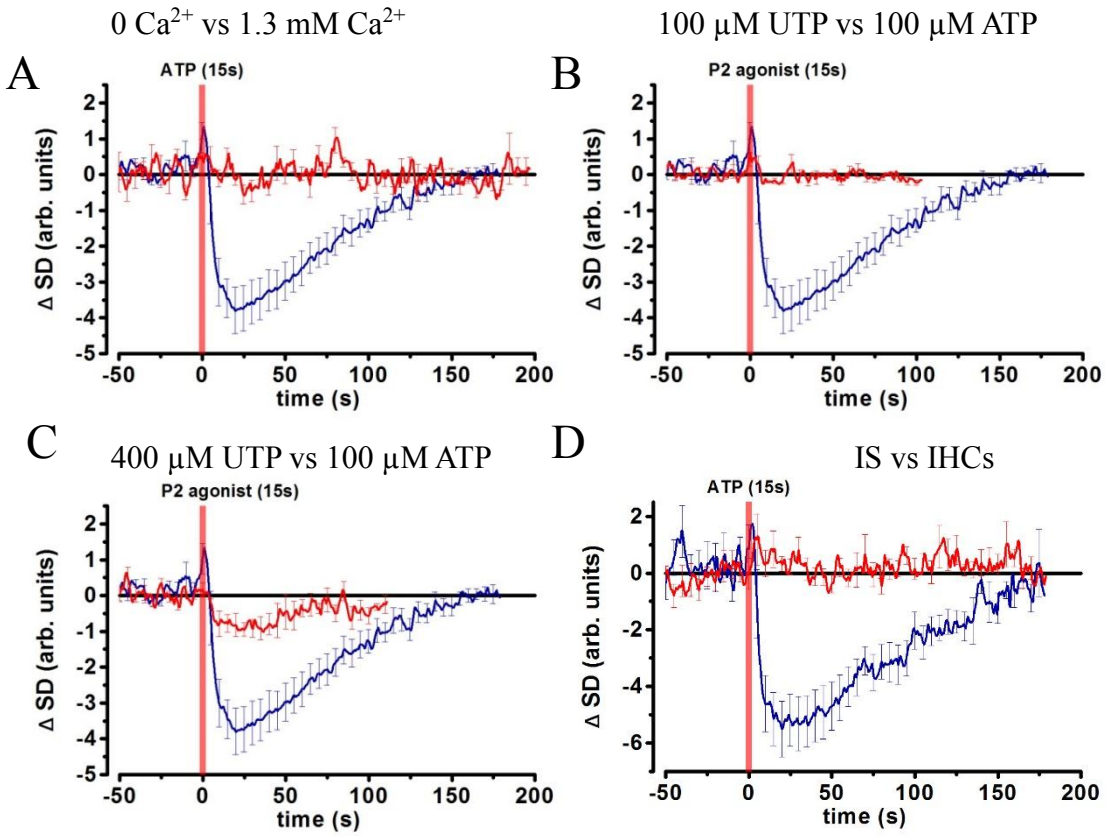

Figure 3.19 The changes in the cytoplasms properties are mediated through P2X receptors and are not present in IHCs.
The SD measured in a 30 x 30 µm ROIs when applying 100 µM ATP in ES with 1.3 mM extracellular Ca^{2+} **(A, B** and **C,** blue, n = 17, 5 cochleas**)** was compared to the SD measured when applying: 100 µM ATP when no additional Ca^{2+} and 10 mM EGTA were present in the ES **(A,** red, n = 7, 3 cochleas**)**, 100 µM UTP in ES with 1.3 mM extracellular Ca^{2+} **(B,** red, n = 4, 2 cochleas**)** and 400 µM UTP in ES with 1.3 mM extracellular Ca^{2+} **(C,** red, n = 5, 2 cochleas**)**. **(D)** SD was also observed in 10 x 10 µm ROIs in the IS (blue, n = 17, 5 cochleas) and IHCs (red, n = 17, 5 cochleas) in ES with 1.3 mM Ca^{2+}.

time-lapse image. Standard deviation (SD) was then monitored in 30 x 30 µm ROIs placed over the IS region n = 17 ATP applications, 5 cochleas (Figure 3.18 B). To determine if the observed changes could be solely mediated by P2Y receptors ATP was

applied in solution containing no additional Ca^{2+} and 10 mM EGTA. No response was observed (Figure 3.19 A n = 7 applications 3 cochleas). Puff application of UTP (100 µM) with 1.3 mM Ca^{2+} in the ES also did not produce a measurable response (Figure 3.19 B n = 4 applications 2 cochleas). After averaging the traces a response of 0.27 of the one elicited by 100 µM ATP was observed after puff applying 400 µM UTP (Figure 3.19 C n = 5 observations 2 cochleas). At such high > 100 µM concentrations UTP might act as a weak P2X receptor agonist (Evans et al., 1995; Froldi et al., 1997; Gever et al., 2006). SD was also monitored in 10 x 10 µm ROIs placed over IHCs and as a positive control over the IS (n = 17, 5 cochleas in both cases). No changes were detected in IHCs (Figure 3.19 D).

The time-course of the recovery in the cytoplasm's mobility appeared to correlate with the recovery of R_m after ATP application in coupled IS cells and both have been plotted for convenience in Figure 3.20.

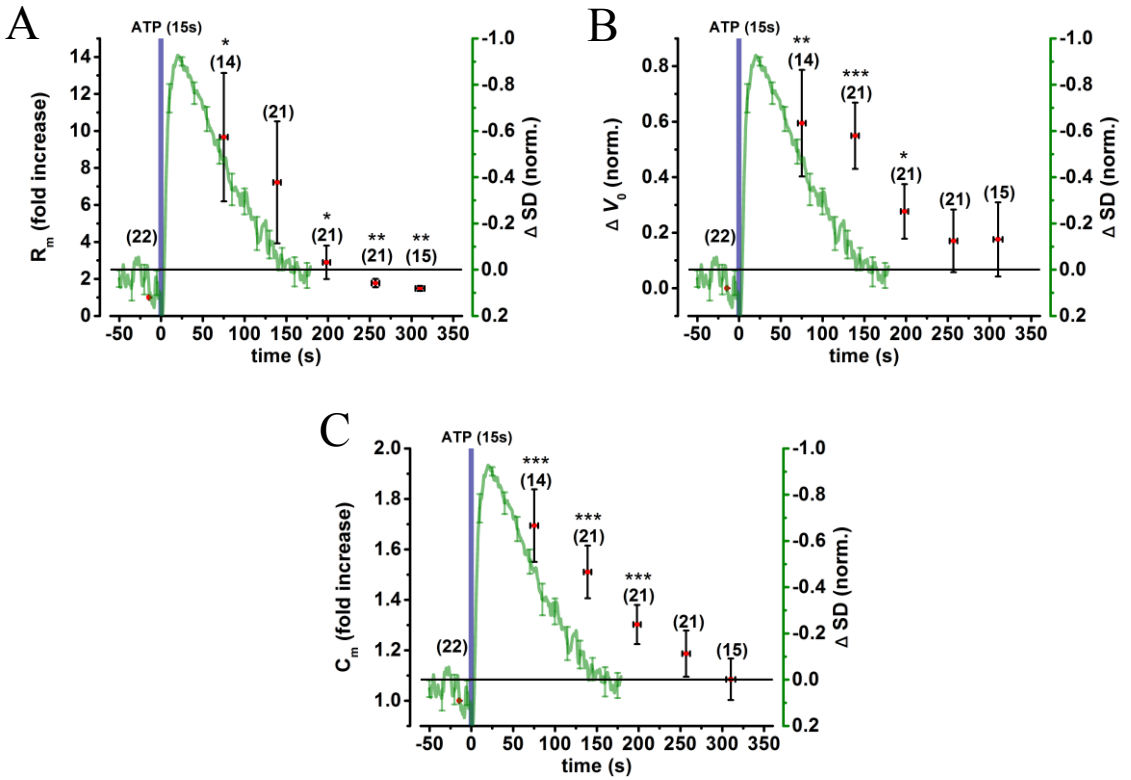

Figure 3.20 The time course of optical changes in the IS corresponds with the electrophysiological changes in R_m, V_0 and C_m.

The membrane resistance **(A)**, current reversal potential **(B)** and capacitance **(C)** were measured during whole cell electrophysiological recordings before and at different time points post-ATP application in coupled IS cells (red points, black bars SEM, number of cells indicated above in parentheses).

To compare the time course of these changes to the differential image SD changes observed post-ATP application the latter was plotted in the same figure (green).

3.2.4 ATP activates two different conductances in border cells of the adult mouse organ of Corti

The periodic spontaneous crenation observed in Köllikers organ prior to the onset of hearing has been hypothesized to be initiated by an extracellular ATP evoked Ca^{2+}_i increase and subsequent opening of CaCCs (Tritsch and Bergles, 2010; Tritsch et al., 2010b). This spontaneous activity ceases after the onset of hearing, however the physiological mechanisms which contribute to this change remain unknown and the role of ATP receptors in the organ of Corti and IS of hearing animals is unclear. As described in section 3.2.3 no crenation was observed in adult IS cells. To determine the effects of ATP on membrane currents in single IS and border cells of the adult mouse cochlea, whole cell recording conditions were established and cells were decoupled with either 1-octanol (1 mM) or FFA (100 µM). FFA in addition to blocking gap junctions is a known Cl^- channel blocker (Bodendiek and Raman, 2010).

	R_m (MOhm)	**C_m (pF)**	**V_0 (mV)**
Border cells octanol	3910 ± 610	11.7 ± 0.8	-39.5 ± 4.7
Border cells FFA	3630 ± 894	10.7 ± 0.7	-39.6 ± 6.2
IS cells octanol	1300 ± 290	16.9 ± 1.4	-21.8 ± 2.5
IS cells FFA	1580 ± 594	19.8 ± 1.6	-20.0 ± 5.5
Border octanol vs Border FFA	0.79	0.34	0.99
Border octanol vs IS octanol	0.0012	0.013	0.0040
Border FFA vs IS FFA	0.086	0.0011	0.039
IS octanol vs IS FFA	0.68	0.19	0.78

Table 3.1 Showing the R_m, C_m and V_0 values for Border and IS cells decoupled with FFA and octanol.
Listed is also the significance of the difference between the various groups. Values were compared using two sample t-tests as detailed in section 2.7.

10kDa dextran conjugated fluorescein was added to the patch pipette to facilitate cell identification (Figure 3.21 A and B). The characteristic phalange of border cells was visible and could be imaged using confocal microscopy, in cochleas fixed for 30 minutes in 4% paraformaldehyde after conducting the electrophysiological recordings.

Both IS and border cells were found to have outward voltage dependent currents of a few hundred picoamps. These currents were found to decrease with time after patching (Figure 3.21 C-D). The membrane resistance of border cells was found to be 3910 ± 610

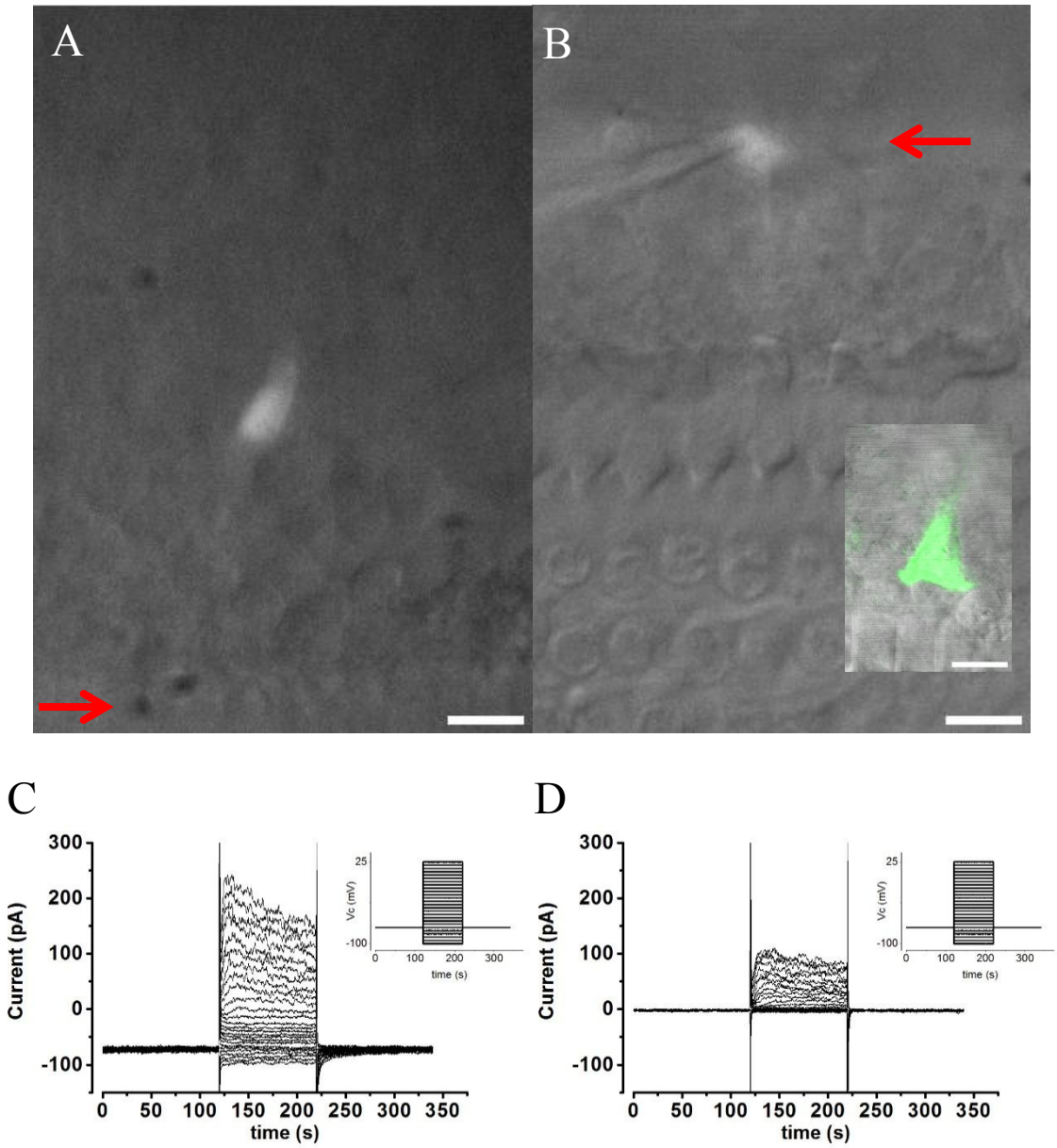

Figure 3.21 Patch clamp electrophysiological recordings were made from IS and border cells in the adult mouse cochlea.
10kDa dextran conjugated fluorescein was added to the intracellular solution to mark patched IS **(A)** and border cells **(B)** red arrow points to the row of border cells, inset shows a fluorescein filled border cell imaged using confocal microscopy. Fluorescence was evoked at 488 nm. 1 mM 1-octanol was used to decrease gap junctional coupling. Both IS **(C)** and border cells **(D)** were found to have voltage dependent outward currents. (Note the small leak current in border cells). Scale bars: 10 µm.

MOhm n = 14 for cells decoupled with 1-octanol and 3630 ± 894 MOhm n = 7 for cells decoupled with FFA (Using a V_c step from -55 to -75 mV). These differences were statistically insignificant (P = 0.79). Single cell capacitance was found to be 11.7 ± 0.8 pF and 10.7 ± 0.7 pF respectively. The difference between these values were

statistically insignificant ($P = 0.34$). The cells V_0 was found to be respectively -39.5 ± 4.7 mV and -39.6 ± 6.2 mV in 1-octanol and FFA decoupled cells, which was not a statistically significant difference ($P = 0.99$). The 1-octanol decoupled border cells were found however to have statistically significantly different values of R_m ($P = 0.0012$), C_m ($P = 0.013$) and V_0 ($P = 0.0040$) compared to 1-octanol decoupled IS cells (n = 6 IS cells). These values apart from R_m were also significantly different in FFA decoupled border cells when compared to FFA decoupled IS cells: R_m ($P = 0.086$), C_m ($P = 0.0011$), V_0 ($P = 0.039$) (n = 6 IS cells). These parameters were not significantly different for IS cells decoupled with 1-octanol R_m 1300 ± 290 MOhms and FFA 1580 ± 594 MOhms ($P = 0.68$). Capacitance of IS cells decoupled with 1-octanol was 16.9 ± 1.4 pF n = 6 and 19.8 ± 1.6 n = 6 ($P = 0.19$) for FFA decoupled cells. V_0 was -21.8 ± 2.5 mV for 1-octanol and -20.0 ± 5.5 ($P = 0.78$) for FFA decoupled IS cells.

To further confirm that the patched cells were indeed border cells recordings were conducted to determine if the glutamate transporter GLAST was present. Border cells have been previously shown to express the GLAST (Furness and Lehre, 1997; Glowatzki et al., 2006). Stimulation of GLAST has been shown to activate an associated Cl^- conductance (Wadiche et al., 1995). This ligand-activated conductance has a higher selectivity for thiocyanate (SCN^-) than Cl^- (Glowatzki et al., 2006). To verify that recordings were indeed being made from border cells, 130 mM of KCl in the intracellular solution was substituted with 130 mM KSCN and 300 µM D-aspartate a substrate for GLAST was puff applied for 250 ms to the patched cell. Patched cells had an R_m of 834.7 ± 54.8 MOhms a capacitance of 13.3 ± 0.7 pF and a mean V_0 of 2.4 ± 4.3 mV n = 9 cells (Figure 3.22). D-aspartate application elicited currents of a magnitude of -50.4 ± 9.0 pA which could be fit with a single exponential and recovered to baseline levels with a τ of 61 ± 22 s. The change in R_m can be ascribed to an increased leak conductance below 0 mV in the presence of KSCN (Figure 3.22 A). In contrast in none of 4 IHCs were D-aspartate-activated currents observed confirming the observations of (Glowatzki et al., 2006) that IHCs do not express these transporters.

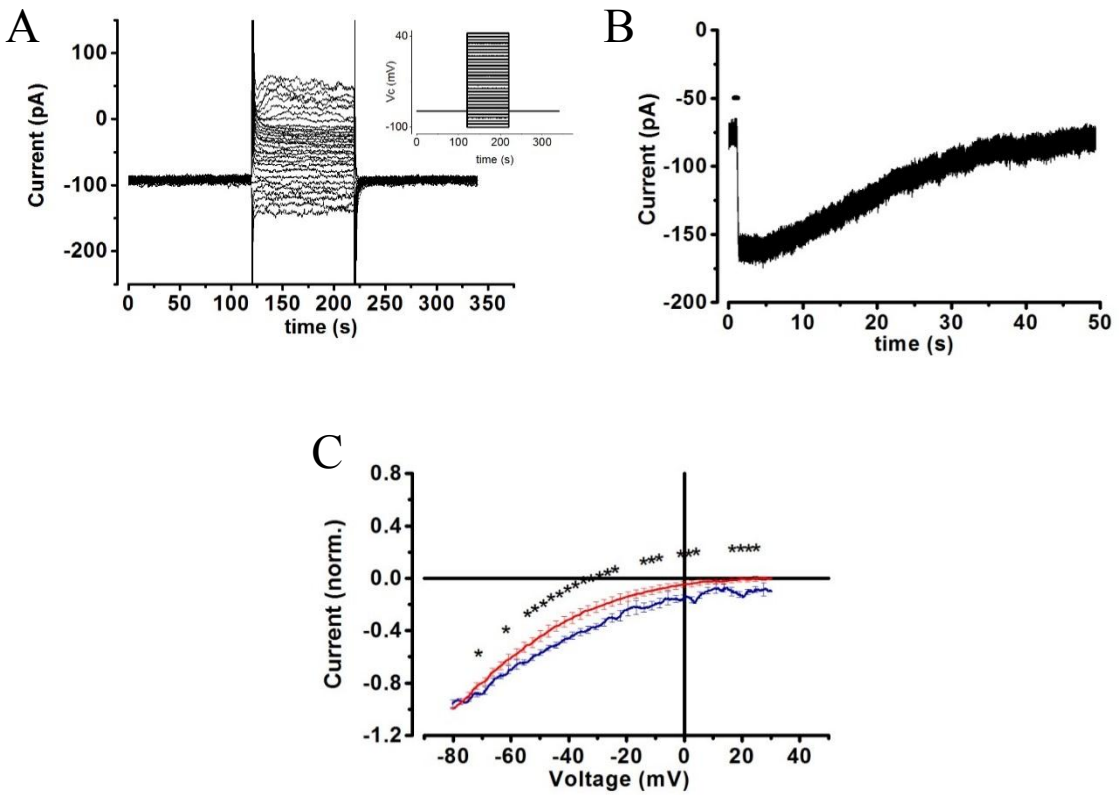

Figure 3.22 Puff application of 300 µM D-aspartate elicited currents in border cells which had different characteristics from ATP-activated currents.
(A) A current-voltage plot typical of a border cells patched with 130 mM KSCN in the intracellular solution. **(B)** 250 ms application of 300 µM D-aspartate to patched border cells (black bar) with 130 mM KSCN in the intracellular solution elicited a current (mean -50.4 ± 9.0 pA $\tau = 61 \pm 22$ s $n = 7$). **(C)** The rectification properties of this current were consistent with those of the GLAST glutamate transporter (Glowatzki et al., 2006) and differed significantly from the rectification properties of currents elicited by ATP application with 130 mM KSCN and 10 mM BAPTA in the intracellular solution $n = 6$ (described further in section 3.2.6), stars indicate regions of significant difference (student t-test $P < 0.05$) between the plotted groups. (blue – D-aspartate application, red - 100 µM ATP).

When recorded from with KCl in the intracellular solution application of 100 µM ATP elicited desensitizing currents in IS cells of -472 ± 166 pA n = 6 cells when cells were decoupled with 1-octanol and -655 ± 144 pA n = 6 when cells were decoupled with FFA, which was not a significant difference ($P = 0.43$) (Figure 3.23 A). The

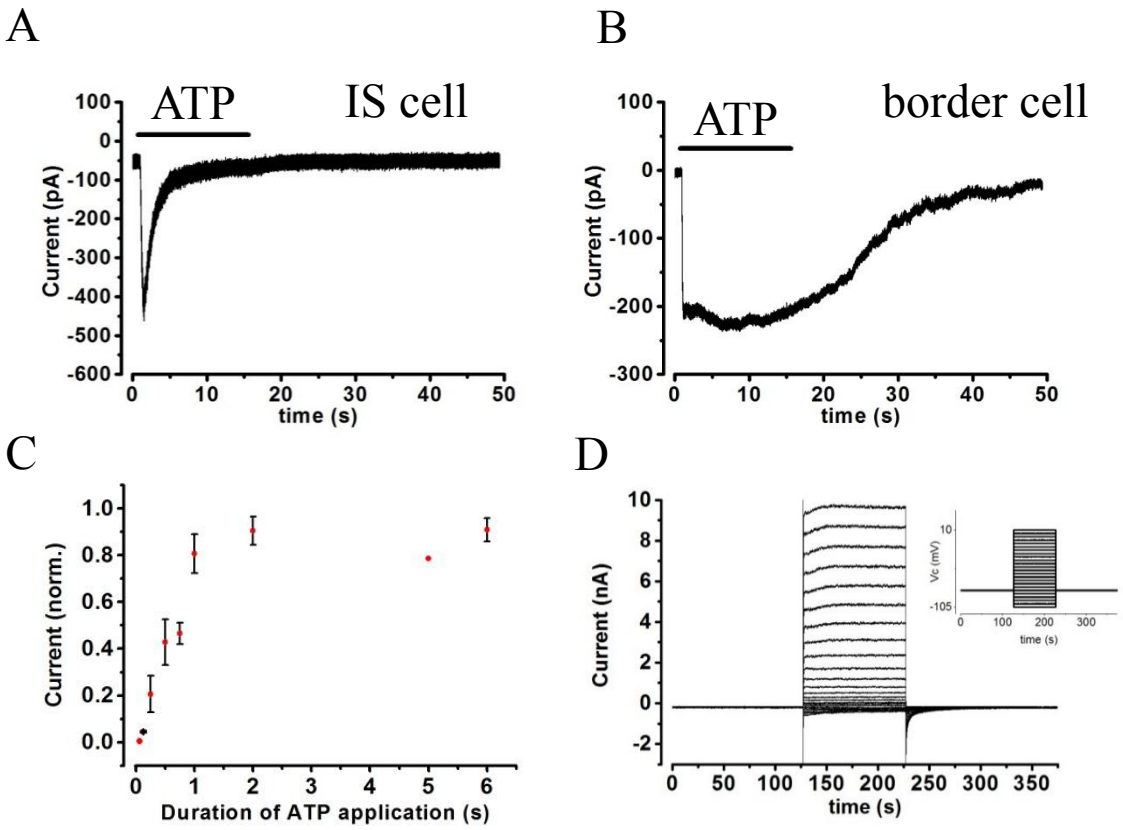

Figure 3.23 Puff application of 100 µM ATP elicited currents in decoupled inner sulcus and border cells but not IHCs.
1 mM 1-octanol was used to decrease gap junctional coupling and ATP (100 µM) was puff applied for 15 s to IS **(A)** and border cells **(B)**. **(C)** A time of ATP application based dose response curve was made for IS cells.
(D) Patched IHCs showed characteristic voltage dependent currents, but ATP application failed to activate any currents in 8/8 IHCs.

desensitization rate could be fit with a single exponential with a time constant (τ) of 2020 ± 405 and 1980 ± 367 ms respectively. This was not a statistically significant difference ($P = 0.95$). Repeated ATP stimulation desensitized currents. Currents re-sensitized to pre-stimulation levels within 5 minutes of applying ATP. These characteristics are consistent with those of the $P2X_{2b}$ and $P2X_{2e}$ receptor subtypes (Koshimizu et al., 2006). These $P2X_2$ receptor isoforms have been localized to the rat vestibular end organs and the guinea pig cochlea (Chen et al., 2000; Troyanovskaya and Wackym, 1998).

A simple dose response curve could be constructed for 1-octanol decoupled IS cells by varying the duration of puff application of 100 µM ATP (Figure 3.23 C).

Border cells decoupled with 1 mM 1-octanol were found to have two ATP-activated current components (Figure 3.23 B). A fast initial current component of a magnitude of -387 ± 55.1 was followed by a more sustained response of a magnitude of -297 ± 57.3 pA n = 14 cells within 2 s of the onset of ATP application. The second component was

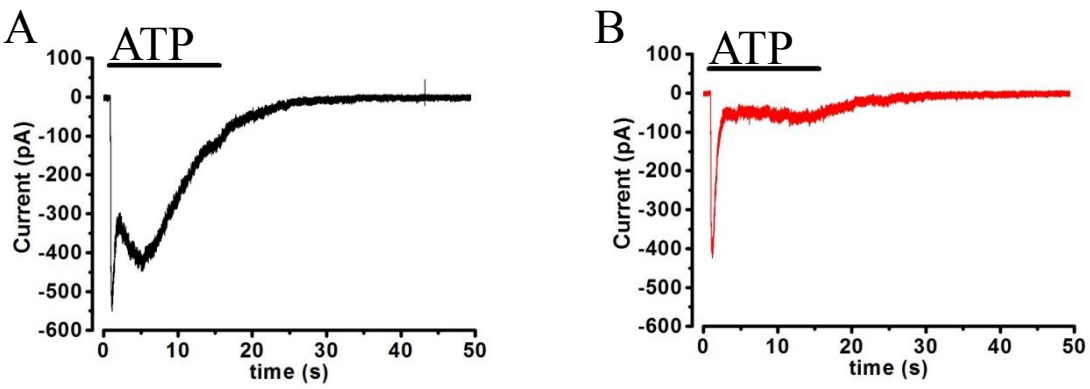

Figure 3.24 The ATP elicited current in border cells consists of two components.
Border cells were patched, decoupled with 1-octanol (1 mM) and 100 µM ATP was puff applied to the cell **(A)**. Subsequently 1-octanol was substituted with FFA (100 µM) **(B)**. The 2nd component is blocked by FFA (n = 7 cells).

blocked by FFA and the remaining first component had a magnitude of -256 ± 33.9 pA (n = 7), which was significantly smaller ($P = 0.039$) than the ATP-activated current magnitude of FFA decoupled IS cells (-655 ± 144 pA). The τ value of the current in FFA decoupled border cells (1350 ± 318 ms) was not significantly different form the τ value of the current in FFA decoupled IS cells (1980 ± 367 ms, n = 6) ($P = 0.22$) (Figure 3.24 B).

The second component was observed to desensitize after >5 s of puff application of 100 µM ATP. The two current components were found to desensitize differentially upon repeated (every minute) 5 s puffs of 100 µM ATP (Figure 3.25 A, B).

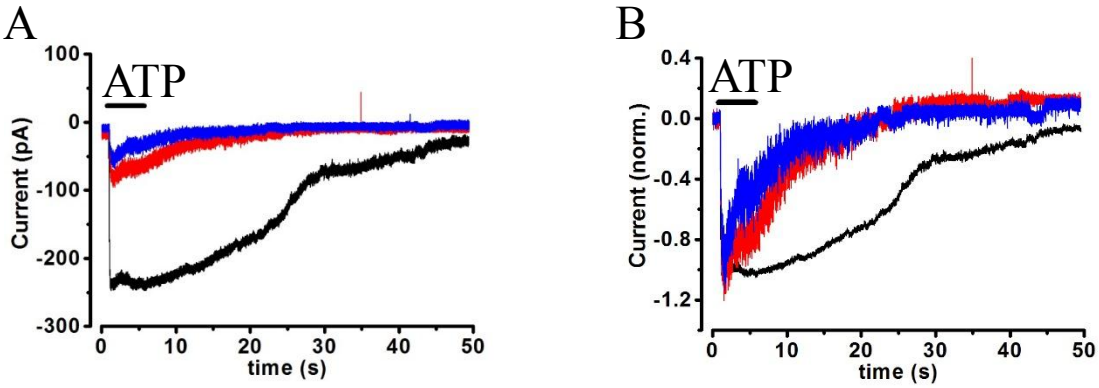

Figure 3.25 Repeated stimulation of border cells with 100 µM ATP (5 s puff, every minute) differentially desensitized both current components.
Typical desensitization profile **(A)** and after normalizing the responses **(B)**.

To determine the rectification properties of the identified ATP-activated conductances, 500 ms voltage ramps (-80 to +30 mV) were applied at 2.5 s after the onset of ATP application. The ATP-activated current component in IS cells was found to be highly inwardly rectifying, consistent with properties of some P2X receptors (Brake et al., 1994; Zhou and Hume, 1998).

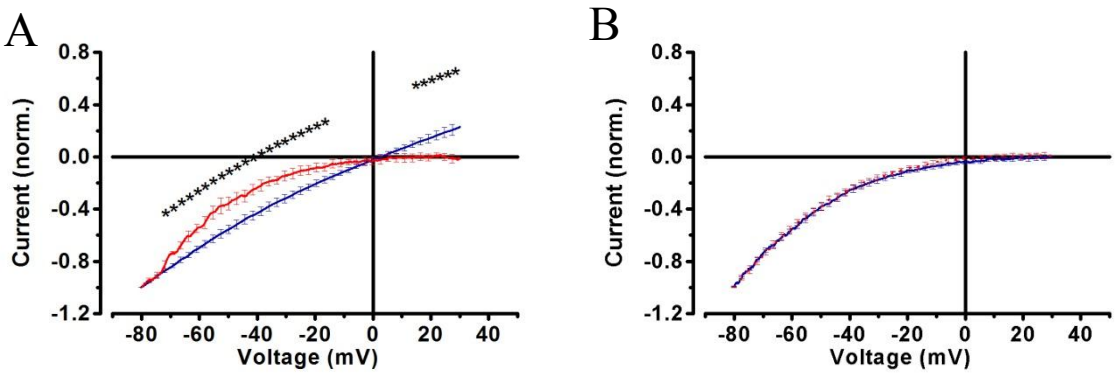

Figure 3.26 The voltage dependent conductance of the ATP-activated current in border cells decoupled with 1-octanol differs from that of border cells in which the second component has been blocked by FFA.
Voltage ramps (-80 to +30 mV) were applied to cells 1.5 s after the start of ATP application. The voltage-dependent conductance properties of the ATP-activated currents were found to be significantly different in border cells decoupled with 1-octanol (1 mM) and FFA (100 µM) **(A)** blue – 1-octanol n = 7, red – FFA n = 3, stars indicate a significant difference at the 0.05 level or lower. Such differences were not observed in IS cells **(B)** (blue - FFA n = 6, red – 1-octanol n = 5).

In contrast in border cells decoupled with 1-octanol the compound current elicited by ATP stimulation showed less inward rectification then in IS cells and reversed at 2.0 mV ± 2.8 mV n = 7 in intra and extracellular solutions containing equimolar Cl^- levels

(Figure 3.26 A). Superfusion with solution containing 100 µM FFA fully blocked the slower component, leaving only the fast initial component which could be ascribed to P2X receptor activation. In the presence of FFA (100 µM) and after puff application of ATP currents elicited by voltage ramps showed strong inward rectification resembling those obtained in recordings from IS cells (Figure 3.26 A). Indeed no statistically significant differences in rectification properties were observed between border and IS cells decoupled with FFA (Figure 3.27).

To try to better distinguish between the rectification properties of both ATP-

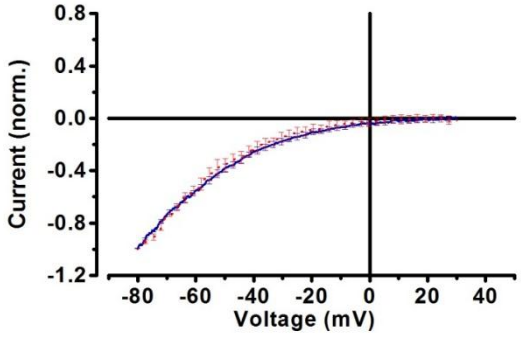

Figure 3.27 After blocking the second component the ATP-activated current, rectification properties of the ATP-activated current in border cells are not different from the rectification properties of ATP-activated currents in IS cells.
There were no significant differences in the voltage dependent conductance properties between IS cells decoupled with FFA n = 6 (blue) and border cells decoupled with FFA n = 3 (red).

activated current components in 1-octanol decoupled border cells an additional voltage ramp was applied at 7 s after the onset of ATP application in 4 cells. No significant differences were found in the reversal potential or rectification properties although the current elicited at 7 s did appear to trend towards a more linear current-voltage relationship (Figure 3.28). No ATP-activated currents were detected in IHCs, even though they exhibited characteristic voltage dependent outward currents (8/8 cells) (Figure 3.23 D).

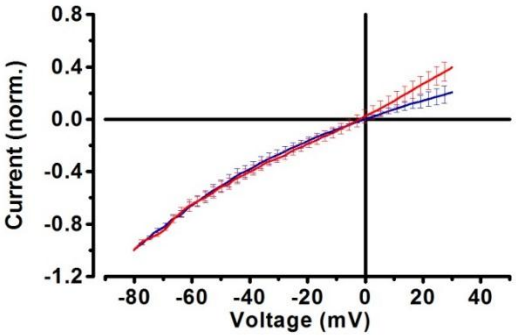

Figure 3.28 Voltage ramps applied at 1.5 and 7 s after the onset of ATP application do not differ significantly from each other in border cells.
In border cells decoupled with 1-octanol the current elicited by a voltage ramp applied at 1.5 s n = 4 (blue) did not significantly differ from one elicited by a voltage ramp at 7 s n = 4 (red), although a trend was visible.

3.2.5 The delayed component has characteristics of a chloride channel

Apart from being a Cl^- channel blocker FFA is known to block cationic channels such as TRP and connexins. To help determine the identity of the channel responsible for the delayed current component in border cells 130 mM Cl^- in the intracellular solution was substituted for an equimolar amount of SCN^- which is known to have an increased permeability through Cl^- channels. If a Cl^- permeability is present a shift in current reversal potential (V_0) towards more positive values should occur. Indeed this was found to be the case and with SCN^- in the intracellular solution V_0 shifted significantly from 2.0 mV ± 2.8 n = 7 cells to 33.3 ± 10.0 n = 6 (two sample t-test P = 0.025) (Figure 3.29 A-B). With SCN^- in the patch pipette the max currents were measured at -325 ± 83.8 for the initial component and -249 ± 57.6 pA for the secondary component n = 9 cells. Cells were found to have an R_m of 853 ± 152, a capacitance of 12.5 ± 1.3 and a V_0 of 0.1 ± 5.5 mV. These values were not significantly different from the R_m (P = 0.91), C_m (P = 0.62) and V_0 (P = 0.74) values found for cells tested for the presence of GLAST, which were also recorded from with SCN^- present in the intracellular solution.

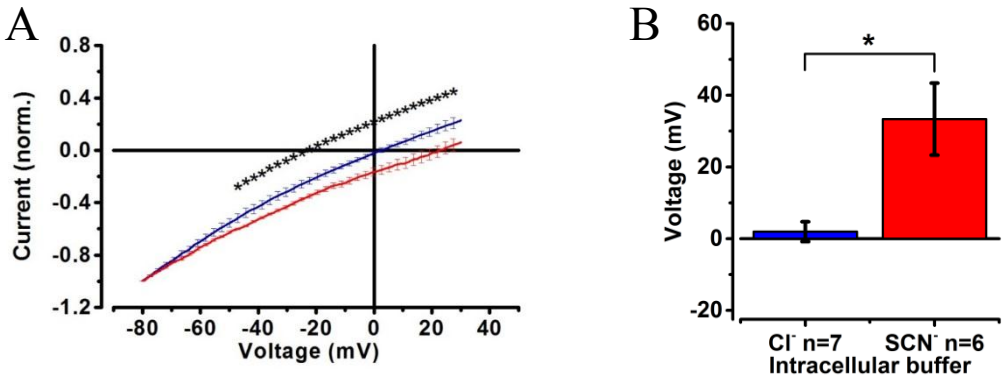

Figure 3.29 The reversal potential of the ATP-activated current in border cells is significantly shifted towards positive values with SCN^- in the intracellular solution.
After substituting intracellular Cl^- (blue n = 7 cells) with SCN^- (red n = 6 cells) the ATP elicited current's reversal potential shifted from 2.0 mV ± 2.8 to 33.3 ± 10.0, shown in normalized traces **(A)** and as a bar graph **(B)**.

3.2.6 The delayed ATP-activated current component in border cells is dependent on the intracellular Ca^{2+} concentration

To determine if the second component is sensitive to Ca^{2+}_i concentration the Ca^{2+} buffering capacity of the intracellular solution was increased. Replacement of 0.5 mM EGTA with 10 mM BAPTA in an intracellular solution in which 130 mM KCl was replaced with KSCN completely abolished the second current component in 1-octanol decoupled border cells. Cells had a R_m of 766 ± 176 MOhms a capacitance of 16.1 ± 0.7 pF and a V_0 of 5.5 ± 3.1 mV.

Cells showed a desensitizing current component of -656 ± 203 pA with a desensitization time constant of 2610 ± 827 ms. The values of R_m, V_0, and τ of desensitization were not significantly different from the values of these parameters obtained from border cells decoupled with FFA ($P = 0.71$, $P = 0.41$, $P = 0.22$ respectively). The membrane capacitance was found to be significantly higher ($P = 0.036$).

The rectification properties of the ATP-activated current under these high Ca^{2+}_i buffering conditions were significantly different from those of cells patched with intracellular SCN^- but under low Ca^{2+}_i buffering (0.5 mM EGTA) conditions (Figure 3.30 A). They were not significantly different however from the ATP-activated current rectification properties in cells in which the second current component was blocked with FFA (Figure 3.30 B). To try to better differentiate between the two current components in addition to the voltage ramp at 1.5 s an additional voltage ramp was applied 9 s after the onset of ATP application. No significant differences were observed in cells patched under low Ca^{2+}_i buffering conditions. Some significant differences were present between the different time points above 0 mV in high Ca^{2+}_i buffering conditions. These are most likely the result of high noise as ATP-evoked currents had a low magnitude in this group at 9 s after the onset of ATP application (Figure 3.31 A and B).

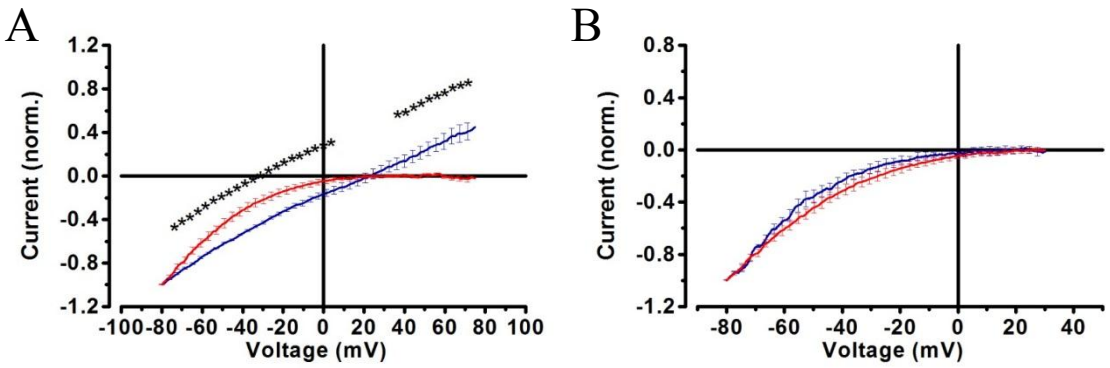

Figure 3.30 The voltage dependent conductance properties of the ATP-activated current significantly differ between cells patched under low and high Ca^{2+}_i buffering conditions.
(A) Border cells were patched with 130 mM KSCN in the intracellular solution under low (0.5 mM EGTA n = 6, blue trace) or high (10 mM BAPTA, n = 6, red trace) Ca^{2+}_i buffering conditions. 1-octanol was used to decouple the cells from the surrounding syncytium and voltage ramps (-80 to +75 mV) were applied.
(B) No statistically significant difference in rectification properties of the ATP elicited current were found between border cells recorded from with 130 mM KCl in the intracellular solution and in which the second component was blocked by FFA (100 µM), n = 3 (blue) and border cells patched with 130 mM of KSCN and 10 mM BAPTA in the intracellular solution, n = 6 (red).

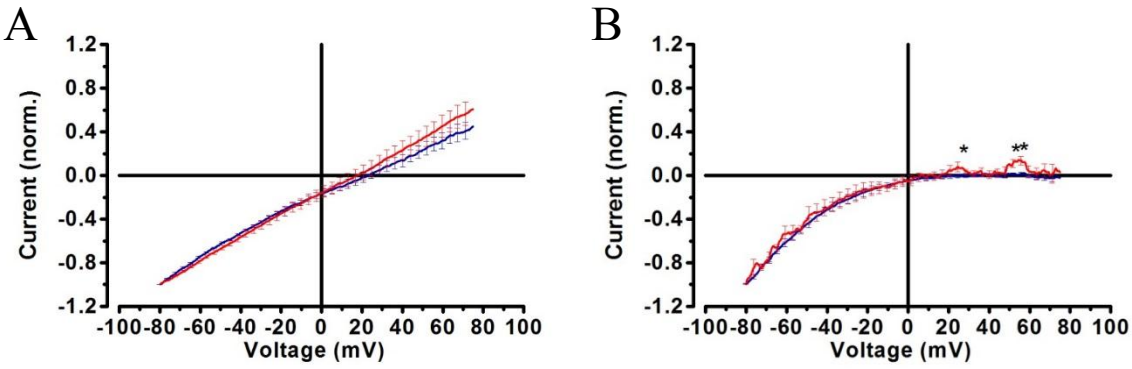

Figure 3.31 Currents elicited by voltage ramps at 1.5 s and 9 s after the onset of ATP application did not differ significantly.
(A) In border cells decoupled with 1-octanol and in the presence of 130 mM SCN^- in the intracellular solution normalized current evoked by a voltage ramp (-80 to +75 mV) applied at 1.5 s after the onset of ATP application (blue) did not significantly differ from one elicited by a voltage ramp at 9 s (red) in cells patched with 0.5 mM EGTA in the intracellular solution, n = 6. **(B)** When 10 mM BAPTA was present, n = 6, some significant differences were found. These can be ascribed to a high noise to current ratio at 9 s post-ATP application as currents in BAPTA patched cells desensitized with a time constant of 2610 ± 827 ms.

3.2.7 The FFA sensitive ATP-activated current component in border cells was not activated by stimulation with extracellular UTP.

To determine if the $Ca^{2+}{}_i$ increase mediated by UTP was sufficient to activate the 2nd ATP-activated component of border cells (Described in section 3.2.4) after establishing whole cell recording conditions 100 µM ATP and UTP were puff applied separately in 5 minute intervals to the same border cell from a double barrel puff pipette. Application of ATP elicited currents with two components, however UTP (100 µM) failed to elicit any visible currents in 4/4 border cells (Figure 3.32 A and B).

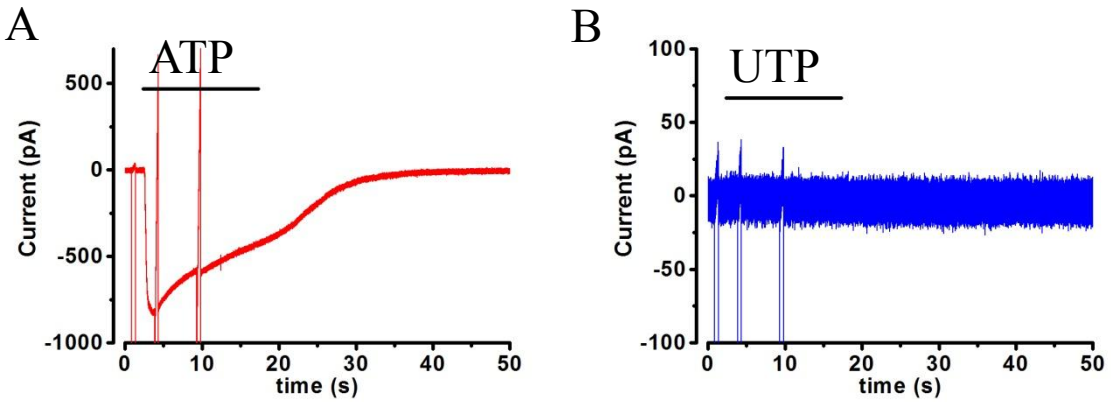

Figure 3.32 Stimulation with 100 µM UTP did not elicit the second component in border cells decoupled with 1-octanol (1 mM).
ATP (100 µM) was puff applied whilst recording from border cells to determine if two components were present **(A)**. UTP (100 µM) was applied to the same cells. **(B)**.In 4/4 cells puff application of 100 µM UTP did not elicit currents even though a current with two components was elicited by application of 100 µM ATP.

3.2.8 ATP does not affect the membrane potential of IHCs

Border and phalangeal cells are thought to play a crucial role in re-uptake of excess glutamate from the IHC afferent synapse as IHCs do not appear to express glutamate transporters (Glowatzki et al., 2006). Their role in maintaining the IHC afferent synapse has been compared to the role of glial cells. Indeed cochlear phalangeal and border cells are known to produce neurotrophins such as BDNF. The ATP-activated Cl^- efflux from border cells could be another mechanism through which these cells can affect signalling at the IHC – spiral ganglion synapse.

The local concentration of K^+ is thought to increase in the vicinity of the IHC during sound stimulation as K^+ is extruded from the hair cell into the extracellular environment. Indeed such increases in K^+ concentration around neurons have been documented in the cortex (Singer and Lux, 1975). Cl^- efflux from the border cell

neighbouring the IHC synapse could change the osmolarity of the ES enriched in K^+

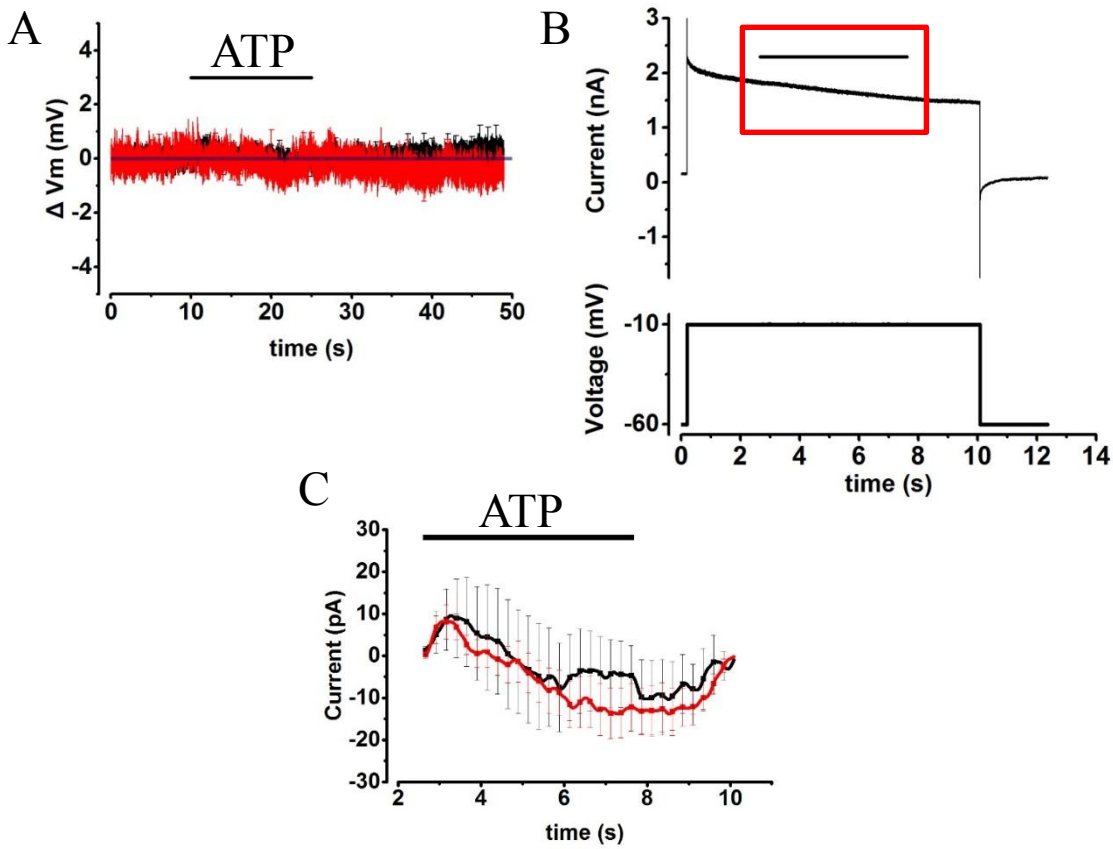

Figure 3.33 Exposure to ATP does not change the IHC membrane potential. **(A)** Patched IHCs were current clamped while puff applying 100 µM ATP in ES or ES with no P2 agonist. Puff application of ATP failed to elicit any change in resting membrane voltage (red) n = 5 when compared to pre-ATP application levels and control cells (black) n = 10, to which ES without ATP was puff applied. **(B)** Patched IHCs were depolarized to -10 mV and ATP (100 µM) was applied to determine its effect on the current. **(C)** Averaged and base current subtracted view of the depolarization evoked current during the application of ATP for the time period shown in the red box in (B). **Black** (control - ES was puff applied. n = 9 observations from 3 cells.) **Red** (ATP was puff applied, n = 9 observations from 3 cells).

extruded from the hair cell. To equalize osmolarity water from the cell would have to move into the extracellular environment. This water movement could have the potential to dilute the extracellular concentration of K^+ and thus help restore the resting membrane potential of surrounding IHCs. Thus application of ATP to the organ of Corti might result in a decrease of the IHC membrane potential. To test this hypothesis patch clamp electrophysiological recordings were made from IHCs and the cells resting membrane potential was monitored during and immediately after puff application of 100 µM ATP. Puff application of ATP did not affect the IHC resting membrane potential (V_m) and no significant differences were found between groups of cells treated

with ATP and control solution (Figure 3.33 A). V_m was estimated at -56.4 ± 3.4 mV n = 10 cells for IHCs treated with control solution and -64.1 ± 1.8 mV n = 5 cells for cells to which 100 µM ATP was puff applied. These differences were not significant (P = 0.065).

IHCs express voltage-activated K^+ channels and any change in extracellular K^+ concentration should affect the magnitude of the K^+ current when the IHC is depolarized. This approach would have the added benefit of increasing the sensitivity to detection of any effects of ATP on the IHC membrane potential.

To use this approach to determine if ATP can affect IHC membrane currents whole cell patch clamp electrophysiological recordings were made from IHCs held at a V_c of -60 mV. After increasing V_c from -60 mV to -10 mV to activate K^+ channels 100 µM ATP was puff applied for 5 s. No significant differences between cells treated with control and ATP containing solution were found n = 3 in both groups (Figure 3.33 B and C).

3.2.9 Summary of results

Exposure of IS cells to extracellular ATP was found to change the membrane resistance, current reversal potential and capacitance of coupled IS supporting cells. These changes appear to be accompanied by a decrease of Brownian motion in the cytoplasm of IS cells. Investigation of single cell currents in border cells neighbouring the IHC afferent synapse found that in addition to a P2X type conductance ATP activates a Cl^- conductance in these cells. No such Cl^- conductance was observed in IS cells, even though a P2X type conductance was present. ATP did not elicit any currents in IHCs nor change their membrane potential.

3.3 Extracellular ATP independent intracellular Ca^{2+} signalling in the adult organ of Corti

3.3.1 Introduction

While conducting observations of extracellular ATP-dependent Ca^{2+} signalling detailed in section 3.1.3, Ca^{2+} signalling events that did not appear to be related to application of

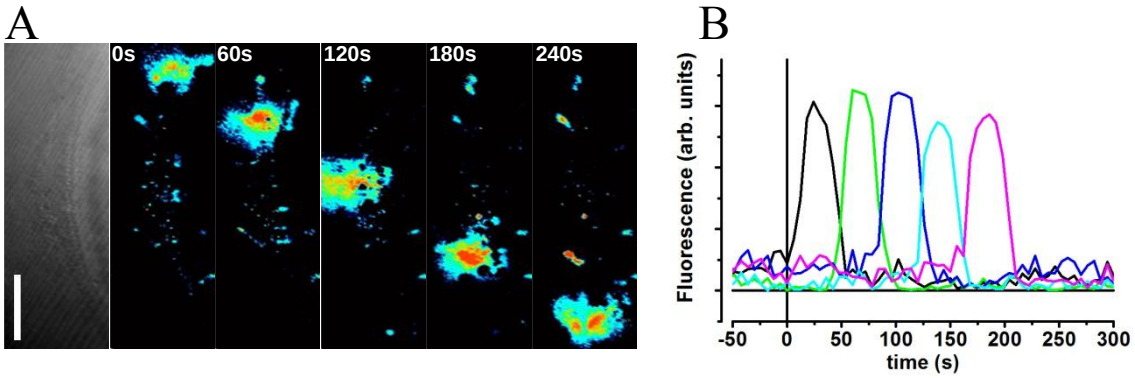

Figure 3.34 Slow Ca^{2+} waves were observed in the adult organ of Corti.
(A) Transmitted light image of the dissected and Fluo4-AM loaded organ of Corti (leftmost pane) and the same fragment observed every 60 seconds after background subtraction and false colouring (5 consecutive panes to the right of the transmitted light view). Visible are increases in Ca^{2+}_i, which propagate as a wave from cell to cell. (black - lowest Ca^{2+}_i levels, red - highest Ca^{2+}_i levels. **(B)** Fluorescence was measured every 50 µm along the wave travel path. Wave travels at a constant speed. Scale bar: 100 µm.

extracellular ATP were also observed (Figure 3.34). These events appeared to initiate 'spontaneously' and did not appear to be directly correlated with physical damage to any part of the organ of Corti. The spontaneous Ca^{2+}_i increases propagated as an intercellular Ca^{2+} wave along the length of the organ of Corti. The waves were first observed in cochleas in which the TM was removed and were limited to the Deiters' and Hensen's cell region. The aim of the investigations described below was to characterize the properties of these waves and determine their mechanism of propagation.

3.3.2 Spontaneous Ca^{2+} waves propagate slower than extracellular ATP mediated Ca^{2+} waves

Equally spaced ROIs were placed every 50 µm along the waves travel path to determine the waves speed and distance of propagation. Once initiated the Ca^{2+} signal was found to propagate between supporting cells at a constant speed of 0.9 ± 0.1 µm/s, n = 19 waves in 4 different cochleas, and for distances that could exceed 300 µm (Figure 3.34 A and B). The propagation speed of Ca^{2+} waves in supporting cells of the immature

organ of Corti has been found to be 10-13 µm/s (Gale et al., 2004; Lahne and Gale, 2008). On the basis of these measurements and to better differentiate these events from Ca^{2+} signalling in the immature organ of Corti, the new type of signalling will be hereby referenced to as 'slow Ca^{2+} waves'.

3.3.3 Slow Ca^{2+}waves were not affected by extracellular Ca^{2+} concentration but affected by the presence of the tectorial membrane

To study slow Ca^{2+} waves in greater detail time-lapse $Ca^{2+}{}_i$ imaging was conducted on Fluo4-AM loaded cochleas. To increase the signal to noise ratio background fluorescence was subtracted (Figure 3.35 A-C). Kymographs were made for the Deiters' cell and IS cell regions (Figure 3.35 D-G, described in Methods). The kymographs were a convenient way to measure individual slow Ca^{2+} wave travel distance, and duration, and after obtaining these values the waves propagation speed (Figure 3.35 H). Wave travel distance could be read from the x-axis of the kymograph, while information on wave duration was obtained from the y-axis. When the TM was left attached slow Ca^{2+} waves were also observed in the IS and kymographs were similarly made for the IS region (Figure 3.35 D, E). When Ca^{2+} was omitted from the ES and when measured from kymographs in cochleas that had the TM removed the speed of slow Ca^{2+} waves in Deiters' cells was found to be 1.04 ± 0.04 µm/s and the average propagation distance 148 ± 9 µm n = 50 waves, 3 cochleas. Increasing extracellular Ca^{2+} levels to 1.3 mM did not appear to affect slow Ca^{2+} wave signalling. Under these conditions slow Ca^{2+} waves were found to propagate at 1.05 ± 0.10 µm/s for 130 ± 8 µm n = 29 waves, 3 cochleas. Differences in wave speed and propagation distance were analysed using Kruskal-Wallis ANOVA. The differences in speed (P = 0.32) and distance (P = 0.32) of propagation in low and high extracellular Ca^{2+} conditions were statistically insignificant. These speeds corresponded well with the speed measured using equally spaced ROIs (Figure 3.34, Figure 3.35 H) and for further analysis kymographs were used.

All observations in which the TM was left intact were conducted in ES containing 1.3 mM Ca^{2+}. With the TM left attached slow Ca^{2+} waves were found to propagate at 1.44 ± 0.05 µm/s and for 185 ± 11 µm n = 137 waves, 4 cochleas in the Deiters' cell region and 2.48 ± 0.07 µm/s; 136 ± 7 µm n = 96, 3 cochleas in the IS. The speed difference between slow Ca^{2+} waves in the Deiters' cell region and the IS was highly statistically significant (Figure 3.35 H, P = 9.8e-27). Propagation distance was found to be

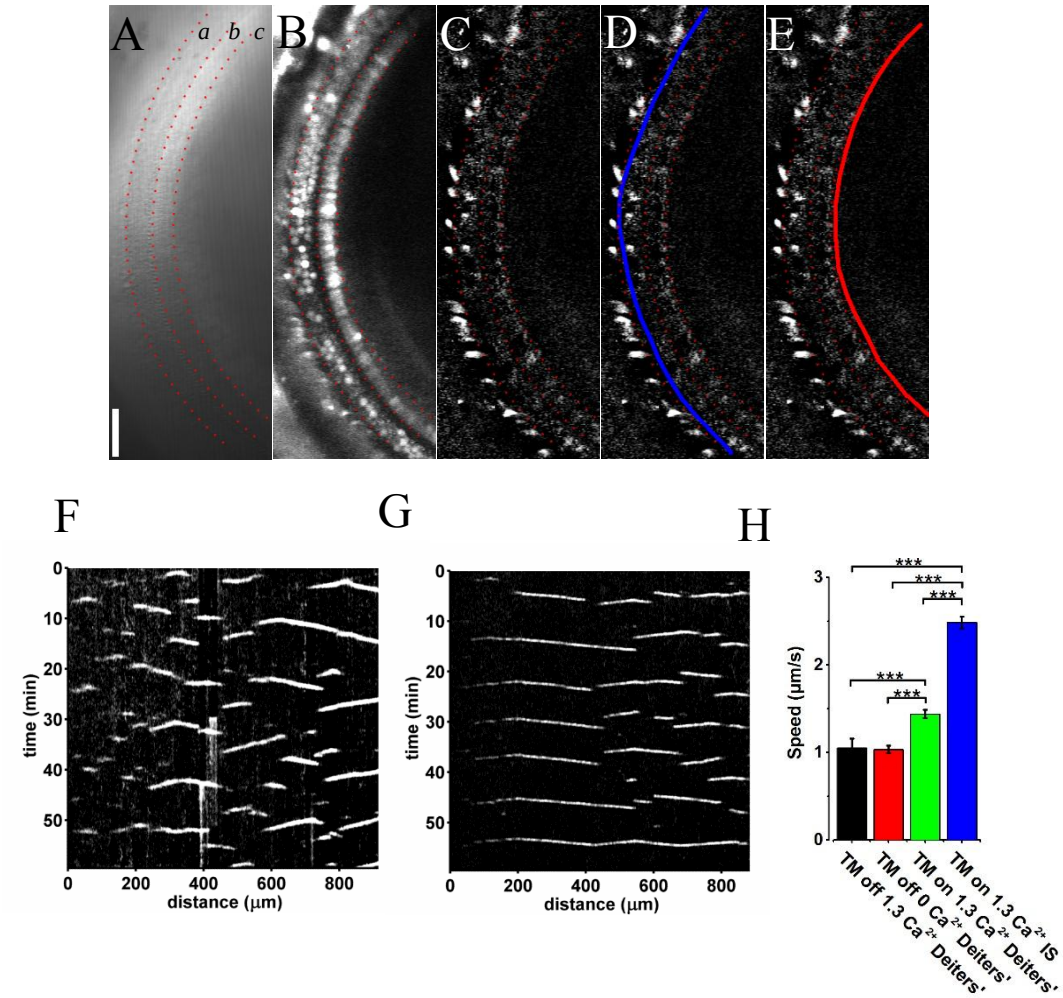

Figure 3.35 Properties of Ca^{2+} waves in the organ of Corti can be captured in kymographs.
(A) Transmitted light view of the Fluo4-AM loaded organ of Corti, the areas between the red dashed lines correspond to: *a* – The Deiters' cell region, *b* – IHCs, *c* – IS cells. **(B)** Same view as in (A) after evoking fluorescence. Inner and outer hair cells can be readily discerned as they have higher nominal fluorescence levels than surrounding supporting cells (See Figure 3.4). **(C)** Background fluorescence was subtracted. **(D)** Pixel values were measured along a line in the Deiters' cell region (blue) and in the IS (red) **(E)**. **(F, G)** Kymographs were constructed using the pixel values found along the lines shown in (D) and (E). **(H)** Wave propagation speed was plotted for different extracellular Ca^{2+} concentrations, different organ of Corti regions and in the presence and absence of the TM. Kruskal-Wallis ANOVA, ***$P < 0.001$. Scale bar: 100 μm.

significantly higher (P = 6.4e-5) in the Deiters' cell region. A significant difference in slow wave speed was observed in the Deiters' cells region between cochleas with an intact TM in solution with 1.3 mM extracellular Ca^{2+} and without the TM both when Ca^{2+} was omitted (P = 1.2e-7) and present at 1.3 mM in the ES (P = 2.6e-5). Propagation distance tended to be increased in the Deiters' cell region when the TM was left intact when compared to low Ca^{2+} no TM conditions (P = 0.10) and was

significantly higher with an intact TM compared to 1.3 mM Ca^{2+}, no TM conditions (P = 0.024). A significant difference was also found between wave travel distance in the Deiters' cell region and IS (P = 6.4e-5).

Region and extracellular Ca^{2+}	***Speed***	***Distance***
Deiters' cell region, 0 Ca^{2+}	1.04 ± 0.04	148 ± 9
Deiters' cell region, 1.3 Ca^{2+}	1.05 ± 0.1	130 ± 8
Deiters' cell TM on 1.3 Ca^{2+}	1.44 ± 0.05	185 ± 11
IS cell region, TM on 1.3 Ca^{2+}	2.48 ± 0.07	136 ± 7

Table 3.2 Wave travel speed and distance measured from kymographs.
TM – tectorial membrane

3.3.4 Slow Ca^{2+} waves have properties which are different from other Ca^{2+} signalling events in the organ of Corti

The slow Ca^{2+} wave parameters detailed above were measured manually from kymographs. To gain a better and more impartial view of the distribution of Ca^{2+} wave speeds and travel distances kymographs were analysed in MATLAB (detailed in section 2.6.9) and the results of this analysis for the Deiters' and IS regions when the TM was left intact are shown in (Figure 3.36). Scatter plots showing wave travel distance plotted against wave duration and wave speed, together with histograms showing the distribution of wave speeds for automatically detected waves have all been constructed.

Scatter plots showing wave travel distance plotted against wave duration could be best fit with a linear function of a slope of 1.3 ± 0.02 µm/s for the Deiters' cell region and 2.6 ± 0.05 µm/s for the IS (Figure 3.36 A, B).

In accordance the speeds of the detected waves cluster at values below 2 µm/s in the Deiters' cell region and between 2-3 µm/s in the IS region as shown in (Figure 3.36 B, C). These values corresponded closely to the measured speed of slow Ca^{2+} waves of 1.44 ± 0.05 µm/s and 2.48 ± 0.07 µm/s in these regions respectively (Detailed in section 3.3.3). All further detection of Ca^{2+} wave parameters was done automatically unless stated otherwise (as described in section 2.6.9).

In the scatter plots waves traveling considerably faster than slow Ca^{2+} waves (above 5 µm/s) are also visible. These constituted ~ 4 % and ~ 10 % of waves in the Deiters' and IS cell regions respectively. Their initiation correlated with loss of fluorescent signal from OHCs and their spread was found to decrease after addition of the purinergic receptor antagonists PPADS (pyridoxalphosphate-6-azophenyl-2',4'-disulfonic acid) (50 µM) and suramin (150 µM) to the ES (described in detail in section 3.3.9). These types of Ca^{2+} waves will be from hereby termed fast Ca^{2+} waves to differentiate them from slow Ca^{2+} waves. Indeed laser-induced damage (described in detail in section 3.3.10) elicited fast Ca^{2+} waves with similar properties.

Spontaneous increases in $Ca^{2+}{}_i$ levels were also found to occur occasionally in Hensen's cells. The oscillations in these cells appeared to be independent of slow Ca^{2+} waves. The periodicity of these oscillations was variable and on average they had a frequency of 12.2 ± 1.3 per hour. The mean interval between oscillations in minutes in cells in which multiple oscillations was observed was 7.4 ± 0.7 and the SD of the mean intervals in individual cells was found to be 3.3 ± 0.4, n = 54 cells.

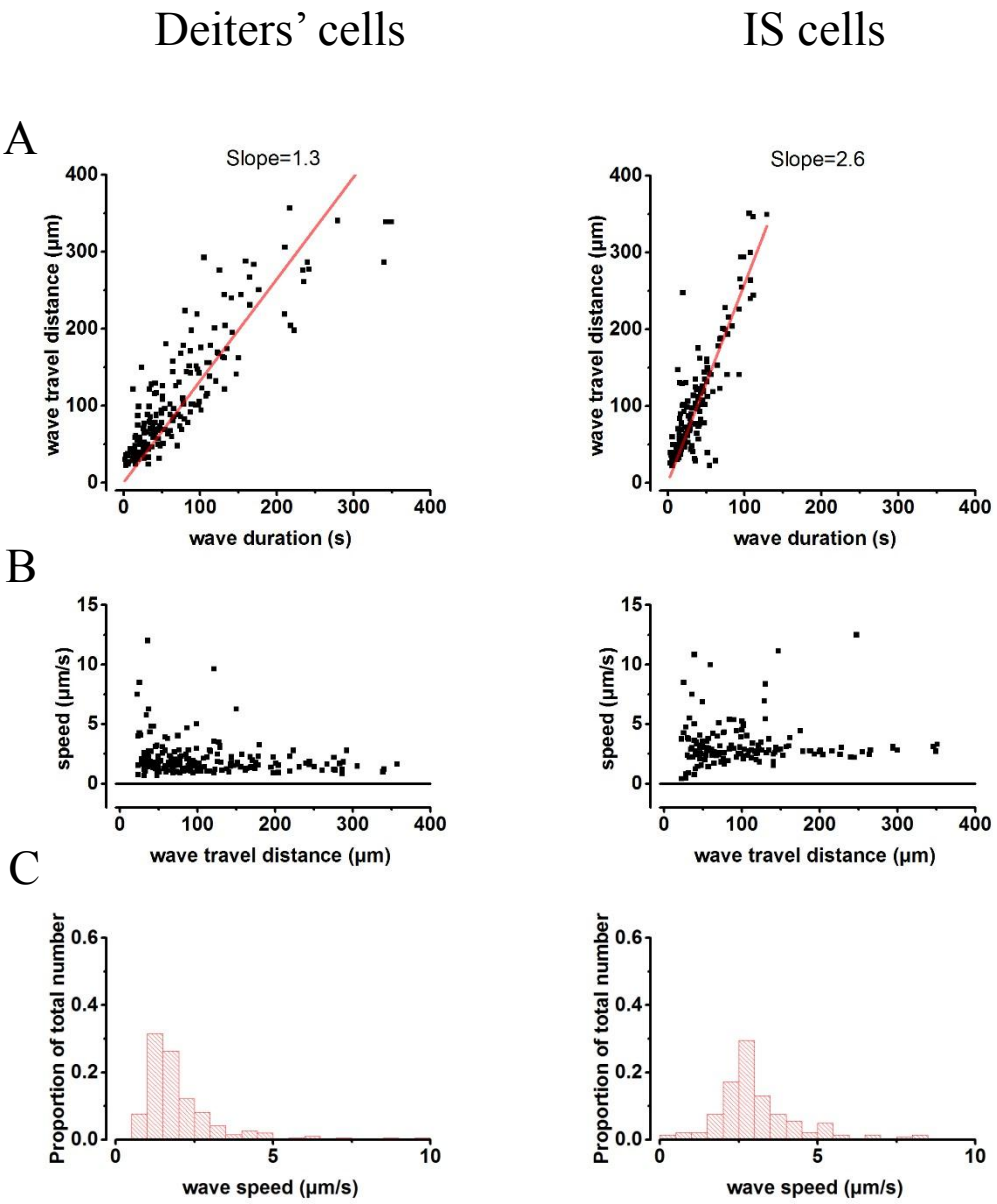

Figure 3.36 The majority of the detected Ca^{2+} waves traveled at a speed below 5 µm/s.

(A) Wave travel distance was plotted against wave travel duration for the Deiters' cell region (left) and IS region (right). Scatter plots were best fit with a linear function of a slope of 1.3 and 2.6 respectively (R-squared > 0.9 in both cases). **(B)** Scatter plots showing wave speed plotted against wave travel distance for the data shown in (A). **(C)** Histograms showing the distribution of wave speeds in both regions.

3.3.5 Slow Ca^{2+} are not dependent on extracellular ATP

To determine if the spread of slow Ca^{2+} waves depended on extracellular ATP release via unpaired gap junction hemichannels extracellular Ca^{2+} levels were increased to 1.3 mM a level believed to close hemichannels. With the TM removed 1.3 mM extracellular Ca^{2+} did not stop slow Ca^{2+} wave signalling in the Deiters' cell region (Figure 3.37, n = 3 cochleas for both control and 1.3 mM extracellular Ca^{2+} groups). The P2 receptor antagonists PPADS (50 µM) and suramin (150 µM) (n = 4 cochleas) also failed to inhibit or stop slow Ca^{2+} wave signalling when the TM was left attached (Figure 3.38 and Figure 3.39, n = 3 cochleas). In both cases the slope of the travel distance and wave duration scatter graphs were similar to that of the control group (Deiters' cell region: slope 1.1 compared to 1.3 for control and IS slope 3.0 compared to 2.6 in the control group).

Slow Ca^{2+} wave signalling also appeared unaffected by the enzyme apyrase (40 U) which catalyzes the cleavage of phosphate from ATP and ADP. In these experiments the TM was removed and Ca^{2+} was omitted from the ES. Under these conditions the slope of the travel distance and wave duration scatter graph of the apyrase treated group was similar to that of the control (Figure 3.40, n = 2 cochleas for the apyrase group and n = 3 cochleas for control).

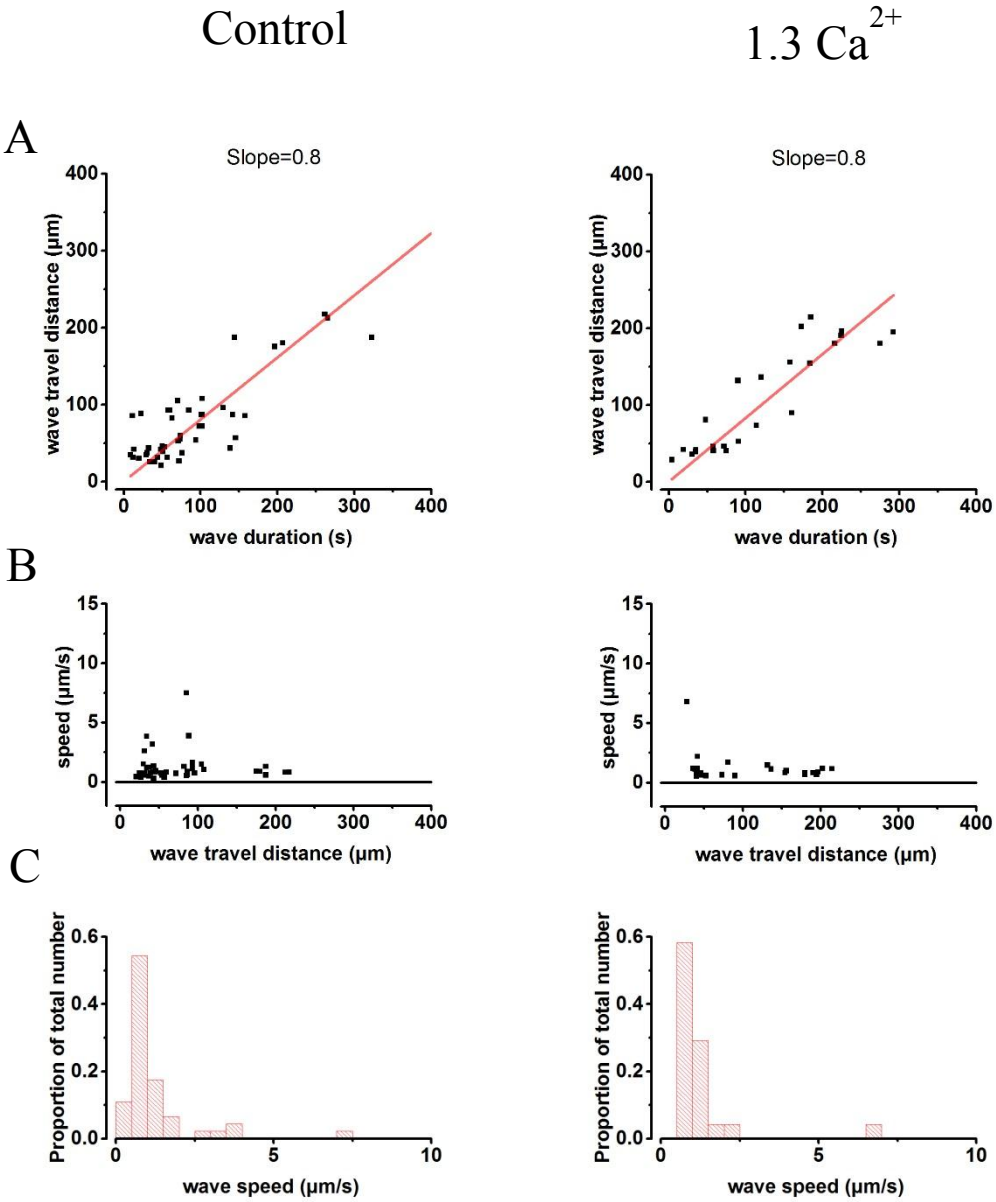

Figure 3.37 Increasing extracellular Ca^{2+} concentration to 1.3 mM does not affect slow Ca^{2+} wave signalling in the Deiters' cells in the organ of Corti.
(A) Wave travel distance was plotted against wave travel duration for the Deiters' cell region when Ca^{2+} was omitted from the ES (left) and with 1.3 mM Ca^{2+} present in the ES (right). Both scatter plots could be best fit with a linear function of a slope of 0.8 (R-squared > 0.9 in both cases). **(B)** Scatter plots showing wave speed plotted against wave travel distance for the data in (A). **(C)** Histograms showing the distribution of wave speeds under both conditions.

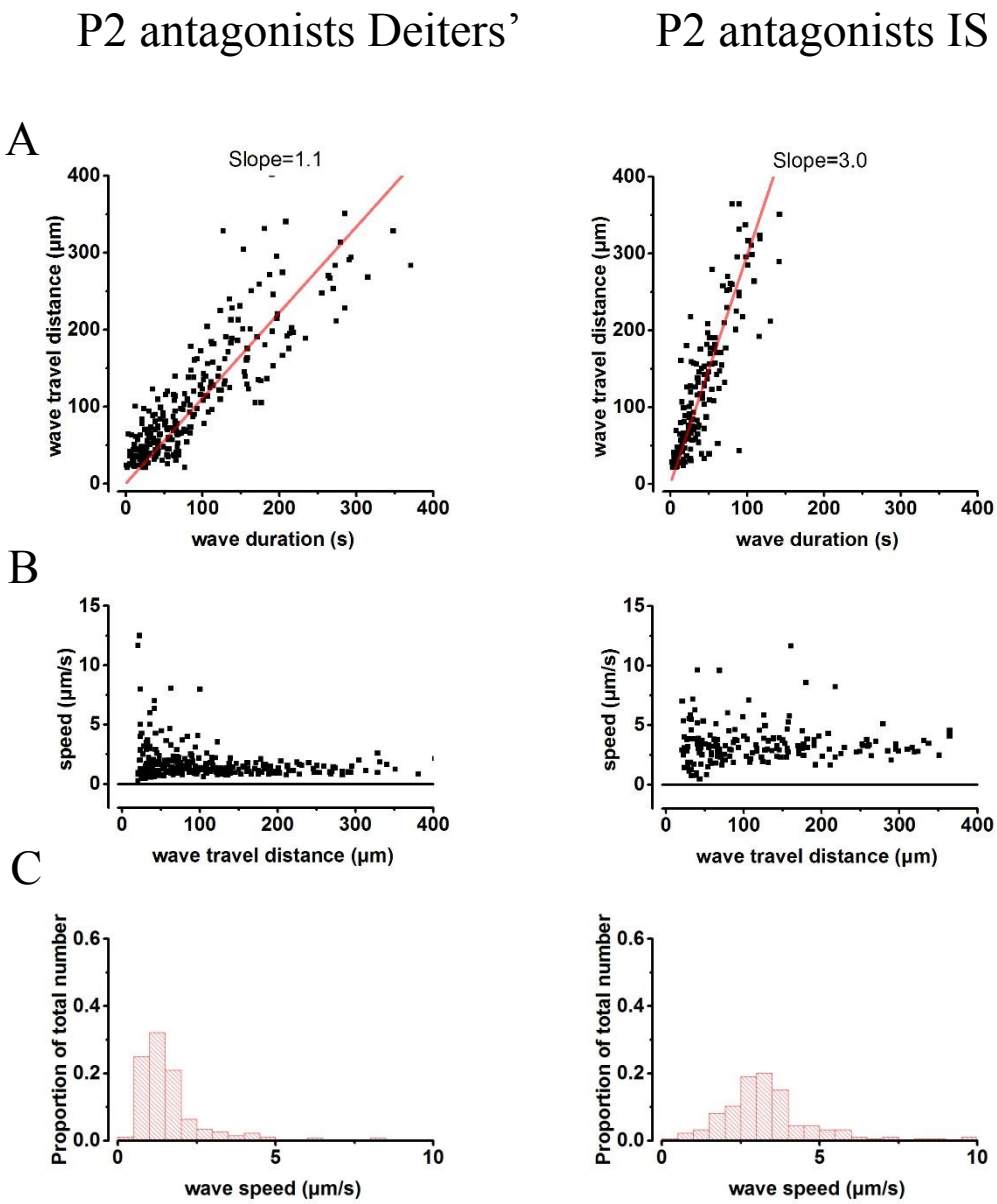

Figure 3.38 P2 receptor antagonists do not inhibit slow Ca^{2+} wave signalling. **(A)** Wave travel distance was plotted against wave travel duration for the Deiters' cell region (left) and IS region (right) in organs of Corti incubated with the P2 receptor antagonists suramin (150 µM) and PPADS (50 µM). Scatter plots were best fit with a linear function of a slope of 1.1 and 3.0 respectively (R-squared > 0.9 in both cases). **(B)** Scatter plots showing wave speed plotted against wave travel distance for the data shown in (A). **(C)** Histograms showing the distribution of wave speeds in both regions.

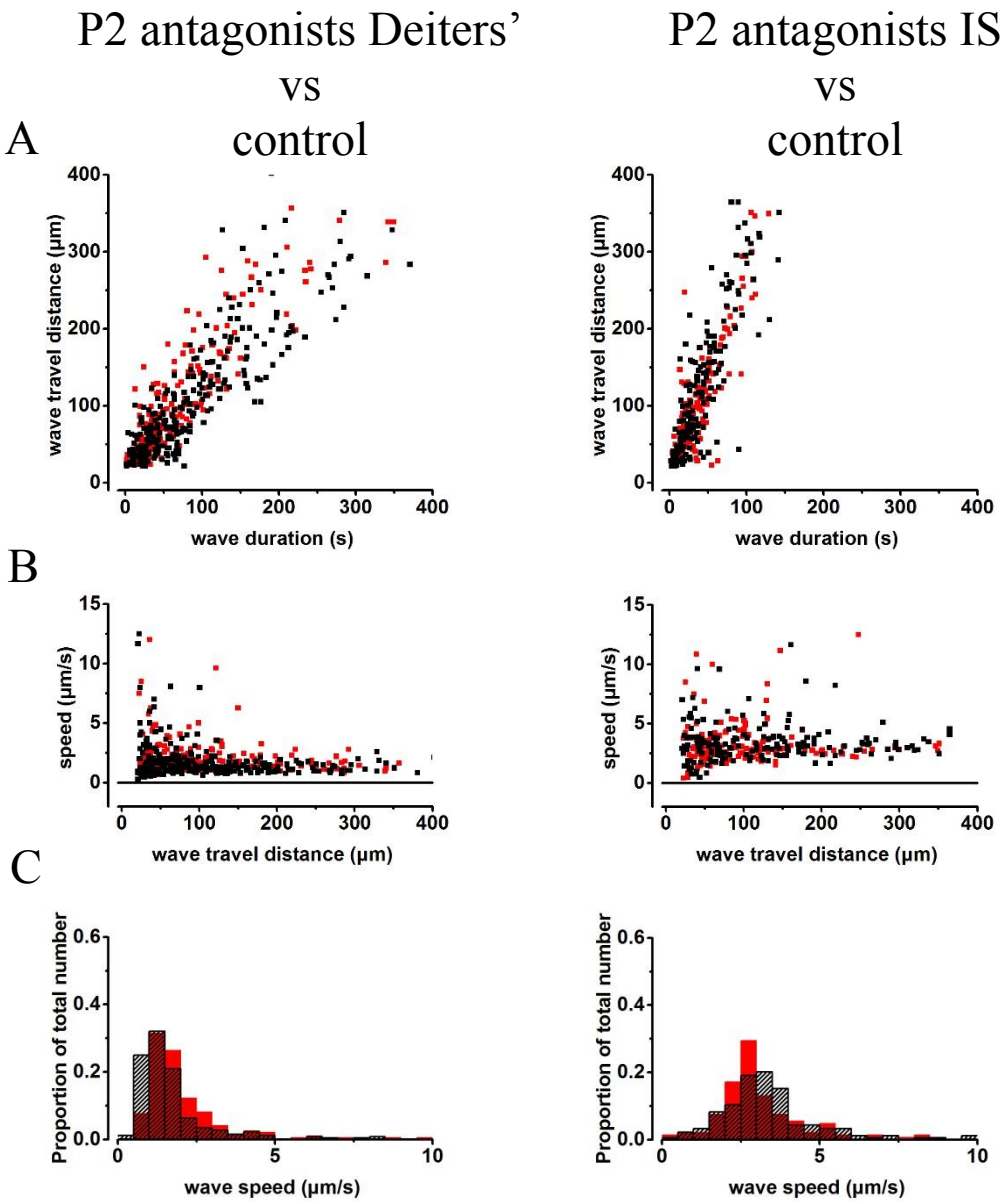

Figure 3.39 P2 receptor antagonists do not inhibit slow Ca^{2+} wave signalling (II).
The Ca^{2+} wave scatter plots **(A, B)** and histograms **(C)** for organs of Corti treated with P2 receptor antagonists shown in Figure 3.38 (black), are shown overlying results obtained under control conditions with no antagonists present (red).

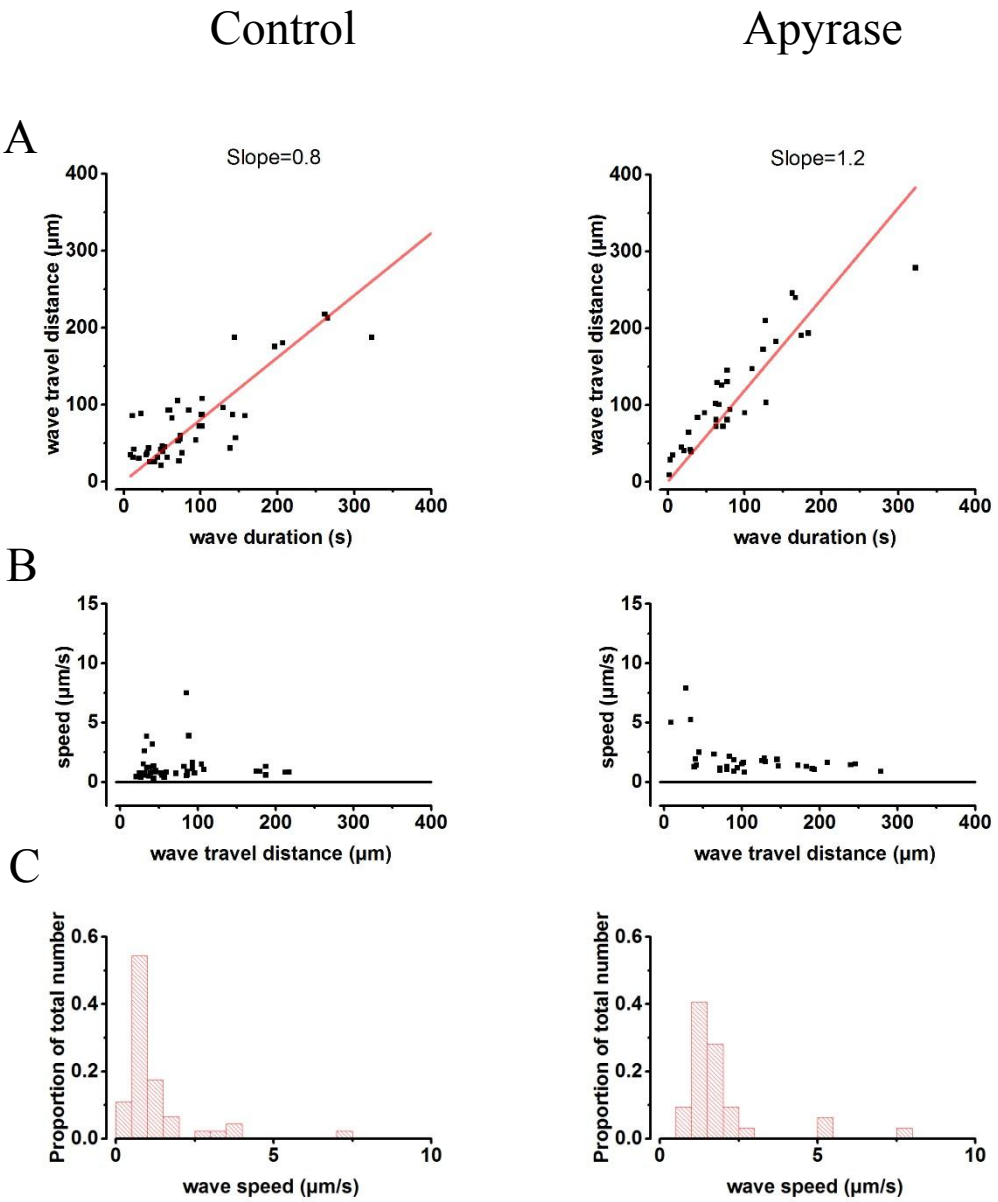

Figure 3.40 Treatment with apyrase does not inhibit slow Ca^{2+} waves in the Deiters' cell region.
(A) Wave travel distance was plotted against wave travel duration for the Deiters' cell region in control conditions (left) and with 40 U of apyrase (right) in the ES. Scatter plots were best fit with a linear function of a slope of 0.8 and 1.2 respectively (R-squared > 0.9 in both cases). **(B)** Scatter plots showing wave speed plotted against wave travel distance for the data shown in (A). **(C)** Histograms showing the distribution of wave speeds in both regions.

3.3.6 Slow Ca^{2+} waves are gap junction mediated

Ca^{2+} waves in the immature organ of Corti have been shown to be mediated by extracellular ATP and to a lesser extent by IP_3 propagation through gap junctions. To determine if slow Ca^{2+} waves required connexins to spread into neighbouring cells, 1 mM 1-octanol, a gap junction blocker was added to the ES. This stopped slow Ca^{2+} wave signalling (n = 3 cochleas). Treatment with the gap junction blocker 100 µM carbenoxolone (CBX) also blocked slow Ca^{2+} waves (n = 3 cochleas) (Figure 3.41). Although oscillations in Ca^{2+}_i levels did not propagate as waves, oscillations in Ca^{2+}_i were still visible in individual Deiters' cells in 2 out of 3 1 mM octanol treated cochleas. Oscillations had a frequency of 6.4 ± 0.7 Ca^{2+}_i increases per hour. The mean interval between Ca^{2+}_i increases was 13.7 ± 1.2 minutes and the mean SD of intervals in individual cells 3.1 ± 0.4 as measured in n = 53 cells. Similar oscillations were also visible in 1 out of 3 100 µM CBX treated cochleas. Upon washout of gap junction blockers slow Ca^{2+} wave signalling recovered.

Connexin 30 has been shown to be the main connexin present in the Deiters' cell region in the mature mouse organ of Corti (Jagger and Forge, 2006). To determine if the observed Ca^{2+} waves were mediated via a connexin dependent process, Ca^{2+} fluorescence was monitored in dissected cochleas from connexin 30 knockout mice. No slow Ca^{2+} waves were observed both when the TM was removed and left intact (Figure 3.42, Figure 3.43 and Figure 3.44 n = 3 cochleas in both cases, n = 6 cochleas in total). Additionally in Cx30 knockout mice Ca^{2+}_i oscillations were visible in individual IS cells in 2 of 3 cochleas when the TM was removed (Frequency 7.0 ± 0.3 Ca^{2+}_i increases/hour, mean interval between increases 12.3 ± 0.7 minutes, mean SD of intervals in individual cells 4.9 ± 0.3, measured in n = 182 cells showing oscillations) and in 1 of 3 cochleas when the TM was preserved (Frequency 8.9 ± 0.7, Interval 9.5 ± 0.8, mean SD of intervals in individual cells 5.4 ± 0.5, n = 59). These oscillations were not synchronized with Ca^{2+}_i oscillations in neighbouring cells and did not spread into neighbouring cells.

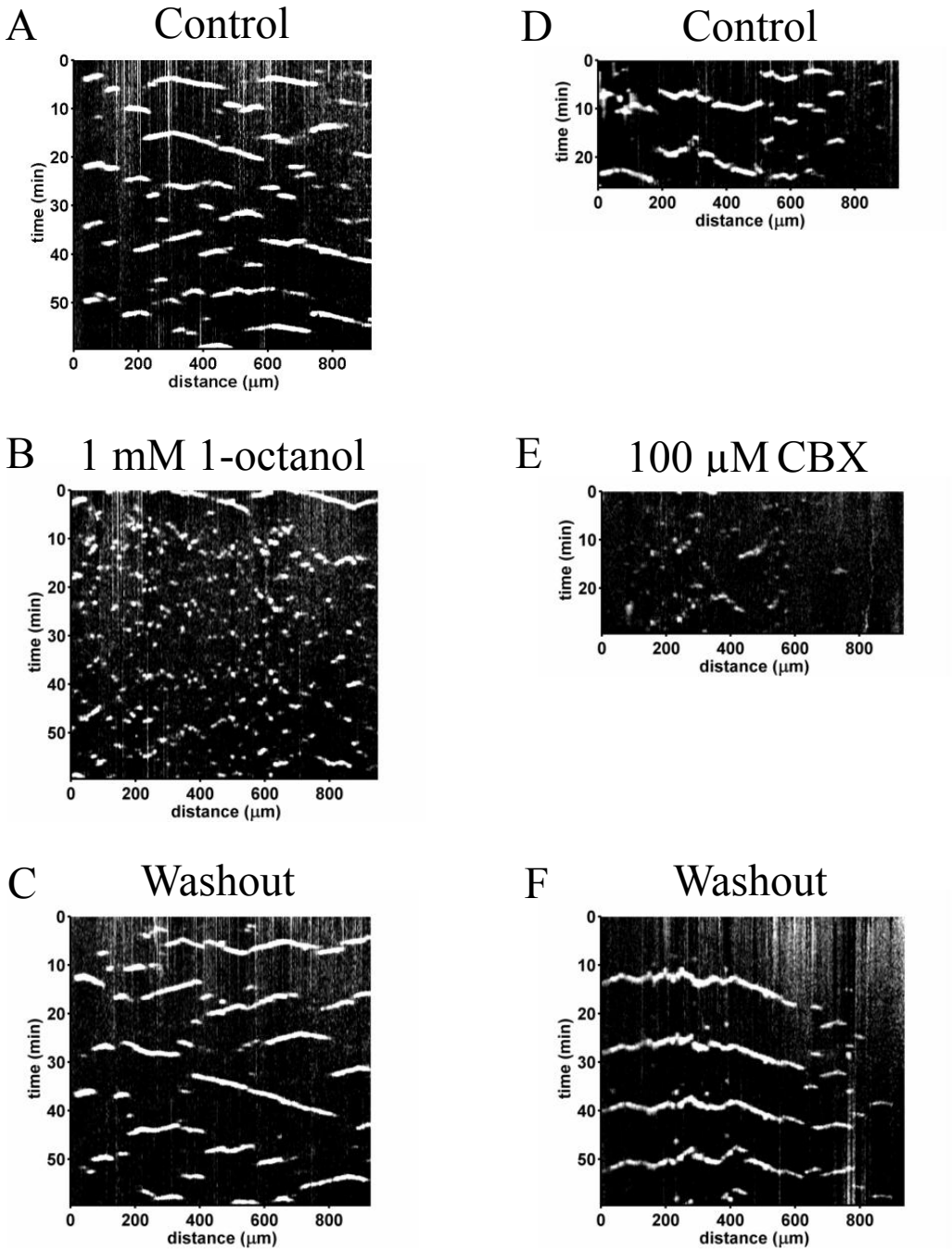

Figure 3.41 Slow Ca^{2+} wave propagation is blocked by gap junction blockers 1-octanol (1 mM) and carbenoxolone (100 µM).
Slow Ca^{2+} waves in the Deiters' cell region before **(A)** and after **(B)** adding 1-octanol to the ES. Slow Ca^{2+} waves were restored after washout **(C)** A similar effect was obtained by adding CBX to the ES **(D-F)**.

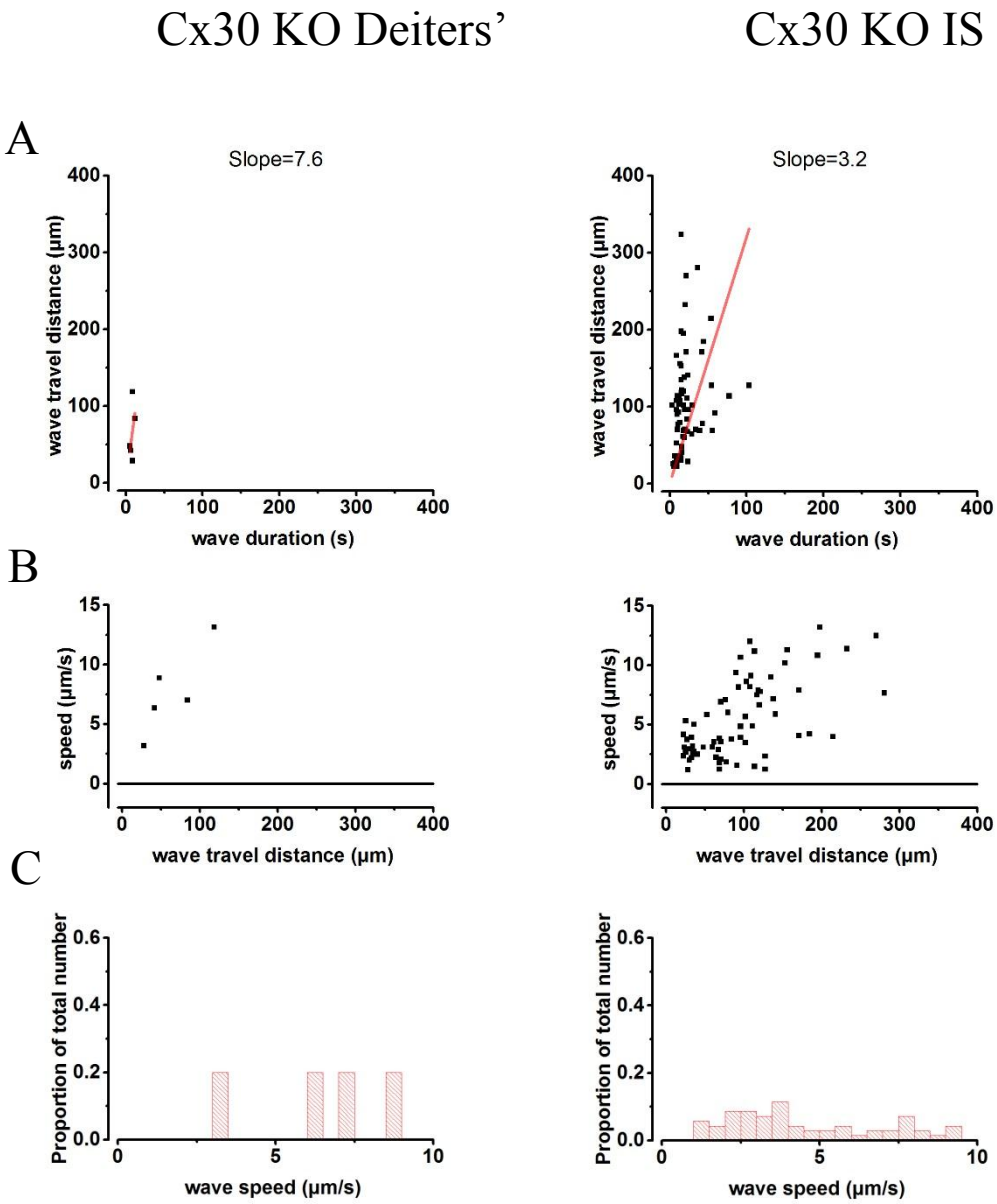

Figure 3.42 Slow Ca^{2+} waves are not present in the organ of Corti of connexin 30 knockout mice.
(A) Wave travel distance was plotted against wave travel duration for the Deiters' cell region (left) and IS region (right) in organs of Corti from connexin 30 knockout mice. Scatter plots were best fit with a linear function of a slope of 7.6 and 3.2 respectively (R-squared equal to 0.9 in the Deiters' cell region and 0.7 in the IS). **(B)** Scatter plots showing wave speed plotted against wave travel distance for the data shown in (A). **(C)** Histograms showing the distribution of wave speeds in both regions. KO – knockout.

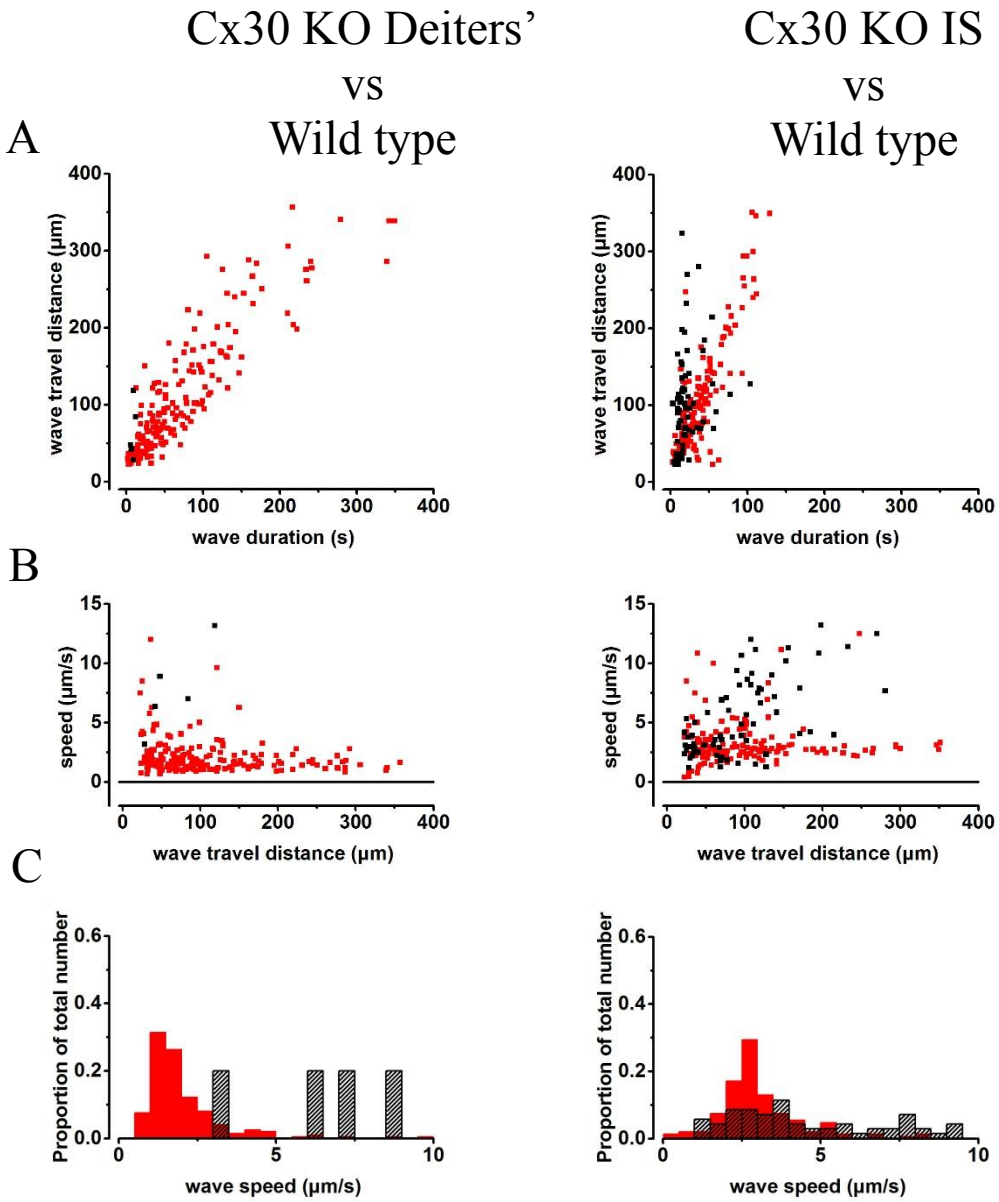

Figure 3.43 Slow Ca^{2+} waves are not present in the organ of Corti of connexin 30 knockout mice (II).
The Ca^{2+} wave scatter plots **(A, B)** and histograms **(C)** for organs of Corti from connexin 30 knockout mice shown in Figure 3.42 (black), are shown overlying results obtained from wild type animals (red). KO – knockout.

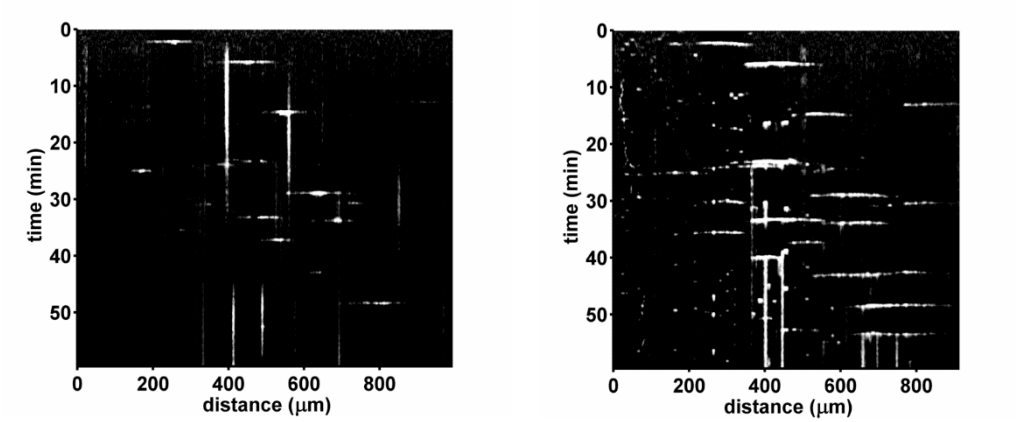

Figure 3.44 Slow Ca^{2+} waves are not present in the organ of Corti of connexin 30 knockout mice (III).
Kymographs were plotted in the Deiters' cell region (left) and the IS cell region (right) after observing fluorescence in the organ of Corti of connexin 30 knockout mice. No slow Ca^{2+} waves are visible. The observed increases in $Ca^{2+}{}_i$ correspond to fast Ca^{2+} waves and $Ca^{2+}{}_i$ oscillations in individual supporting cells.

3.3.7 Slow Ca^{2+} waves are periodic

Slow Ca^{2+} waves repeated in regular intervals (Figure 3.45). This appeared to be similar in different organ of Corti regions (as shown at different points on the x-axis of the kymograph in Figure 3.45). To measure the periodicity of slow Ca^{2+} waves, fluorescence was monitored in multiple 10 x 5 µm ROIs in the Deiters' cell or IS

Region and superfusate	***Wave frequency (waves/hour)***	***Inter-wave interval (minutes)***	***SD of inter-wave interval (minutes)***	***Observation time (min), number of waves & cochleas***
Deiters' cell region, 0 Ca^{2+}	6.4 ± 0.6	10.1 ± 0.8	2.8 ± 0.5	230, 64, 3
Deiters' cell region, 1.3 Ca^{2+}	6.9 ± 0.7	9.6 ± 1.1	2.5 ± 0.9	140, 36, 3
Deiters' cell region, apr.	5.6 ± 0.4	11.3 ± 0.8	2.4 ± 0.4	330, 66, 2
Deiters' cell region, TM on	7.3 ±0.3	8.5 ± 0.3	2.0 ± 0.2	540, 184, 4
IS cell region, TM on	6.3 ± 0.5	11.2 ± 1.3	2.3 ± 0.6	420, 100, 3

Table 3.3 Properties of slow Ca^{2+} waves under various conditions.
Listed is the average wave frequency, average inter-wave interval and average SD of the inter-wave interval as well as the observation time shown in minutes, number of waves used for obtaining parameter information and cochleas used to estimate these values. 0 Ca^{2+} - no additional Ca^{2+} in the ES, 1.3 Ca^{2+} - 1.3 mM Ca^{2+} in ES, apr. – with 40 U of apyrase in ES, no additional Ca^{2+}, TM on – TM left attached and 1.3 mM Ca^{2+} in ES.

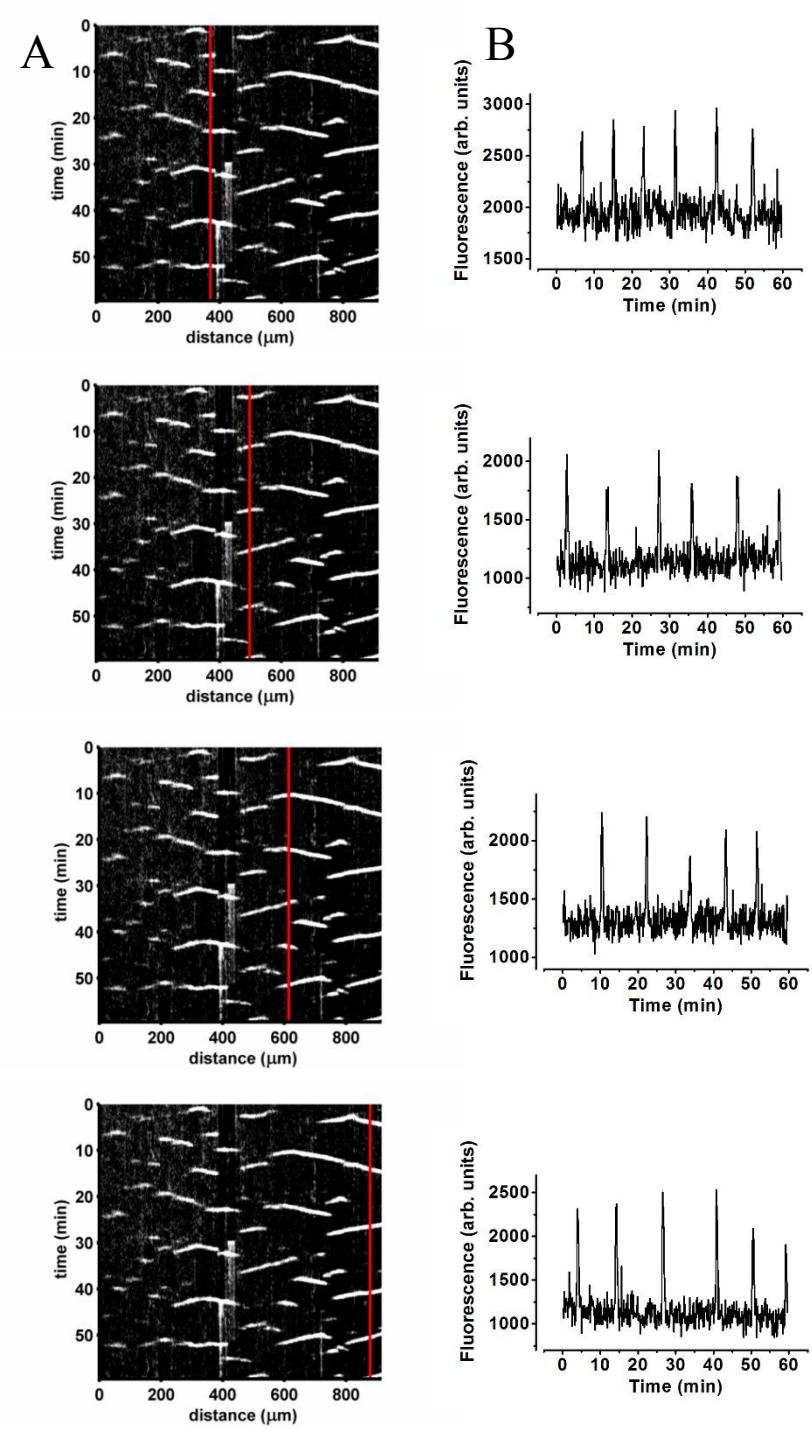

Figure 3.45 The frequency of slow Ca^{2+} waves is similar in different regions of the organ of Corti.
(A) Fluorescence was measured at different locations in the Deiters' cells region of the organ of Corti (red lines) during 60 minutes of observation. **(B)** The resulting fluorescence values were plotted for each location.

regions of Fluo4-AM loaded organs of Corti. Slow Ca^{2+} wave parameters were initially measured in cochleas which had the TM removed and when Ca^{2+} was omitted from the ES. Under such conditions slow Ca^{2+} wave frequency was found to be 6.4 ± 0.6 waves

per hour (3 cochleas, n = 64 waves). The mean inter-wave interval was 10.1 ± 0.8 minutes with the mean SD of the inter-wave interval equal to 2.8 ± 0.5. In total 230 minutes of observation were conducted. For convenience these values for organs of Corti observed under different conditions have been listed in Table 3.3 and plotted in (Figure 3.46). When apyrase (40 U) was added to the ES the frequency of slow waves was not significantly different ($P = 0.28$), the inter-wave interval also did not show a significant difference ($P = 0.31$) (Figure 3.46). Addition of 1.3 mM Ca^{2+} to the ES did

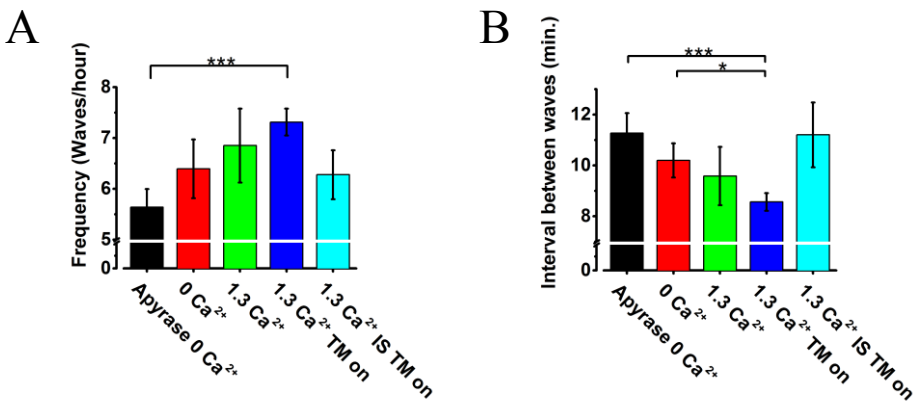

Figure 3.46 Slow Ca^{2+} wave frequencies and slow Ca^{2+} wave inter-wave intervals as measured under different conditions.
(A) The frequencies and **(B)** inter-wave intervals of slow Ca^{2+} for cochleas observed in different conditions and ES Ca^{2+} levels as shown in Table 3.3 were plotted as bar graphs. 0 Ca^{2+} - no additional Ca^{2+} present in ES, 1.3 Ca – 1.3 mM Ca^{2+} in ES, **P*<0.05; ****P*<0.001.

not affect the wave frequency or inter-wave interval ($P = 0.16$ and $P = 0.65$ respectively). Significant differences were present however when cochleas which had the TM removed were compared to cochleas in which the TM was left attached. Wave frequency in the Deiters' cell region was significantly lower in the apyrase treated group when Ca^{2+} was omitted from the ES compared to frequency in Deiters' cells when the TM was left on and with 1.3 mM Ca^{2+} in the ES ($P = 7.8e\text{-}4$), this was also the case for the inter-wave interval ($P = 0.0056$). The inter-wave interval was significantly higher in the Deiters' cell region when the TM was removed and with no additional Ca^{2+} in ES when compared to the Deiters' cell region with the TM intact and with 1.3 mM Ca^{2+} in ES ($P = 0.042$). Finally, wave frequency tended to be increased in the Deiters' cell region when compared to the IS region when the TM was left intact ($P = 0.070$) similarly to the inter-wave interval ($P = 0.060$).

Slow Ca^{2+} wave frequencies were also measured from kymographs (as shown in Figure 3.45 B) to verify the ROI obtained data. When kymographs were used to obtain information about slow Ca^{2+} wave periodicity in cochleas in which the TM was left attached, slow Ca^{2+} wave frequency was measured at 6.8 ± 0.3 waves per hour for the

Region and superfusate	***Wave frequency (waves/hour)***	***Inter-wave interval (minutes)***	***SD of inter-wave interval (minutes)***	***Observation time (min), number of waves & cochleas***
Deiters' cells, control	6.8 ± 0.3	9.1 ± 0.4	1.6 ± 0.2	540, 60, 4
IS cells, control	6.1 ± 0.8	11.0 ± 1.4	3.9 ± 1.3	420, 45, 3
Deiters' cells, P2 antg	7.3 ± 0.8	9.0 ± 0.9	1.6 ± 0.3	650, 67, 3
IS cells, P2 antg	6.9 ± 1.1	12.0 ± 2.5	2.9 ± 0.6	540, 70, 2

Table 3.4 Showing slow Ca^{2+} wave parameters in cochleas in which the TM was left attached.
P2 antg – Both suramin (150 µM) and PPADS (50 µM) were added to the ES. 1.3 mM Ca^{2+} was present in the ES in all groups. The above frequencies were obtained from waves detected on kymographs (as in Figure 3.45 B).

Deiters' cell region and 6.1 ± 0.8 for the IS cell region. This was not a significant difference ($P = 0.49$). The inter-wave interval could be measured at: 9.1 ± 0.4 minutes for the Deiters' cell region and 11.0 ± 1.4 minutes for the IS. The difference was not significant ($P = 0.22$). Measurements were based on n = 60 and n = 45 waves respectively for the Deiters' cells and IS regions. In cochleas treated with PPADS (50 µM) and suramin (150 µM) in which the TM was also left attached wave frequency was found to be 7.3 ± 0.8 in the Deiters' cell region and 6.9 ± 1.1 in the IS. The inter-wave interval was measured at 9.0 ± 0.9 minutes in the Deiters' cell region and 12.0 ± 2.5 in the IS. These values were obtained after analysing n = 67 and n = 70 waves in the Deiters' and IS regions respectively. Neither the wave frequency in the Deiters' cell ($P = 0.52$) and IS regions ($P = 0.57$) nor the inter-wave intervals in the Deiters' cell ($P = 0.95$), and IS regions ($P = 0.74$), were significantly different from the values obtained from P2 antagonist untreated cochleas (Table 3.4).

In all cochleas in which the TM was removed (9 of 9), slow Ca^{2+} waves were already present at the start of observations (approximately 120 minutes post-sacrifice). Leaving the TM intact appeared to delay the onset of slow Ca^{2+} wave signalling as long as the

organ of Corti remained undamaged during the dissection process. For the following measurements the first experimental observations were assumed to take place at 90 minutes post sacrifice to account for the dissection, Ca^{2+} indicator loading and configuring the microscope for experimental observations. To simplify the measurements wave frequency was measured in 60 minute time bins. In 3 cochleas in which the gradual onset of slow Ca^{2+} wave signalling could be observed waves initiated at 170 ± 53 minutes post dissection in the Deiters' cell region and at 190 ± 40 in the IS region (Figure 3.47).

The use of the P2 receptor antagonists PPADS (50 µM) and suramin (150 µM) did not appear to affect the onset time. With these antagonists in the ES in 2 cochleas the onset time of wave signalling in the Deiters' cell region was found to be 180 ± 30 minutes and 210 ± 0 minutes in the IS.

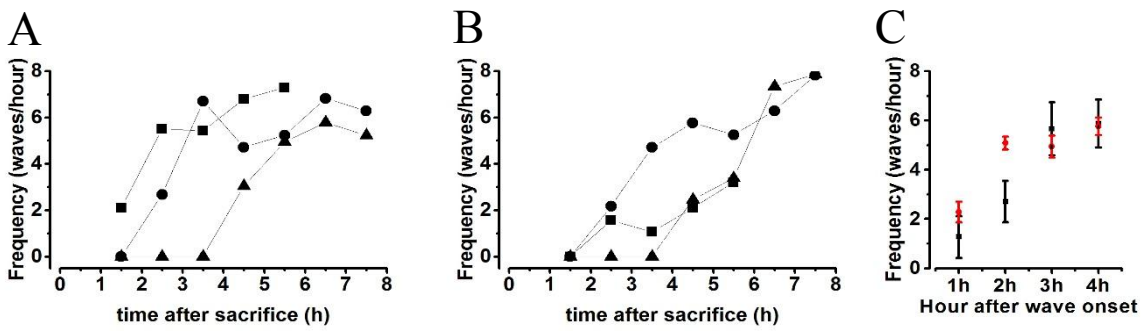

Figure 3.47 Slow Ca^{2+} waves onset is gradual and its frequency does not decrease up to 7 hours post-sacrifice.

(A) The frequency of slow Ca^{2+} waves was plotted at different times post-sacrifice in 3 cochleas in the Deiters' cell region and in 3 cochleas in the IS **(B)**. **(C)** Slow Ca^{2+} wave frequency was determined for every hour after the onset of slow Ca^{2+} wave signalling (red – Deiters' cells region, n = 6 ROIs, in 3 cochleas, black – IS region n = 5 ROIs, 3 cochleas).

In 2 out of 2 cochleas in which a small (< 100 µm) section of the organ of Corti was damaged during the dissection, slow Ca^{2+} waves were found at the start of experimental observations and their frequency did not substantially increase further nor decrease during 3 hours of observation. Furthermore in these damaged cochleas no slow Ca^{2+} waves were observed in the IS. IS Ca^{2+} waves were also absent when the TM was removed (9 of 9 cochleas).

3.3.8 The durations of intracellular Ca^{2+} increases elicited by slow Ca^{2+} waves in the Deiters' and IS cell regions are different

The value of the FW 0.5 of passing slow Ca^{2+} waves was taken from measurements obtained from kymographs for the Deiters' cell and IS regions in cochleas in which the TM was left intact (typical measurements used to obtain FW 0.5 values are shown in Figure 3.45 B). FW 0.5 was found to be 34.7 ± 0.9 seconds in Deiters' cell region (n = 60 waves from 4 cochleas) and 24.1 ± 0.3 seconds for the IS (n = 45 waves from 3 cochleas). This compared to FW 0.5 values of 36.7 ± 2.4 seconds, (n = 18 measurements, 3 cochleas for the Deiters' cells region) and 17.2 ± 0.7 seconds (n = 20 measurements, 3 cochleas) for the IS for the $Ca^{2+}{}_i$ increases elicited by puff application of 100 µM ATP (Figure 3.12), under similar experimental conditions (Same experimental setup sampling rate and magnification). The FW 0.5 measurements for slow Ca^{2+} waves support the hypothesis that the different FW 0.5 values measured during puff application of ATP reflect genuine physiological differences in regulation of $Ca^{2+}{}_i$ homeostasis between the different cell populations. Furthermore such physiological differences could contribute to the different speeds of slow wave propagation in the IS and Deiters' cell regions. Indeed, the ratio of IS to Deiters' cell slow Ca^{2+} wave propagation speed is 1.9, while the Deiters' cells to IS ratios of the FW 0.5 values for slow Ca^{2+} waves and puff application of ATP are 1.4 and 2.1 respectively.

3.3.9 Permeabilisation of hair cells elicits fast extracellular ATP dependent Ca^{2+} waves

Fast Ca^{2+} waves were preceded by loss of fluorescent signal from OHCs most likely due

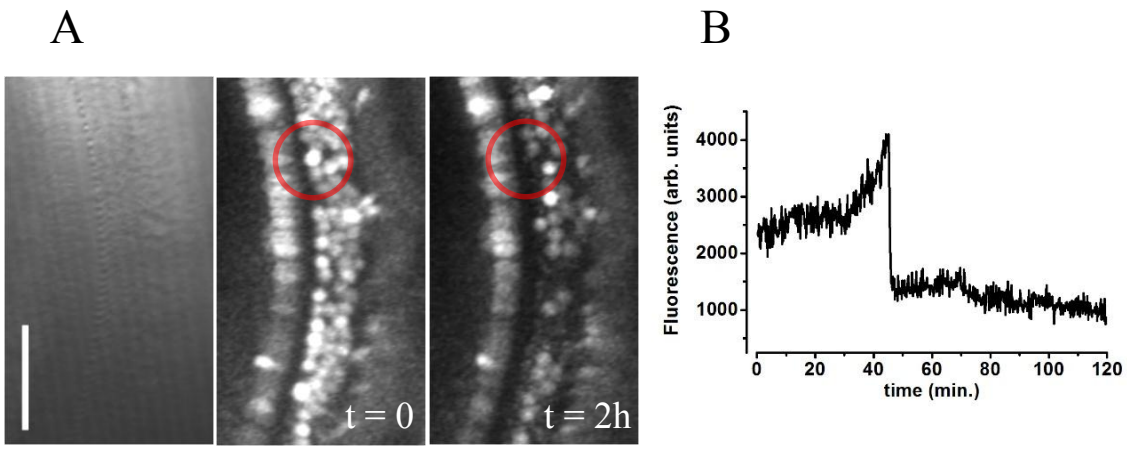

Figure 3.48 Individual OHCs showed fluorescence loss during the course of experimental observations.
(A) Transmitted light (left) and evoked fluorescence views of the organ of Corti at the start of experimental observations (middle) and after 2 hours (right). During this time period several OHCs (one shown in red circle) lost fluorescent signal.
(B) Fluorescence was tracked in a pixel in a single OHC. Fluorescence loss was preceded by an increase in $Ca^{2+}{}_i$ levels. Scale bar is 100 µm.

to permeabilisation of the OHC membrane and washout of the cells content (Figure 3.48). Such waves were initiated by only 5% of OHCs which lost fluorescence, based on measurements on 2 cochleas. The rest of OHCs observed to lose fluorescence did not appear to initiate any Ca^{2+} waves. Each of the observed fast Ca^{2+} waves appeared to be coincident with fluorescence loss from a particular OHC. No factor other then permeabilising cells could be identified as triggering fast Ca^{2+} waves. Fast Ca^{2+} waves could be initiated by ATP released from the permeabilised OHCs cytoplasm. To test this hypothesis the purinergic receptor antagonists suramin (final concentration: 150 μM) and PPADS (50 μM) were added to the ES. P2 receptor antagonists decreased the average distance of fast wave propagation from the permeabilising OHC as measured in the Deiters' cell region from 104.1 ± 12.9 μm, n = 10 fast waves, to 51.8 ± 5.0 μm n = 15 fast waves ($P = 0.0027$). Waves propagated with an average speed of 6.5 ± 1.1 and 10.4 ± 3.8 μm/s ($P = 0.34$). The above measurements were done manually from kymographs. The fast Ca^{2+} waves were not fully inhibited. It is possible that this result is due to the presence of P2Y receptors not sensitive to PPADS or suramin. In Cx30 knockout mice the percentage of permeabilising OHCs triggering fast Ca^{2+} waves appeared larger and was found to be 30% based on measurements in 3 cochleas.

3.3.10 Fast Ca^{2+} waves can be elicited by hair cell photo-ablation

To further determine if permeabilisation of the cells membrane was required to elicit fast Ca^{2+} waves, laser damage to cells in the Deiters' cell region was elicited by using a Ti-Saphire laser at 720 nm (Figure 3.49). Laser-induced damage elicited fast Ca^{2+} waves which spread from the site of damage and into the surrounding supporting cells for distances of on average 130.0 ± 11.0 μm with an average speed of 7.2 ± 0.9 μm/s, n = 13 waves from 2 cochleas when measured manually from kymographs. The difference in the extent of spread of waves elicited by laser-induced damage and the ones observed to originate from permeabilised hair cells could be due to the larger extent of damage elicited by the laser. The Ca^{2+} waves induced by photo-ablation had similar properties to the waves observed in the IS of connexin 30 knockout animals (Figure 3.50).

Interestingly in several instances a fast Ca^{2+} wave appeared to initiate a slow Ca^{2+} wave. This was observed to happen both when fast Ca^{2+} waves were triggered by OHC permeabilisation or laser induced damage (Figure 3.51).

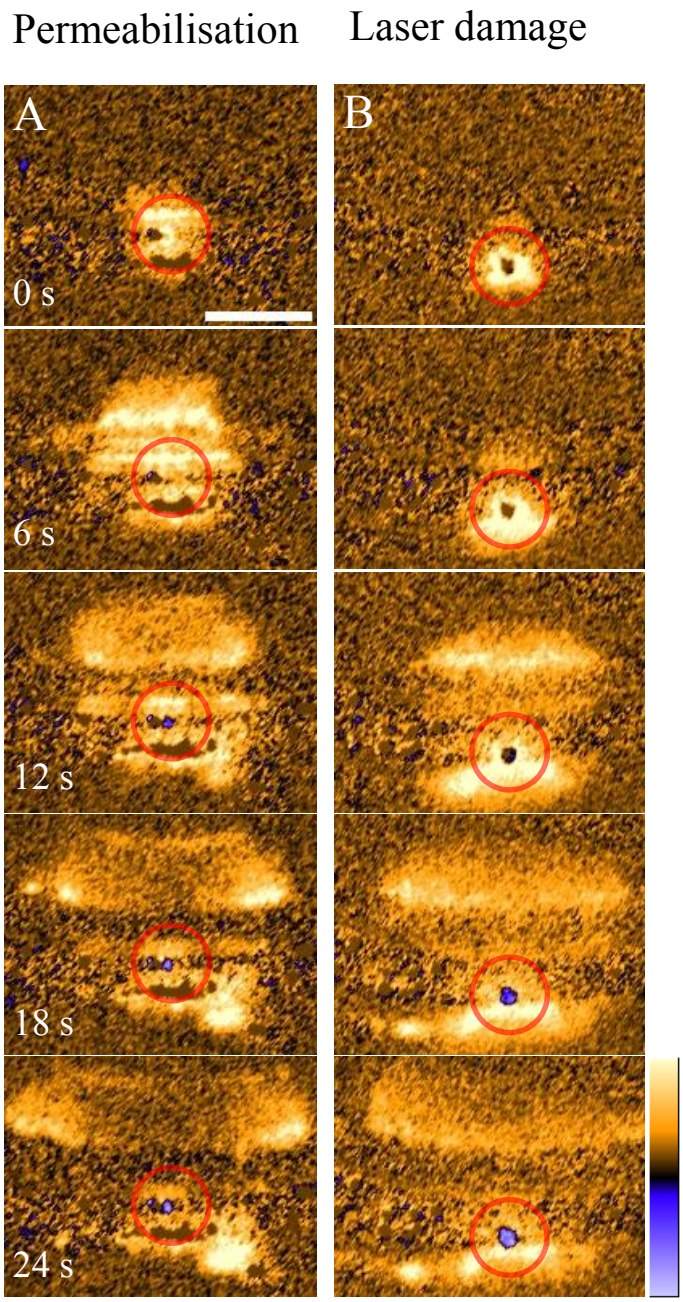

Figure 3.49 Fast Ca^{2+} waves could be replicated by laser induced damage.
(A) A differential image (obtained as outlined in section 2.5.1) showing a fast Ca^{2+} wave (bright yellow) in the organ of Corti which initiated concurrently with permeabilisation and loss of fluorescent signal from an OHC (as shown in Figure 3.48). **(B)** Similar fast Ca^{2+} waves could be initiated by laser induced damage. Note the decrease in fluorescence of the targeted cell (centre of red circle - blue). Colourbar: yellow is increase in fluorescent signal, blue is decrease in fluorescent signal. Scale bar is 100 µm.

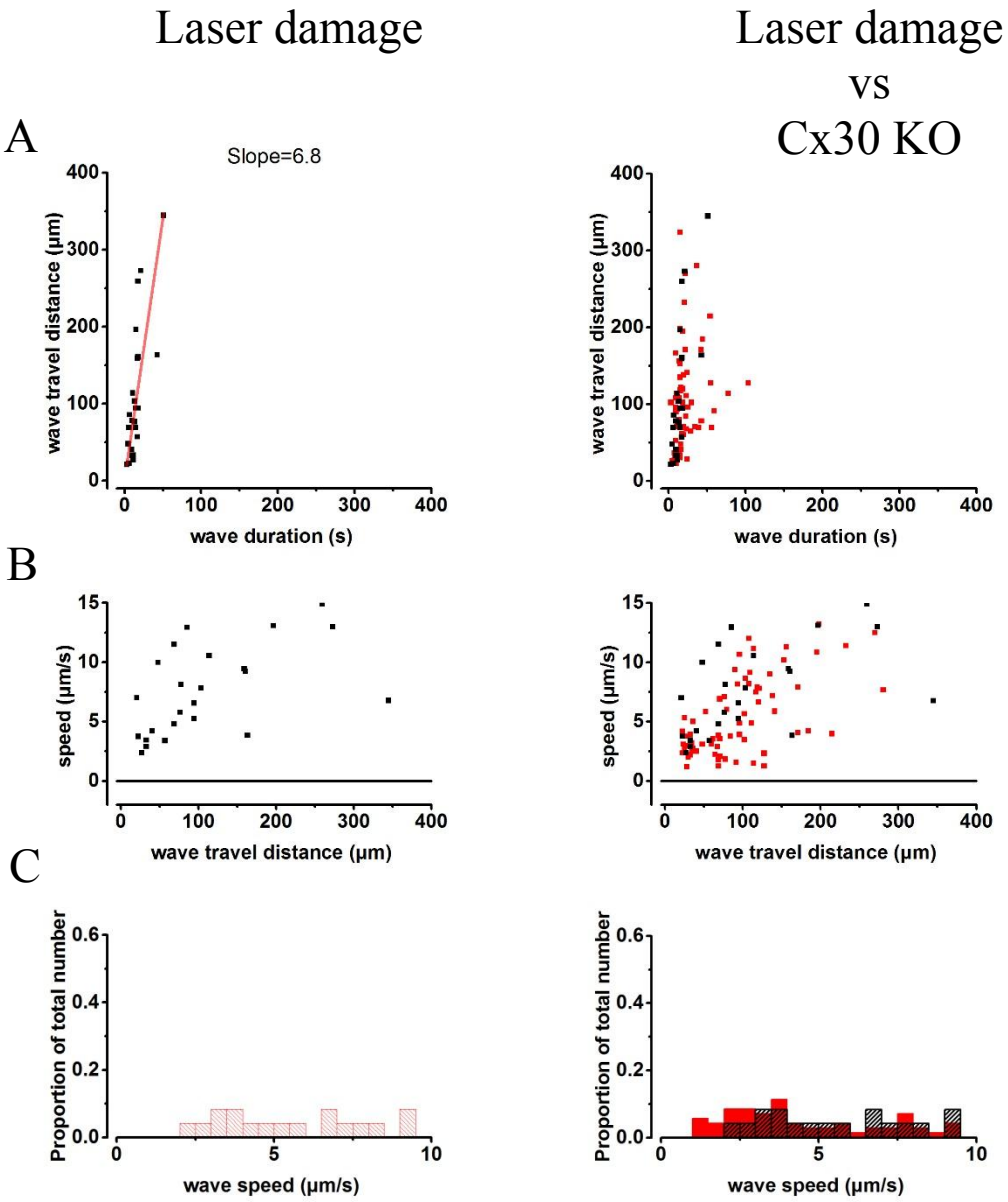

Figure 3.50 IS Ca^{2+} waves evoked by laser damage and Ca^{2+} waves in the IS of connexin 30 knockout mice had similar properties.
(A) Fast Ca^{2+} wave travel distance was plotted against wave travel duration in the IS cell region after targeting cells in the Deiters' cell region with a laser (left, R-squared > 0.9), this plot was overlaid over fast Ca^{2+} wave data obtained for the IS of connexin 30 knockout animals (right, black – waves induced by laser damage, red – connexin 30 knockout animals) **(B)** Scatter plots showing wave speed plotted against wave travel distance for the data shown in (A). **(C)** Histograms showing the distribution of wave speeds for waves induced by laser damage (black) and observed in tissue from connexin 30 knockout mice (red). Cx30 KO – connexin 30 knockout mouse.

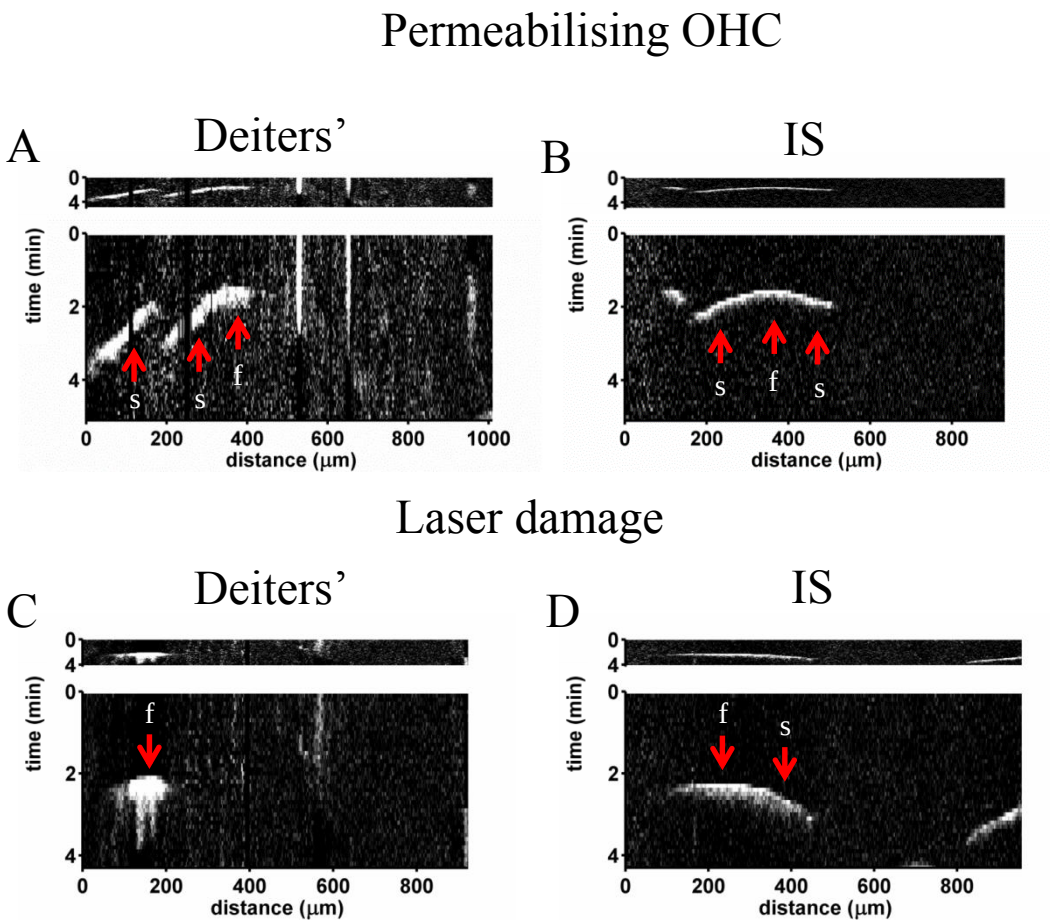

Figure 3.51 Fast Ca^{2+} waves triggered by damage can elicit slow Ca^{2+} waves. Kymographs were created in the Deiters' cell region **(A, C)** standard (upper panel) and stretched (lower panel) and IS region **(B, D)**. Fast Ca^{2+} waves could in some instances induce a slow Ca^{2+} wave in both the Deiters' cell and IS regions (for example: A and B, same permeabilising OHC triggers fast Ca^{2+} waves ('f') in both regions, the fast wave in turn initiates slow Ca^{2+} waves ('s')). The same incident of laser damage induced fast Ca^{2+} waves in both the Deiters' cell and IS cell regions. Laser induced fast Ca^{2+} waves could also trigger slow Ca^{2+} waves. The onset of the fast Ca^{2+} waves coincided with the permeabilisation of an OHC or laser damage. Transition from a fast to slow Ca^{2+} wave coincides with a change in the slope of the waves visible on the kymographs.

3.3.11 Summary of results

Spontaneous extracellular ATP-independent Ca^{2+} waves which propagated along the length of the adult organ of Cort with constant speeds between 1-3 μm/s were observed in the Deiters' and IS cell regions. These waves were found to initiate after animal sacrifice and thereafter repeat periodically with a frequency of approximately 6 waves per hour. Removal of the TM was found to fully stop waves in the IS region. In addition faster Ca^{2+} waves which had an average speed of 6.5 μm/s and were caused most likely

by damage-induced ATP release were found to be present. In some instances such faster waves were found to precipitate the slower extracellular ATP-independent waves.

4 Discussion

4.1 Immunohistochemistry

4.1.1 P2X receptor staining

The $P2X_2$ receptor immunostaining results shown in this thesis are in broad agreement with results of investigations in mice and other animal species (Housley et al., 1998; Huang et al., 2002; Jarlebark et al., 2002). In a mouse $P2X_2$ antiserum peroxidase study the $P2X_2$ receptors were localized to the IS, tops of Deiters' and Hensen's cells. Low expression was found in IHCs (Jarlebark et al., 2002).

Rat $P2X_2$ mRNA was found to have a similar distribution (Housley et al., 1998). $P2X_2$ receptor mRNA was found in IS cells and organ of Corti supporting cells. Moderate $P2X_2$ receptor mRNA levels were detected in OHCs in the basal turn. IHCs showed very little $P2X_2$R mRNA staining.

P2X receptors have also been localized to Deiters', Hensen's and the apex of inner and outer hair cells electrophysiologically (Sugasawa et al., 1996b). In IHCs ATP was shown to activate only small currents, which were not present in all IHCs tested (Jarlebark et al., 2002; Tritsch and Bergles, 2010). ATP did not evoke any response in IHCs in the current study, however only cells of the apical cochlear turn could be accessed. Low currents could be present in other cochlear regions as $P2X_2$ receptor expression in the guinea pig was found to vary along the tonotopic axis and was higher in hair cells of the basal cochlear turn (Housley et al., 1998; Raybould and Housley, 1997).

Altogether the pattern of $P2X_2$ receptor staining obtained in this study indicates that in mice $P2X_2$ expression is present mostly in supporting cells. Stereocilliary $P2X_2$ staining could not be verified functionally. A novel observation is that $P2X_2$ receptors might be found below the cuticular plate in the perilymph facing membranes of supporting cells. Taken together the immunohistochemistry results clearly demonstrate that $P2X_2$ receptors are broadly distributed in cochlear supporting cells among them IS cells, while hair cells show $P2X_2$ receptor staining limited mostly to the stereocilia.

4.1.2 P2Y receptor staining

In the current study $P2Y_2$ and $P2Y_4$ receptor staining showed a broad unspecific distribution. An exception were the membranes of OHCs which showed clear $P2Y_2$ staining. However $P2Y_2$ staining was still broad in other regions of the cochlea.

Unfortunately as P2Y receptor staining appeared unspecific conclusions based on the obtained results can only be limited.

In an immunohistochemistry study by (Huang et al., 2010) $P2Y_2$ receptor staining was limited in the adult rat organ of Corti to the pillar cells and did not show a broad distribution. No OHC membrane $P2Y_2$ staining was present. Instead moderate $P2Y_4$ receptor staining was found in the IHCs and OHCs. Additionally weak $P2Y_4$ staining was present in the pillar cells. In an immunohistochemical study on the guinea pig $P2Y_4$ was found distributed in many different cochlear cell types, however staining appeared strongest in Hensen's and the outer row of Deiters' cells (Parker et al., 2003).

Altogether the distribution of $P2Y_2$ and $P2Y_4$ receptors shows more interspecies heterogeneity then that of the $P2X_2$ receptor. Of note was the presence of $P2Y_2$ receptors in the OHC membrane found in the current study. Indeed, ATP has been shown to decrease the cochlear microphonic (CM) chiefly a measure of OHC function (Munoz et al., 1995; Patuzzi et al., 1989). This change is thought to be mostly the result of P2Y receptor stimulation as it is not affected by the P2X receptor antagonist PPADS (Bobbin and Salt, 2005). Thus this study provides further evidence that the function of OHCs could be affected by ATP through P2Y receptor stimulation.

4.2 Intracellular Ca^{2+} imaging

4.2.1 Resting intracellular Ca^{2+} levels in organ of Corti cells

The Ca^{2+}-imaging results obtained in this study indicate that resting $Ca^{2+}{}_i$ concentration in cochlear hair cells might be significantly higher than the $Ca^{2+}{}_i$ levels found in organ of Corti supporting cells. The high Ca^{2+} indicator signal observed in hair cells could be also the result of more Ca^{2+} indicator permeating into hair cells. This issue could be resolved by using a ratiometric Ca^{2+} dye. The higher hair cell Ca^{2+} signal is not due to cell permeation and Ca^{2+} influx from the extracellular environment as a significant fraction of the Ca^{2+} indicator remained unbound and cell depolarization increased fluorescence levels. Cell permeation would also result in washout of the Ca^{2+} dye. These observations indicate that extracellular ATP should still increase IHC $Ca^{2+}{}_i$ levels if P2 receptors are present. OHCs were also observed to show a higher Ca^{2+} dye signal in this study. Other investigators have found that OHCs show elevated $Ca^{2+}{}_i$ levels when compared to surrounding supporting cells (Yuan et al., 2010). The importance of the increased $Ca^{2+}{}_i$ in hair cells remains unclear. The resting $Ca^{2+}{}_i$ levels measured by (Yuan et al., 2010) are however similar to $Ca^{2+}{}_i$ levels measured by other investigators

in isolated guinea pig OHCs (Ikeda et al., 1991; Szucs et al., 2006b). This might indicate that these are indeed physiological resting Ca^{2+}_i levels. In accordance OHCs show high levels of Ca^{2+} buffers, which are thought to play an important role in regulating adaptation of the MET channel and OHC membrane potential via Ca^{2+}-activated K^+ channels (Hackney et al., 2005). Even less is known about the importance of resting Ca^{2+}_i levels in supporting cells. This area warrants further investigation as differences in supporting cell Ca^{2+}_i homeostasis mechanisms became apparent during the course of this study (discussed in section 4.2.3).

4.2.2 Extracellular ATP increases intracellular Ca^{2+} and elicits currents in supporting cells but not IHCs

In agreement with the lack of IHC $P2X_2$ staining apart from the stereocilia and lack of Ca^{2+}_i increase in IHCs upon ATP application no ATP-activated currents were detected when conducting whole cell electrophysiological recordings from IHCs. Complete lack of ATP-activated currents was however unexpected. $P2X_2$ receptor immunohistochemical staining was found in the current and other studies in hair cell stereocilia (Housley et al., 1999). Furthermore electrophysiological evidence for P2X receptors at the apex of guinea pig hair cells exists (Housley et al., 1992; Sugasawa et al., 1996b).

The removal of the TM could possibly damage the IHC stereocilia and thus result in the lack of ATP-activated currents. Another possibility is that the P2 receptors in stereocilia do not form functional channels. Multiple $P2X_2$ splice variants have been localized to the cochlea (Brandle et al., 1997; Chen et al., 2000; Housley et al., 1995). Proteins can have different roles depending on how they are spliced and where they are located (Huberts and van der Klei, 2010). Thus the $P2X_2$ receptors located in the hair cell stereocilia might not necessarily act as ion channels. Seemingly non-functional $P2X_2$ mRNA transcripts have indeed been isolated (Lynch et al., 1999). These did not form functional channels when transfected into oocytes even though they were found to form a considerable percentage of the total detected transcript number (Lynch et al., 1999).

Overall the Ca^{2+}_i imaging data is mostly consistent and in agreement with the immunohistochemistry and indicates that at the apex of the mouse cochlea P2X receptors appear to be present mostly in cochlear supporting cells and possibly in IHC stereocilia.

4.2.3 Differences in intracellular Ca^{2+} homeostasis between cochlear supporting cells

The observed differences in the values of FW between supporting cells appear to be the result of genuine differences in physiology and mechanisms governing Ca^{2+} homeostasis in the different cochlear supporting cell types. Such differences have also been observed in cochlear cultures from the neonatal cochlea, in which some cells were more prone to ATP induced $Ca^{2}{}_{i}$ oscillations (Majumder et al., 2010; Piazza et al., 2007). The importance of variability in $Ca^{2+}{}_{i}$ homeostasis in cochlear supporting cells has been demonstrated in Kölliker's organ, in which spontaneous $Ca^{2+}{}_{i}$ increases might play an important role in precipitating the spontaneous spiking observed in immature IHCs (Tritsch et al., 2007). No such spontaneous activity has been observed in other regions of the neonatal cochlea.

One possibility which should be mentioned is that due to the topology of the organ of Corti ATP from the puff pipette would reach the IS region at a lower concentration than Deiters' cells or Hensen's cells. Although this argument cannot be wholly discarded if this was the case the FW 0.5 of the $Ca^{2+}{}_{i}$ increase in IS cells should show a higher standard deviation because of the variability in the position of the puff pipette. No such increase was detected. Additionally in some recordings the overall magnitude of the $Ca^{2+}{}_{i}$ increase in IS cells is higher than in the same recording in Deiters' cells, but FW 0.5 still remains shorter. Finally, in kymographs showing slow Ca^{2+} waves the $Ca^{2+}{}_{i}$ increase elicited by a passing wave is briefer in the IS when compared to Deiters' cells. This difference could also partially or wholly underlie the observed difference in speeds of Ca^{2+} wave propagation (section 3.3.3), although other factors such as variation in different connexin subtype permeability to intracellular messengers could also play a role. Altogether the differences in the values of the FW 0.5 appear to reflect genuine differences in $Ca^{2+}{}_{i}$ homeostasis mechanisms in the different cochlear supporting cell types.

4.2.4 Two receptor populations are present in the organ of Corti

$P2Y_2$ and $P2Y_4$ receptors have a lower EC_{50} (typically 1 – 2 μM) for ATP then $P2X_2$ receptors (15 – 60 μM) (Bogdanov et al., 1998; Brake et al., 1994; Godecke et al., 1996; Lustig et al., 1993; Navarro et al., 2011; Suarez-Huerta et al., 2001).

These differences could be verified experimentally and above a certain distance from the puff pipette at which the agonist concentration was sufficiently diffuse the $Ca^{2+}{}_{i}$

increase was similar when stimulating only P2Y receptors and both P2X and P2Y. Together with the observed sensitivity to UTP and ATP in low extracellular Ca^{2+} conditions these observations indicate that at least two populations of ATP receptors are present in the adult organ of Corti with characteristics consistent with them belonging to the P2X and P2Y families.

4.3 Electrophysiology

4.3.1 P2 receptor dependent gap junction regulation

In coupled IS cells puff application of ATP evoked inward currents consistent with the presence of P2X receptors. The resting membrane conductance did not immediately return to pre-ATP application levels and stabilized for a limited time at a new higher level. Similar changes in resting membrane conductance after ATP application have been described in studies on *in situ* guinea pig Deiters and Hensen's cells (Lagostena et al., 2001; Lagostena and Mammano, 2001). The change in resting membrane conductance has been ascribed to a Ca^{2+}_i dependent closure of gap junctions (Lagostena et al., 2001). Indeed in the experiments described herein Ca^{2+}_i increased after stimulation with ATP. However Ca^{2+}_i recovered to resting levels sooner than the resting membrane conductance and SD of the differential image (FW 0.5 ~20 seconds for extracellular ATP Ca^{2+}_i fluorescence compared to ~50 seconds for SD changes). Thus the opening of gap junctions after the return of Ca^{2+}_i to resting levels appears to be delayed and does not support a simple direct relationship between gap junction open state and Ca^{2+}_i levels. Indeed studies have found that the effect of Ca^{2+} on gap junctions is most likely mediated by calmodulin (CaM) (reviewed in (Peracchia, 2004)).

The time course of the changes in membrane conductance correlated better with the time course of the ATP induced cytoplasmic changes in the IS, then the duration of the Ca^{2+}_i increase. The cytoplasmic changes were found to be mediated mostly through P2X receptors activation and were absent when selectively stimulating P2Y receptors with 100 µM UTP. Ca^{2+}_i dependent gap junction closure relies in some cells on the route of Ca^{2+} entry (Chanson et al., 1999). For example in pancreatic acinar cells extracellular Ca^{2+} is more effective at decreasing gap junctional coupling then Ca^{2+}_i store release (Chanson et al., 1999). This is likely due to cytoplasmic Ca^{2+} buffering and slow rates of cytoplasmic Ca^{2+} diffusion compared to other messengers (Allbritton et al., 1992). The observed morphological changes could be affected by the route of Ca^{2+} entry in a similar manner.

4.3.2 Importance of intracellular Ca^{2+} dependent gap junction closure and cytoplasmic changes

Gap junctions in cochlear supporting cells have been proposed to be part of a K^+ transport pathway. In this pathway K^+ extruded from hair cells is transported through cochlear supporting cells and eventually back into the scala media. Thus Ca^{2+}_i dependent gap junction closure should effectively stop any K^+ recycling activity if present (Gomez-Hernandez et al., 2003). The recordings from IS supporting cells obtained during this study show that IS cells possess voltage-activated outward currents. Such outward currents have also been observed in Deiters' cells and were identified as K^+ channels (Chung et al., 2013; Nenov et al., 1998). These could be activated by depolarization with ATP. Based on the results obtained in this study exposure of the IS cells to ATP could indeed stop K^+ movement through the gap junction network and activate outward K^+ channels. $P2X_2$ antibody staining obtained in this study also supports the proposed role of P2X receptors as a K^+ shunt pathway, as staining was observed among other on the apical membranes of the supporting cells in the medial and lateral gap junction connected compartments (Jagger and Forge, 2006).

The importance of the observed cytoplasmic changes after stimulation of P2X receptors remain unclear. The observed cytoplasmic changes appear to depend on extracellular Ca^{2+} influx through P2X receptors. The apical ends of IS supporting cells face endolymph which has a low extracellular Ca^{2+} concentration. The rest of the cells membrane is bathed in perilymph which has a Ca^{2+} concentration of 1.3 mM. Thus the location of the $P2X_2$ receptors on the IS cell membrane is crucial to determine if the observed morphological changes are physiologically relevant.

$P2X_2$ receptors have been immunohistochemically localized to cochlear supporting cells in both observations undertaken during this study and in the guinea pig cochlea (Housley et al., 1999). Immunohistochemistry indicates that $P2X_2$ receptors are present both on the reticular lamina which faces the endolymph and on the perilymph facing membrane of Deiters' cells, pillar cells, OHCs and as shown in this study IS cells (Housley et al., 1992; Housley et al., 1999). Thus it appears that in the mature adult cochlea perilymphatic Ca^{2+} could enter the IS cells although further studies are needed to determine this unequivocally.

The mechanism of the observed cytoplasmic changes is also unclear. A possible explanation is that the cytoplasm transitions from a sol to gel state. Sol to gel transitions

have been shown to be crucial for cell movement (Ananthakrishnan and Ehrlicher, 2007). In these models the cytoplasmic state is governed by the polymerization state of cytoplasmic actin.

A simple change in intracellular ion concentration can precipitate actin polymerization. Changes in $Ca^{2+}{}_i$ and intracellular Mg^{2+} levels have been found to play an important role in regulating actin polymerization and influx of these ions from the ES could initiate spontaneous actin polymerization (Gordon et al., 1977; Yin and Stossel, 1979).

Actin polymerization also underlies the growth and movement of neuronal and astrocyte processes. In this case the process is highly regulated and dependent on calmodulin and Ca^{2+} (Cheng et al., 2002; Molotkov et al., 2013). Proteins such as profilin and gelsolin which regulate the actin polymerization state are present in astrocytes and neurons, and could potentially also be involved in the changes observed in the IS.

Some evidence for such processes in the mature organ of Corti has been found already. Extracellular ATP has been observed to induce stalk movement in isolated Deiters' cells from adult guinea pigs (Bobbin, 2001). The observed movements could be the result of a change in the mechanical properties of the Deiters' cell actin cytoskeleton. Indeed Deiters' cells and particularly the stalks of Deiters' cells have been found to be enriched in F-actin fibres (Dallos et al., 1996; Kuhn and Vater, 1995). Even though no comparable F-actin enrichment has been found in IS cells the change in stiffness of the IS could affect the sound induced wave traveling down the basilar membrane and thus the perception of sound. Altogether ATP could affect hearing through its action on the IS by stopping K^+ cycling and changing the stiffness of the basilar membrane (Steele and Lim, 1999).

4.4 P2 agonist evoked single cell currents

One of the goals of the current study was to determine what types of ATP-activated currents are present in the adult mouse IS. In Köllikers organ in rat immature organ of Corti organotypic cultures cell shrinkage or crenation accompanied by spontaneous increases in $Ca^{2+}{}_i$ levels has been observed. The morphological changes in Köllikers organ have been shown to depend on extracellular ATP. The spontaneous morphological changes are accompanied by membrane currents (Tritsch and Bergles, 2010). These currents are thought to consist of two components. It has been hypothesized that one of them is a CaCC as both puff application of ATP or UTP elicits

currents. In this model activation of the Cl^- channel would lead to water movement resulting in a change in osmolarity and cell shrinkage. The results obtained in this study indicate that two component currents are no longer found in the majority of the cells of the IS region in adult mice. This is further supported by the lack of observable crenation in the IS.

4.4.1 Importance of the border cell Cl^- conductance

Border and phalangeal cells are found in close proximity to the afferent IHC synapse and express glial cell markers. Due to their unique position in the organ of Corti and parallels with glia they could play an active role in signalling at the afferent synapse (Rio et al., 2002). In this study it was found that in contrast to IS cells border cells have a unique Ca^{2+}-activated Cl^- conductance. The importance and role of this current is currently unclear. A change in osmolarity due to Cl^- movement could cause water to diffuse out of the cell and into the extracellular environment. Such water movement could dilute the extracellular K^+ concentration around the afferent synapse during intense noise stimulation, and help reduce the IHC membrane potential, thus affecting sound information encoding and exerting a protective effect on the hair cell and afferent bouton.

Indeed, aquaporins, which form water permeable membrane pores, that enable fast water movement through the cells membrane have been found to be expressed in the IS in rats (Takumi et al., 1998). Unfortunately no extracellular ATP elicited changes in IHC membrane potential were detected in the current study. The close opposition of border cells and IHCs and the small volume of the extracellular space between these cells could be crucial for such a system to work. By their nature patch clamp electrophysiological recordings in tissue, disrupt the extracellular environment surrounding the patched cell. Thus the close opposition of border and IHCs could become disturbed as a result of the recording. Border cells have a long thin phalange which runs along the IHC from the IHC base to its apex and a small cell body (diameter ~ 5 µm). This could make the extracellular space between the border cell and IHC membranes especially prone to disruption.

Activation of the Cl^- current might also prolong the depolarization of the border cell after exposure to extracellular ATP. The increased membrane potential would activate any voltage-dependent K^+ channels, increase the K^+ driving force and enhance the KCC cotranporter function. In this model the K^+ channels would be located below the

cuticular plate and away from the synaptic region of the IHC. The increased Ca^{2+}_i concentration following stimulation with ATP would possibly decrease gap junctional coupling and thus make the border cell more susceptible to depolarization, thus enhancing any outward voltage activated K^+ currents. In addition extracellular Cl^- ions would also be needed for both glutamate and K^+ symport by GLAST and KCC cotransporters Figure 4.1.

The models detailed above rely on the border cell having a relatively high Cl^- content, which would ensure that a driving force for Cl^- efflux is present. Such a high Cl^- concentration is present in glial cells in which it has been estimated to be at approximately 40 mM (Walz, 2002). In addition the gap junction connected syncytium in the inner ear has been found to exhibit relatively high negative resting membrane potentials of approximately -70 mV when measured *in vivo*, which would further increase the driving force for Cl^- anions (Oesterle and Dallos, 1989).

UTP failed to elicit currents in mouse border cells in the present study. Due to the relatively small size of border cells, the intracellular factors necessary for successful P2Y signal transduction could become rapidly washed out from the cell. Another possibility is that Cl^- channels could be located close to the $P2X_2$ receptors so that only Ca^{2+} influx through P2X receptors would activate them.

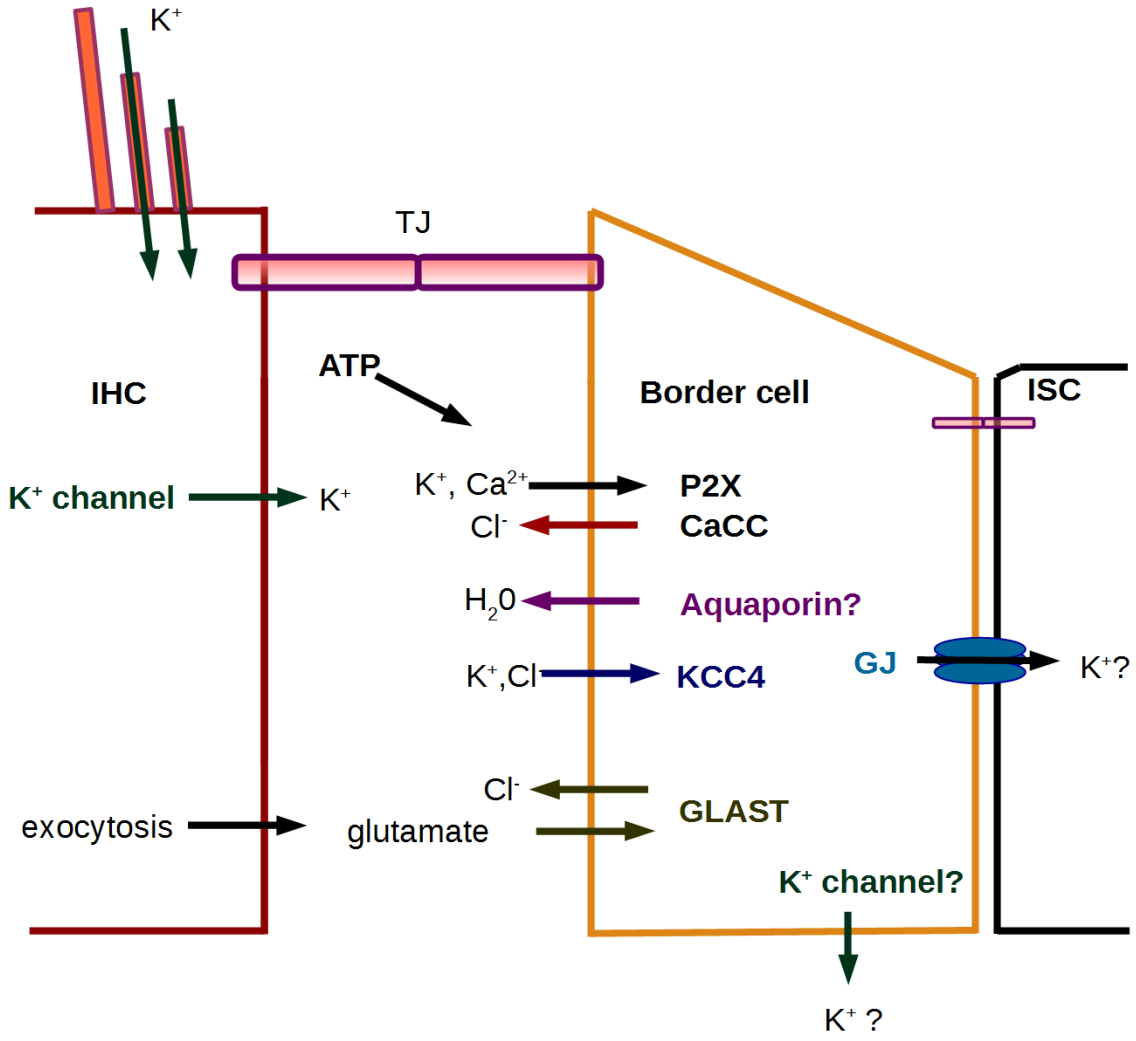

Figure 4.1 Ionic fluxes in border cells.
Hair cells, border cells and IS supporting cells are connected at their apex via tight junctions (TJ). K^+ which enters the hair cells through MET channels is thought to eventually exit into the perilymph. Border cells express the K^+-Cl^- cotransporter KCC4 and glutamate cotransporter GLAST and thus potentially play an important role in K^+ and glutamate removal from the vicinity of the IHC. K^+ removal away from the IHC could be further potentiated by extracellular ATP-dependent activation of Ca^{2+}-activated Cl^- channels (CaCCs), which could lead to a prolonged depolarization of the cell and activation of outward voltage-dependent K^+ channels below the cuticular plate. Additionally, the change in intracellular Cl^- concentration could lead to a change in the cells osmolarity causing water to move into the extracellular space between the IHC and border cell, diluting K^+ and protecting the IHC from excessive depolarization.
In addition to removal through voltage-activated channels, K^+ could also be transported away from the afferent synapse in the border cell through gap junctions (blue) into IS cells (ISC). Gap junction dependent K^+ transport could be inhibited by increases in $Ca^{2+}{}_i$ levels.

4.4.2 The delayed current in border cell is due to activation of a Ca^{2+}-activated Cl^- channel

Studies on P2X channels have found that in some channel subtypes under conditions of prolonged exposure to ATP, the ATP elicited current is biphasic with two current components I1 and I2. After an initial desensitizing current (I1) a second delayed and more sustained current activates (I2) (Khakh et al., 1999; Virginio et al., 1999b). The mechanism of this has been elucidated. When the ATP receptor is exposed to agonist for long time periods the membrane spanning pore dilates and becomes more permeable to substances of a higher molecular weight. In an extracellular solution containing 90 mM $NMDG^+$ and a Na^+ based intracellular solution the change in permeability manifests itself as a change in the direction of the I2 current relative to I1 (Khakh et al., 1999; Surprenant et al., 1996; Virginio et al., 1999b). P2X pore dilation was first observed in P2X7 receptors (Surprenant et al., 1996; Virginio et al., 1999a). Later it has been also found among other to be present in rat $P2X_2$ receptors (Khakh et al., 1999). The diameter of the rat $P2X_2$ channel when in the I2 state is at least 3Å larger than when in I1 (Eickhorst et al., 2002). I2 current has been shown to be sensitive to extracellular Ca^{2+} levels. Studies have found that under low extracellular Ca^{2+} conditions very little or no desensitization of I2 is present (Khadra et al., 2012). When millimolar extracellular Ca^{2+} levels are present the I2 current becomes susceptible to desensitization. These characteristics could cause pore dilation to be mistaken for a Ca^{2+}-activated conductance.

In border cells the delayed current does not appear to be the result of P2X receptor dilation as marked change in reversal potential was observed in border cells when Cl^- was substituted with SCN^-. P2X pore dilation is also facilitated by low extracellular Ca^{2+} concentration and should not be affected by the presence of BAPTA in the intracellular solution (Virginio et al., 1999b). The Ca^{2+} sensitive domain of the P2X channel governing pore dilation has been localized to the extracellular region of the P2X receptor (Ding and Sachs, 2000). However in border cells 10 mM intracellular BAPTA fully blocked the delayed component. Finally studies on mouse $P2X_2$ receptors have determined that pore dilation is not present in mouse $P2X_2$ channels. The reason is that two C-terminal amino acids: I432 and G444 which are required for dilation are substituted for by S432 and D444 (Brandle et al., 1997; Coddou et al., 2011; Eickhorst et al., 2002; He et al., 2002; Koshimizu et al., 2006; Navarro et al., 2011).

The possibility still exists that another dilating P2X receptor is present in the mouse. However to date the only other P2X receptor detected in abundance in the organ of Corti is $P2X_3$, which does not have the ability to dilate and has not been found after hearing onset (Huang et al., 2005; Huang et al., 2006). Additionally the $P2X_2$ transcript detected in the guinea pig organ of Corti was $P2X_{2b}$, which also is a desensitizing variant (Housley et al., 1999).

Other cationic Ca^{2+}-activated channels could also be present in border cells. However activation of only cationic channels would not produce the observed shift in reversal potential. Thus the most likely explanation is that a Ca^{2+}-activated channel is present in mice border cells. The possibility still exists that in addition to a Cl^- channel a cationic Ca^{2+}-activated conductance contributes to the observed delayed current (Qu and Hartzell, 2000). Possible candidates for Ca^{2+}-activated cationic channels in the organ of Corti would be members of the TRP channel family. Many of these channels have been localized to the organ of Corti by qPCR (Asai et al., 2010).

An unexpected observation of the current study was that border cells patched with SCN^- in the intracellular solution had a smaller membrane resistance and an increased leak conductance when compared to cells patched with Cl^-. The glutamate-aspartate transporter (GLAST) is present in border cells as shown in this study and by others (Glowatzki et al., 2006). GLAST couples glutamate and Na^+ transport but also has an associated glutamate Cl^- conductance (Wadiche et al., 1995). A constant base GLAST activity would result in a constantly active GLAST Cl^- channel. This activity would be more pronounced with SCN^- as it permeates the endogenous GLAST Cl^- channel much better than Cl^- itself, resulting in an increased leak conductance. The GLAST anion conductance is voltage dependent and indeed increased leak is especially prominent at negative membrane potentials. The argument for high base GLAST activity is supported by the large number of IHC glutamatergic synapses and constant spontaneous rates of afferent neurons (Liberman, 1978; Liberman et al., 1990). Thus relatively large amounts of glutamate could leak into the extrasynaptic space at the IHC basal pole. In addition border and phalangeal cells are the only cells in the vicinity of the IHC synapse which express glutamate transporters (Furness and Lawton, 2003; Furness and Lehre, 1997; Glowatzki et al., 2006).

4.5 Mechanism of propagation and function of cochlear slow Ca^{2+} waves

4.5.1 Slow Ca^{2+} wave characteristics

Slow Ca^{2+} waves in the adult organ of Corti have characteristics which are different from the Ca^{2+} waves observed in organotypic cochlear cultures from prehearing mice. Slow Ca^{2+} waves do not appear to propagate via an extracellular ATP dependent mechanism even though the effect of apyrase on IS slow Ca^{2+} waves still remains to be determined as the removal of the TM was sufficient to fully block slow Ca^{2+} wave signalling in the IS (Discussed below). The tight junctions at the apex of IS supporting cells should not prevent the diffusion of the P2 antagonists below the reticular lamina as the perilymphatic space was also filled with P2 antagonist containing solution.

Milimolar Ca^{2+} levels are known to inhibit hemichannels, however increasing the Ca^{2+} concentration in the ES to 1.3 mM did not appear to have any measureable effect on slow Ca^{2+} waves (Pfahnl and Dahl, 1999). All experiments in which the TM was left attached were indeed conducted with 1.3 mM Ca^{2+} in the ES. Finally cochlear slow Ca^{2+} waves propagated at 1 – 3 µm/s, which is significantly slower than Ca^{2+} waves in the immature organ of Corti which propagate with speeds of approximately 10 – 20 µm/s.

Overall, cochlear slow Ca^{2+} waves were unaffected by extracellular Ca^{2+} concentration, purinergic receptor inhibitors or apyrase. These results argue against slow Ca^{2+} waves being mediated by an extracellular ATP, P2Y and hemichannel dependent signalling mechanism as found in the immature organ of Corti (Gale et al., 2004; Tritsch et al., 2007).

Slow Ca^{2+} waves were however inhibited by the gap junction blockers 1-octanol and carbenoxolone and absent from Cx30 knockout mice. Taken together the data indicates that most likely cochlear slow Ca^{2+} waves are gap junction mediated, and that extracellular ATP signalling is not involved in their propagation. Ca^{2+} waves with similar properties, that propagate through gap junctions have been described in ciliated airway epithelia, astrocytes, vascular smooth muscle cells and in the developing Danio and Xenopus embryo (Leybaert and Sanderson, 2012; Webb and Miller, 2006).

4.5.2 An active propagation model for cochlear slow Ca^{2+} waves?

As no extracellular ATP appears to be involved in cochlear slow Ca^{2+} wave signalling the most likely intracellular messenger responsible for Ca^{2+} wave spread is inositol trisphosphate (IP_3) (Leybaert and Sanderson, 2012). Cochlear slow Ca^{2+} waves were observed to propagate for distances of over 500 µm and at a constant speed. Thus their most likely mode of propagation is active propagation. In such a model propagation does not rely solely on IP_3 or ATP diffusion from the point of origin. Instead IP_3

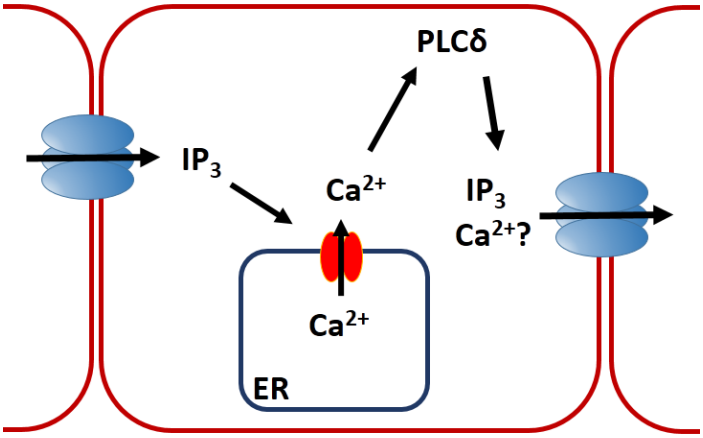

Figure 4.2 A possible model of Ca^{2+} wave propagation through gap junctions in the adult cochlea.
IP_3 entering through gap junctions (blue) from a neighbouring cell might stimulate IP_3 receptors (red) located on the ER (blue). This would precipitate Ca^{2+} release from intracellular stores. The released Ca^{2+} could stimulate PLCδ to produce more IP_3. The newly produced IP_3 could diffuse through gap junctions (blue) further propagating the Ca^{2+} wave into a neighbouring cell. Extracellular signalling is not involved in wave propagation in this model.

diffusion through gap junctions elicits a Ca^{2+} increase and Ca^{2+}-dependent activation of PLC, which cleaves the membrane bound phosphatidylinositol 4,5-bisphosphate (PIP_2) into diacylglycerol (DAG) and IP_3. The released IP_3 diffuses through gap junctions into neighbouring cells, propagating the wave (Hofer et al., 2002) (Figure 4.2).

In an active propagation model Ca^{2+} wave propagation distance depends on the activity of phospholipase C (PLC), the amount of Ca^{2+} in intracellular Ca^{2+} stores and to a lesser extent on the permeability of gap junctions to IP_3 (Hofer et al., 2002). The PLC isoform most likely involved in Ca^{2+} wave propagation is PLCδ, which is activated by micromolar Ca^{2+} levels (Rebecchi and Pentyala, 2000). In the case of cochlear slow Ca^{2+} waves the main limiting factor appears to be the rate of Ca^{2+} store refilling as

waves can propagate across hundreds of micrometres but the period of wave signalling does not increase much above 1 wave per 10 minutes (Hofer et al., 2002).

4.5.3 The tectorial membrane is required for slow Ca^{2+} wave signalling in the inner sulcus

A surprising observation was that the removal of the TM fully stopped slow Ca^{2+} wave signalling and even $Ca^{2+}{}_i$ oscillations in individual cells in the IS. Why the TM should promote or otherwise affect Ca^{2+} signalling in supporting cells in any way is not clear. The IS and the organ of Corti are partially separated from the rest of the scala media by the TM. Thus the possibility cannot be discounted that the endolymph beneath the TM contains a factor, that might make IS cells more susceptible to $Ca^{2+}{}_i$ oscillations and Ca^{2+} wave signalling. Such a factor might remain present in this space even after moving the cochlea into ES, as the space under the TM is limited and could limit diffusion. Removing the TM would dilute such a factor and thus inhibit Ca^{2+} waves. Furthermore if indeed present such a factor might be present on the TM itself. The TM is thought to be composed mostly of collagens and glycoproteins (Richardson et al., 2008). Based on the current state of knowledge none of its identified compositional components would appear to affect $Ca^{2+}{}_i$ levels in the cells beneath it.

If an extracellular messenger was involved in IS slow Ca^{2+} wave propagation the TM might delay its dilution and thus increase the propagation distance of Ca^{2+} waves. However it is unclear why signal would not propagate between neighbouring cells. Furthermore $Ca^{2}{}_i$ oscillations should still be present in individual IS supporting cells after TM removal. No such oscillations were observed in wild type mice. Altogether it seems unlikely that opening the space underneath the TM would completely abolish slow Ca^{2+} waves if these were mediated through extracellular signalling molecules.

4.5.4 Function of slow Ca^{2+} waves

The observation that slow Ca^{2+} wave signalling in the Deiters' cell region appeared to start earlier in cochleas in which the TM was removed argues for the hypothesis that slow Ca^{2+} waves are triggered by damage, and the change in $Ca^{2+}{}_i$ levels might be a signal that activates cell damage repair mechanisms. A similar mechanism might govern the onset of IS slow Ca^{2+} waves even though the TM might have to be physically present for waves to propagate between cells. In the immature organ of Corti ablation of a single hair cell has been shown to initiate a Ca^{2+} wave. These damage-induced, non-repetitive waves, which similarly to Köllikers organ Ca^{2+} waves are mediated by

extracellular ATP, travel at approximately 13 µm/s (Gale et al., 2004). Such damage-induced waves have been shown to increase the phosphorylation of c-Jun N-terminal kinase (JNK) and extracellularly regulated kinase (ERK). The phosphorylated, activated forms of these two mitogen-activated protein kinases have been found to contribute to auditory hair cell loss (Lahne and Gale, 2008; Wang et al., 2003a). Gap junction mediated repetitive Ca^{2+} waves which propagate at a similar speed to cochlear slow Ca^{2+} waves have been observed during convergent extension and somite formation and differentiation during Xenopus embryo development and in the marginal converging zone of the epibolizing blastoderm during the transition to gastrulation in the Danio embryo (Wallingford et al., 2001; Webb and Miller, 2003; Webb and Miller, 2006). These waves are thought to regulate cell migration and specification during development. Ca^{2+} waves have been also found to play an important role in wound healing where they regulate cell migration (Sung et al., 2003).

Slow Ca^{2+} waves in the IS could therefore be a way of regulating and coordinating the response to trauma in the organ of Corti. This is supported by electron microscope studies indicating that noise blast induced damage elicits morphological changes in IS supporting cells and supporting cell migration (Hamernik et al., 1984).

Regular Ca^{2+} waves could metabolically synchronize and coordinate cells which do not neighbour with each other (Leybaert and Sanderson, 2012). Regular $Ca^{2+}{}_i$ oscillations have also been observed in individual cells under many conditions (Smedler and Uhlen, 2014). The periodic increases in $Ca^{2+}{}_i$ concentration can affect gene expression (Dolmetsch et al., 1998). Information regulating gene transcription is encoded in the frequency and pattern of $Ca^{2+}{}_i$ oscillations (Parekh, 2011). Mathematical models predict that the amplitude, frequency and duration of the Ca^{2+} signal could be decoded by Ca^{2+}-activated kinases and phosphatases downstream of target proteins (Salazar et al., 2008; Uhlen and Fritz, 2010).

Transcription factors such as NFAT, NFκB and transcription factor regulators such as CaMKII, PKC, MAPK, and calpain have been shown to act as Ca^{2+} signal and oscillator decoders (De Koninck and Schulman, 1998; Dolmetsch et al., 1997; Hu et al., 1999; Kupzig et al., 2005; Oancea and Meyer, 1998; Tompa et al., 2001). Different decoders can be activated by different frequencies of oscillations and it is thought that the range of recognized frequencies can stretch from 1-10 milliHz (3.6 to 36 oscillations per hour)

for NFκB to 1000-10,000 milliHz (60 to 600 oscillations per hour) for calpain (Smedler and Uhlen, 2014).

In the present study the maximum Ca^{2+} wave frequency has been shown to be around 6 waves/hour in the Deiters' cells and IS. The transcription factors which are sensitive to this frequency range are NF-kB, MAPKs, NFAT (Smedler and Uhlen, 2014). Studies in the neonatal organ of Corti have found that the MAPKs, c-Jun and ERK 1/2 are phosphorylated as the result of damage and the resulting $Ca^{2+}{}_i$ increases in supporting cells (Gale et al., 2004; Lahne and Gale, 2008). Interestingly, recent studies have shown that Notch signalling which plays an important role in regulating the hair cell differentiation pathway can be regulated by both ERK/MEK dependent and CaMKII dependent processes (Mamaeva et al., 2009; Tremblay et al., 2013). The activity of both ERK/MEK and CamKII can be regulated by $Ca^{2+}{}_i$ levels. In organotypic cultures of P6 organs of Corti oscillations of $Ca^{2+}{}_i$ in cochlear supporting cells have been shown to regulate connexin expression through the transcription factor NFκB (Ortolano et al., 2008).

The imaging conducted for this study was conducted at room temperature at 21-24ºC. Temperature is known to regulate both speed of propagation and the frequency of Ca^{2+} waves. An increase in temperature could affect slow Ca^{2+} wave signalling, further increasing the frequency of Ca^{2+} oscillations into a range recognized by additional transcription factors (Jaffe, 2002).

4.5.5 Intracellular Ca^{2+} oscillations in individual supporting cells

The observed variability in single cell $Ca^{2+}{}_i$ oscillations in decoupled Deiters' cells and IS cells in Cx30 mice indicates that gap junctions could be necessary for synchronizing $Ca^{2+}{}_i$ signalling and homeostasis in multiple cochlear supporting cells. Separately in both wild type and Cx30 knockout mice $Ca^{2+}{}_i$ oscillations were present in Hensen's cells. Hensen's cells express CaCCs and such oscillations could play a role in regulating Cl^- homeostasis in the scala media (Lagostena et al., 2001).

4.5.6 Do intracellular Ca^{2+} oscillations and slow Ca^{2+} waves require Ca^{2+} influx from the extracellular environment?

Currently the stimulus, which initiates the increase in $Ca^{2+}{}_i$ in an individual cell and starts a slow Ca^{2+} wave is not known. It is also not clear if the initial Ca^{2+} increase in an individual cell is triggered by extracellular signalling. An influx of extracellular Ca^{2+} does not appear to be required to initiate slow wave signalling as omission of Ca^{2+} from

the extracellular medium did not appear to decrease the frequency or inter-wave interval of slow Ca^{2+} waves compared to 1.3 mM extracellular Ca^{2+} levels.

In the cell at least three intracellular stores of Ca^{2+} are present. These are the ER, mitochondria and Ca^{2+} bound to proteins such as calretinin and calmodulin (reviewed in (Schuster et al., 2002)). Simulations modelling oscillations of Ca^{2+}_i levels have found that the homeostatic mechanisms governing Ca^{2+} release and sequestration to these three sources could be sufficient to maintain Ca^{2+}_i oscillations. A self-activating step

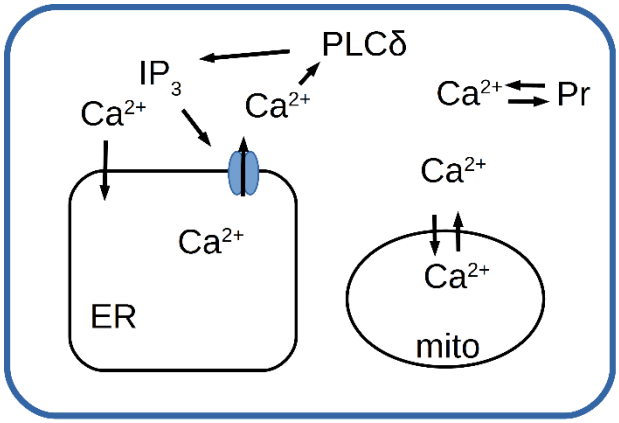

Figure 4.3 Control of Ca^{2+}_i oscillations.
The control of Ca^{2+}_i oscillation frequency is a complex process. Several feedback loops might exist. Stimulation of IP_3Rs (blue) can release Ca^{2+} from the ER. The released Ca^{2+} might in turn regulate IP_3 production through its effects on PLCδ. Ca^{2+}_i can also be buffered by mitochondria (mito) and proteinaceous Ca^{2+} buffers (Pr).

such as CICR is required for these models to function. Extracellular signalling or Ca^{2+} influx from the extracellular space is not necessary for oscillations to occur.

By modifying the rate of cytoplasmic Ca^{2+} influx and efflux it is possible to precisely modulate the rate and magnitude of Ca^{2+} oscillations. Such fine tuning can be achieved by changing the expression profile of genes mediating Ca^{2+} transport, as well as by post-translational modifications of the proteins involved in these processes.

Further studies are needed to determine the exact Ca^{2+} homeostasis mechanisms functioning in slow Ca^{2+} wave signalling in supporting cells. Such studies should help determine how slow Ca^{2+} waves initiate and which processes govern the inter-wave interval (Figure 4.3).

4.6 Fast Ca^{2+} waves in the adult organ of Corti

4.6.1 Dependence of fast Ca^{2+} waves on extracellular ATP and interrelation with slow Ca^{2+} wave signalling

Apart from the slow waves, faster Ca^{2+} waves caused most likely by ATP release from permeabilising OHC were observed. These waves could be initiated by laser-induced damage and were not previously described in the adult organ of Corti. Similar damage evoked waves have been described in organotypic cultures of the immature organ of Corti and were found to depend on extracellular ATP (Gale, personal communication). In some instances these waves were able to trigger slow Ca^{2+} waves, indicating that extracellular ATP can also initiate slow Ca^{2+} wave signalling. Indeed the FW 0.5 time of the $Ca^{2+}{}_i$ increase in supporting cells was similar for both slow Ca^{2+} waves and treatment with extracellular ATP. This indicates that the same $Ca^{2+}{}_i$ clearing mechanisms could be in use during both slow Ca^{2+} wave signalling and fast extracellular ATP-dependent Ca^{2+} signalling.

4.7 Future directions

4.7.1 Inner sulcus P2 receptors

Future studies should verify functionally the location of P2X receptors localized in this study to the perilymph facing membrane of IS cells. Such experiments would certainly help determine if the observed effects of P2 receptor stimulation on gap junction conductance and cytoplasm state can indeed occur *in vivo*. It is also unclear if P2Y receptors can also contribute to regulation of the gap junction conductance. When caged IP_3 was liberated in the cytoplasm of guinea pig Hensen's cells, membrane resistance increased (Lagostena et al., 2001). However in a different study the P2Y agonist UTP failed to decouple isolated guinea pig Hensen's cells, even though cells were transiently decoupled by puff application of ATP (Zhu and Zhao, 2012). Thus further experiments should address this discrepancy and the physiological importance of P2Y receptors in the adult cochlea.

An important future direction will be to determine the distribution of CaCCs in the cochlea. Multiple Cl^- channel types could be present and as the cochlear Cl^- channel distribution is currently unknown perhaps the best approach would be to use fluorescent Cl^- indicators in conjunction with confocal microscopy to verify the electrophysiological observations of this study and determine in which other cells CaCCs might be present (Woll et al., 1996). Such an investigation could provide more

insight into the importance and physiological role of Cl^- transport within the cochlea. In addition functional electrophysiological studies would be helpful to determine if K^+ channels are indeed present in the IS and border cells. The location of any such channels should also be determined to help understand if they could have a role in K^+ cycling or could provide a shunt conductance to decrease endolymph K^+ concentration.

Lastly further studies should address the relevance of the P2 receptor staining visible in the stereocilia in the current and other studies (Housley et al., 1999; Jarlebark et al., 2002). Electrophysiological recordings and Ca^{2+} imaging could help determine if functional $P2X_2$ channels are present in mouse hair cell stereocilia. Such an investigation could also be helpful in determining what role stereocilia $P2X_2$ channels play in the physiology of the hair cells.

4.7.2 Slow Ca^{2+} waves

Spontaneous slow Ca^{2+} waves have not been reported to be present in the adult cochlea previously and their importance and exact mechanism of propagation still remains to be elucidated. Perhaps the most significant issue is to determine if such waves are present or can be evoked *in vivo*. One avenue to accomplish this would be through the use of genetically encoded Ca^{2+} indicators such as GCaMP (Nakai et al., 2001). Such an indicator would eliminate the need for loading the organ of Corti cells *in vivo* with exogenous dyes. A way to access the organ of Corti and image it *in vivo* would still however need to be developed. Other experiments to determine if IP_3 is indeed involved in slow Ca^{2+} wave propagation and if other intracellular factors known to be important in Ca^{2+} wave signalling such as mitochondria are involved also remain to be conducted. The effects of slow Ca^{2+} waves on the cells metabolism should also be probed. As often repetitive Ca^{2+} signalling is involved in gene regulation (discussed in section 4.5.4) studies to determine if slow Ca^{2+} waves affect gene expression or could be manipulated to do so could potentially be of therapeutic value.

References

Abbracchio, M.P., and G. Burnstock. 1994. Purinoceptors: are there families of P2X and P2Y purinoceptors? *Pharmacology and Therapeutics*. 64:445-475.

Abbracchio, M.P., G. Burnstock, J.M. Boeynaems, E.A. Barnard, J.L. Boyer, C. Kennedy, G.E. Knight, M. Fumagalli, C. Gachet, K.A. Jacobson, and G.A. Weisman. 2006. International Union of Pharmacology LVIII: update on the P2Y G protein-coupled nucleotide receptors: from molecular mechanisms and pathophysiology to therapy. *Pharmacological Reviews*. 58:281-341.

Ahmad, S., W. Tang, Q. Chang, Y. Qu, J. Hibshman, Y. Li, G. Sohl, K. Willecke, P. Chen, and X. Lin. 2007. Restoration of connexin26 protein level in the cochlea completely rescues hearing in a mouse model of human connexin30-linked deafness. *Proceedings of the National Academy of Sciences of the United States of America*. 104:1337-1341.

Allbritton, N.L., T. Meyer, and L. Stryer. 1992. Range of messenger action of calcium ion and inositol 1,4,5-trisphosphate. *Science*. 258:1812-1815.

Ananthakrishnan, R., and A. Ehrlicher. 2007. The forces behind cell movement. *International Journal of Biological Sciences*. 3:303-317.

Anderson, J.M., and C.M. Van Itallie. 2009. Physiology and function of the tight junction. *Cold Spring Harbor Perspectives in Biology*. 1:a002584.

Anselmi, F., V.H. Hernandez, G. Crispino, A. Seydel, S. Ortolano, S.D. Roper, N. Kessaris, W. Richardson, G. Rickheit, M.A. Filippov, H. Monyer, and F. Mammano. 2008. ATP release through connexin hemichannels and gap junction transfer of second messengers propagate Ca2+ signals across the inner ear. *Proceedings of the National Academy of Sciences of the United States of America*. 105:18770-18775.

Armstrong, C.M., and W.F. Gilly. 1992. Access resistance and space clamp problems associated with whole-cell patch clamping. *Methods in Enzymology*. 207:100-122.

Asai, Y., J.R. Holt, and G.S. Geleoc. 2010. A quantitative analysis of the spatiotemporal pattern of transient receptor potential gene expression in the developing mouse cochlea. *Journal of the Association for Research in Otolaryngology*. 11:27-37.

Ashmore, J. 2008. Cochlear outer hair cell motility. *Physiological Reviews*. 88:173-210.

Ashmore, J.F., and H. Ohmori. 1990. Control of intracellular calcium by ATP in isolated outer hair cells of the guinea-pig cochlea. *Journal of Physiology*. 428:109-131.

Beltramello, M., V. Piazza, F.F. Bukauskas, T. Pozzan, and F. Mammano. 2005. Impaired permeability to Ins(1,4,5)P3 in a mutant connexin underlies recessive hereditary deafness. *Nature Cell Biology*. 7:63-69.

Beutner, D., and T. Moser. 2001. The presynaptic function of mouse cochlear inner hair cells during development of hearing. *Journal of Neuroscience*. 21:4593-4599.

Bobbin, R.P. 2001. ATP-induced movement of the stalks of isolated cochlear Deiters' cells. *Neuroreport*. 12:2923-2926.

Bobbin, R.P., and A.N. Salt. 2005. ATP-gamma-S shifts the operating point of outer hair cell transduction towards scala tympani. *Hearing Research*. 205:35-43.

Bobbin, R.P., and M.H. Thompson. 1978. Effects of putative transmitters on afferent cochlear transmission. *Annals of Otology, Rhinology and Laryngology*. 87:185-190.

Bodendiek, S.B., and G. Raman. 2010. Connexin modulators and their potential targets under the magnifying glass. *Current Medicinal Chemistry*. 17:4191-4230.

Boettger, T., C.A. Hubner, H. Maier, M.B. Rust, F.X. Beck, and T.J. Jentsch. 2002. Deafness and renal tubular acidosis in mice lacking the K-Cl co-transporter Kcc4. *Nature*. 416:874-878.

Boettger, T., M.B. Rust, H. Maier, T. Seidenbecher, M. Schweizer, D.J. Keating, J. Faulhaber, H. Ehmke, C. Pfeffer, O. Scheel, B. Lemcke, J. Horst, R. Leuwer, H.C. Pape, H. Volkl, C.A. Hubner, and T.J. Jentsch. 2003. Loss of K-Cl co-transporter KCC3 causes deafness, neurodegeneration and reduced seizure threshold. *EMBO Journal*. 22:5422-5434.

Bogdanov, Y.D., S.S. Wildman, M.P. Clements, B.F. King, and G. Burnstock. 1998. Molecular cloning and characterization of rat P2Y4 nucleotide receptor. *British Journal of Pharmacology*. 124:428-430.

Boitano, S., E.R. Dirksen, and M.J. Sanderson. 1992. Intercellular propagation of calcium waves mediated by inositol trisphosphate. *Science*. 258:292-295.

Brake, A.J., M.J. Wagenbach, and D. Julius. 1994. New structural motif for ligand-gated ion channels defined by an ionotropic ATP receptor. *Nature*. 371:519-523.

Brandle, U., P. Spielmanns, R. Osteroth, J. Sim, A. Surprenant, G. Buell, J.P. Ruppersberg, P.K. Plinkert, H.P. Zenner, and E. Glowatzki. 1997. Desensitization of the P2X(2) receptor controlled by alternative splicing. *FEBS Letters*. 404:294-298.

Burnstock, G. 1972. Purinergic nerves. *Pharmacological Reviews*. 24:509-581.

Burnstock, G. 1976. Purinergic receptors. *Journal of Theoretical Biology*. 62:491-503.

Burnstock, G. 2006. Purinergic signalling. *British Journal of Pharmacology*. 147 Suppl 1:S172-181.

Burnstock, G. 2007. Purine and pyrimidine receptors. *Cellular and Molecular Life Sciences*. 64:1471-1483.

Burnstock, G., and G.E. Knight. 2004. Cellular distribution and functions of P2 receptor subtypes in different systems. *International Review of Cytology*. 240:31-304.

Burnstock, G., and M. Williams. 2000. P2 purinergic receptors: modulation of cell function and therapeutic potential. *Journal of Pharmacology and Experimental Therapeutics*. 295:862-869.

Chanson, M., P. Mollard, P. Meda, S. Suter, and H.J. Jongsma. 1999. Modulation of pancreatic acinar cell to cell coupling during ACh-evoked changes in cytosolic Ca2+. *Journal of Biological Chemistry*. 274:282-287.

Chen, C., M.S. Parker, A.P. Barnes, P. Deininger, and R.P. Bobbin. 2000. Functional expression of three P2X(2) receptor splice variants from guinea pig cochlea. *Journal of Neurophysiology*. 83:1502-1509.

Cheng, S., M.S. Geddis, and V. Rehder. 2002. Local calcium changes regulate the length of growth cone filopodia. *Journal of Neurobiology*. 50:263-275.

Chung, J.W., E.C. Nam, W.T. Kim, J.B. Youm, and C.H. Leem. 2013. Potassium currents in isolated deiters' cells of Guinea pig. *Korean Journal of Physiology & Pharmacology*. 17:537-546.

Clapham, D.E. 2007. Calcium signaling. *Cell*. 131:1047-1058.

Coddou, C., Z. Yan, T. Obsil, J.P. Huidobro-Toro, and S.S. Stojilkovic. 2011. Activation and regulation of purinergic P2X receptor channels. *Pharmacological Reviews*. 63:641-683.

Cohen-Salmon, M., T. Ott, V. Michel, J.P. Hardelin, I. Perfettini, M. Eybalin, T. Wu, D.C. Marcus, P. Wangemann, K. Willecke, and C. Petit. 2002. Targeted ablation of connexin26 in the inner ear epithelial gap junction network causes hearing impairment and cell death. *Current Biology*. 12:1106-1111.

Cornell-Bell, A.H., S.M. Finkbeiner, M.S. Cooper, and S.J. Smith. 1990. Glutamate induces calcium waves in cultured astrocytes: long-range glial signaling. *Science*. 247:470-473.

Dallos, P., A.N. Popper, and R.R. Fay. 1996. The cochlea. Springer, New York.

De Koninck, P., and H. Schulman. 1998. Sensitivity of CaM kinase II to the frequency of Ca2+ oscillations. *Science*. 279:227-230.

de Roos, A.D., E.J. van Zoelen, and A.P. Theuvenet. 1996. Determination of gap junctional intercellular communication by capacitance measurements. *Pflügers Archiv. European Journal of Physiology*. 431:556-563.

De Vuyst, E., E. Decrock, L. Cabooter, G.R. Dubyak, C.C. Naus, W.H. Evans, and L. Leybaert. 2006. Intracellular calcium changes trigger connexin 32 hemichannel opening. *EMBO Journal*. 25:34-44.

De Vuyst, E., N. Wang, E. Decrock, M. De Bock, M. Vinken, M. Van Moorhem, C. Lai, M. Culot, V. Rogiers, R. Cecchelli, C.C. Naus, W.H. Evans, and L. Leybaert. 2009. Ca(2+) regulation of connexin 43 hemichannels in C6 glioma and glial cells. *Cell Calcium*. 46:176-187.

Demer, L.L., C.M. Wortham, E.R. Dirksen, and M.J. Sanderson. 1993. Mechanical stimulation induces intercellular calcium signaling in bovine aortic endothelial cells. *American Journal of Physiology*. 264:H2094-2102.

Ding, S., and F. Sachs. 2000. Inactivation of P2X2 purinoceptors by divalent cations. *Journal of Physiology*. 522 Pt 2:199-214.

Dolmetsch, R.E., R.S. Lewis, C.C. Goodnow, and J.I. Healy. 1997. Differential activation of transcription factors induced by Ca2+ response amplitude and duration. *Nature*. 386:855-858.

Dolmetsch, R.E., K. Xu, and R.S. Lewis. 1998. Calcium oscillations increase the efficiency and specificity of gene expression. *Nature*. 392:933-936.

Drury, A.N., and A. Szent-Gyorgyi. 1929. The physiological activity of adenine compounds with especial reference to their action upon the mammalian heart. *Journal of Physiology*. 68:213-237.

Dulon, D., C. Blanchet, and E. Laffon. 1994. Photo-released intracellular Ca2+ evokes reversible mechanical responses in supporting cells of the guinea-pig organ of Corti. *Biochemical and Biophysical Research Communications*. 201:1263-1269.

Dulon, D., P. Mollard, and J.M. Aran. 1991. Extracellular ATP elevates cytosolic Ca2+ in cochlear inner hair cells. *Neuroreport*. 2:69-72.

Eickhorst, A.N., A. Berson, D. Cockayne, H.A. Lester, and B.S. Khakh. 2002. Control of P2X(2) channel permeability by the cytosolic domain. *Journal of General Physiology*. 120:119-131.

Endo, M., M. Tanaka, and Y. Ogawa. 1970. Calcium induced release of calcium from the sarcoplasmic reticulum of skinned skeletal muscle fibres. *Nature*. 228:34-36.

Enomoto, K., K. Furuya, S. Yamagishi, and T. Maeno. 1992. Mechanically induced electrical and intracellular calcium responses in normal and cancerous mammary cells. *Cell Calcium*. 13:501-511.

Erbe, C.B., K.C. Harris, C.L. Runge-Samuelson, V.A. Flanary, and P.A. Wackym. 2004. Connexin 26 and connexin 30 mutations in children with nonsyndromic hearing loss. *Laryngoscope*. 114:607-611.

Evans, R.J., C. Lewis, G. Buell, S. Valera, R.A. North, and A. Surprenant. 1995. Pharmacological characterization of heterologously expressed ATP-gated cation channels (P2x purinoceptors). *Molecular Pharmacology*. 48:178-183.

Evans, W.H., and P.E. Martin. 2002. Gap junctions: structure and function (Review). *Molecular Membrane Biology*. 19:121-136.

Fechner, F.P., J.J. Nadol, B.J. Burgess, and M.C. Brown. 2001. Innervation of supporting cells in the apical turns of the guinea pig cochlea is from type II afferent fibers. *Journal of Comparative Neurology*. 429:289-298.

Flagg-Newton, J., I. Simpson, and W.R. Loewenstein. 1979. Permeability of the cell-to-cell membrane channels in mammalian cell juncton. *Science*. 205:404-407.

Flock, A., and H.C. Cheung. 1977. Actin filaments in sensory hairs of inner ear receptor cells. *Journal of Cell Biology*. 75:339-343.

Flock, A., B. Flock, A. Fridberger, E. Scarfone, and M. Ulfendahl. 1999. Supporting cells contribute to control of hearing sensitivity. *Journal of Neuroscience*. 19:4498-4507.

Ford, L.E., and R.J. Podolsky. 1970. Regenerative calcium release within muscle cells. *Science*. 167:58-59.

Forge, A., D.J. Jagger, J.J. Kelly, and R.R. Taylor. 2013. Connexin30-mediated intercellular communication plays an essential role in epithelial repair in the cochlea. *Journal of Cell Science*. 126:1703-1712.

Forge, A., N.K. Marziano, S.O. Casalotti, D.L. Becker, and D. Jagger. 2003. The inner ear contains heteromeric channels composed of cx26 and cx30 and deafness-related mutations in cx26 have a dominant negative effect on cx30. *Cell Communication & Adhesion*. 10:341-346.

Fridberger, A., A. Flock, M. Ulfendahl, and B. Flock. 1998. Acoustic overstimulation increases outer hair cell Ca2+ concentrations and causes dynamic contractions of the hearing organ. *Proceedings of the National Academy of Sciences of the United States of America*. 95:7127-7132.

Froldi, G., K. Varani, A. Chinellato, E. Ragazzi, L. Caparrotta, and P.A. Borea. 1997. P2X-purinoceptors in the heart: actions of ATP and UTP. *Life Sciences*. 60:1419-1430.

Fuchs, P.A. 2010. The ear. Oxford University Press, Oxford ; New York.

Furness, D.N., and D.M. Lawton. 2003. Comparative distribution of glutamate transporters and receptors in relation to afferent innervation density in the mammalian cochlea. *Journal of Neuroscience*. 23:11296-11304.

Furness, D.N., and K.P. Lehre. 1997. Immunocytochemical localization of a high-affinity glutamate-aspartate transporter, GLAST, in the rat and guinea-pig cochlea. *European Journal of Neuroscience*. 9:1961-1969.

Gale, J.E., J.R. Meyers, A. Periasamy, and J.T. Corwin. 2002. Survival of bundleless hair cells and subsequent bundle replacement in the bullfrog's saccule. *Journal of Neurobiology*. 50:81-92.

Gale, J.E., V. Piazza, C.D. Ciubotaru, and F. Mammano. 2004. A mechanism for sensing noise damage in the inner ear. *Current Biology*. 14:526-529.

Gever, J.R., D.A. Cockayne, M.P. Dillon, G. Burnstock, and A.P. Ford. 2006. Pharmacology of P2X channels. *Pflügers Archiv. European Journal of Physiology*. 452:513-537.

Glowatzki, E., N. Cheng, H. Hiel, E. Yi, K. Tanaka, G.C. Ellis-Davies, J.D. Rothstein, and D.E. Bergles. 2006. The glutamate-aspartate transporter GLAST mediates glutamate uptake at inner hair cell afferent synapses in the mammalian cochlea. *Journal of Neuroscience*. 26:7659-7664.

Glowatzki, E., and P.A. Fuchs. 2002. Transmitter release at the hair cell ribbon synapse. *Nature Neuroscience*. 5:147-154.

Godecke, S., U.K. Decking, A. Godecke, and J. Schrader. 1996. Cloning of the rat P2u receptor and its potential role in coronary vasodilation. *American Journal of Physiology*. 270:C570-577.

Gomez-Casati, M.E., J.C. Murtie, C. Rio, K. Stankovic, M.C. Liberman, and G. Corfas. 2010. Nonneuronal cells regulate synapse formation in the vestibular sensory epithelium via erbB-dependent BDNF expression. *Proceedings of the National Academy of Sciences of the United States of America*. 107:17005-17010.

Gomez-Hernandez, J.M., M. de Miguel, B. Larrosa, D. Gonzalez, and L.C. Barrio. 2003. Molecular basis of calcium regulation in connexin-32 hemichannels. *Proceedings of the National Academy of Sciences of the United States of America*. 100:16030-16035.

Goodenough, D.A., and D.L. Paul. 2003. Beyond the gap: functions of unpaired connexon channels. *Nature Reviews: Molecular Cell Biology*. 4:285-294.

Gordon, D.J., J.L. Boyer, and E.D. Korn. 1977. Comparative biochemistry of non-muscle actins. *Journal of Biological Chemistry*. 252:8300-8309.

Gow, A., C. Davies, C.M. Southwood, G. Frolenkov, M. Chrustowski, L. Ng, D. Yamauchi, D.C. Marcus, and B. Kachar. 2004. Deafness in Claudin 11-null mice reveals the critical contribution of basal cell tight junctions to stria vascularis function. *Journal of Neuroscience*. 24:7051-7062.

Gu, B.J., W. Zhang, R.A. Worthington, R. Sluyter, P. Dao-Ung, S. Petrou, J.A. Barden, and J.S. Wiley. 2001. A Glu-496 to Ala polymorphism leads to loss of function of the human P2X7 receptor. *Journal of Biological Chemistry*. 276:11135-11142.

Gulley, R.L., and T.S. Reese. 1976. Intercellular junctions in the reticular lamina of the organ of Corti. *Journal of Neurocytology*. 5:479-507.

Hackney, C.M., S. Mahendrasingam, A. Penn, and R. Fettiplace. 2005. The concentrations of calcium buffering proteins in mammalian cochlear hair cells. *Journal of Neuroscience*. 25:7867-7875.

Hamernik, R.P., G. Turrentine, and C.G. Wright. 1984. Surface morphology of the inner sulcus and related epithelial cells of the cochlea following acoustic trauma. *Hearing Research*. 16:143-160.

He, M.L., T.A. Koshimizu, M. Tomic, and S.S. Stojilkovic. 2002. Purinergic P2X(2) receptor desensitization depends on coupling between ectodomain and C-terminal domain. *Molecular Pharmacology*. 62:1187-1197.

Henn, F.A., and A. Hamberger. 1971. Glial cell function: uptake of transmitter substances. *Proceedings of the National Academy of Sciences of the United States of America*. 68:2686-2690.

Hofer, T., L. Venance, and C. Giaume. 2002. Control and plasticity of intercellular calcium waves in astrocytes: a modeling approach. *Journal of Neuroscience*. 22:4850-4859.

Housley, G.D., D. Greenwood, and J.F. Ashmore. 1992. Localization of cholinergic and purinergic receptors on outer hair cells isolated from the guinea-pig cochlea. *Proceedings: Biological Sciences*. 249:265-273.

Housley, G.D., D. Greenwood, T. Bennett, and A.F. Ryan. 1995. Identification of a short form of the P2xR1-purinoceptor subunit produced by alternative splicing in the pituitary and cochlea. *Biochemical and Biophysical Research Communications*. 212:501-508.

Housley, G.D., R. Kanjhan, N.P. Raybould, D. Greenwood, S.G. Salih, L. Jarlebark, L.D. Burton, V.C. Setz, M.B. Cannell, C. Soeller, D.L. Christie, S. Usami, A. Matsubara, H. Yoshie, A.F. Ryan, and P.R. Thorne. 1999. Expression of the P2X(2) receptor subunit of the ATP-gated ion channel in the cochlea: implications for sound transduction and auditory neurotransmission. *Journal of Neuroscience*. 19:8377-8388.

Housley, G.D., L. Luo, and A.F. Ryan. 1998. Localization of mRNA encoding the P2X2 receptor subunit of the adenosine 5'-triphosphate-gated ion channel in the adult and developing rat inner ear by in situ hybridization. *Journal of Comparative Neurology*. 393:403-414.

Housley, G.D., R. Morton-Jones, S.M. Vlajkovic, R.S. Telang, V. Paramananthasivam, S.F. Tadros, A.C. Wong, K.E. Froud, J.M. Cederholm, Y. Sivakumaran, P. Snguanwongchai, B.S. Khakh, D.A. Cockayne, P.R. Thorne, and A.F. Ryan. 2013. ATP-gated ion channels mediate adaptation to elevated sound levels. *Proceedings of the National Academy of Sciences of the United States of America*. 110:7494-7499.

Hu, Q., S. Deshpande, K. Irani, and R.C. Ziegelstein. 1999. [Ca(2+)](i) oscillation frequency regulates agonist-stimulated NF-kappaB transcriptional activity. *Journal of Biological Chemistry*. 274:33995-33998.

Huang, D., P. Chen, S. Chen, M. Nagura, D.J. Lim, and X. Lin. 2002. Expression patterns of aquaporins in the inner ear: evidence for concerted actions of multiple types of aquaporins to facilitate water transport in the cochlea. *Hearing Research*. 165:85-95.

Huang, L.C., D. Greenwood, P.R. Thorne, and G.D. Housley. 2005. Developmental regulation of neuron-specific P2X3 receptor expression in the rat cochlea. *Journal of Comparative Neurology*. 484:133-143.

Huang, L.C., A.F. Ryan, D.A. Cockayne, and G.D. Housley. 2006. Developmentally regulated expression of the P2X3 receptor in the mouse cochlea. *Histochemistry and Cell Biology*. 125:681-692.

Huang, L.C., P.R. Thorne, S.M. Vlajkovic, and G.D. Housley. 2010. Differential expression of P2Y receptors in the rat cochlea during development. *Purinergic Signalling*. 6:231-248.

Huberts, D.H., and I.J. van der Klei. 2010. Moonlighting proteins: an intriguing mode of multitasking. *Biochimica et Biophysica Acta*. 1803:520-525.

Ikeda, K., Y. Saito, A. Nishiyama, and T. Takasaka. 1991. Effects of pH on intracellular calcium levels in isolated cochlear outer hair cells of guinea pigs. *American Journal of Physiology*. 261:C231-236.

Ikeda, K., M. Suzuki, M. Furukawa, and T. Takasaka. 1995. Calcium mobilization and entry induced by extracellular ATP in the non-sensory epithelial cell of the cochlear lateral wall. *Cell Calcium*. 18:89-99.

Jaffe, L. 2002. On the conservation of fast calcium wave speeds. *Cell Calcium*. 32:217-229.

Jagger, D.J., and A. Forge. 2006. Compartmentalized and signal-selective gap junctional coupling in the hearing cochlea. *Journal of Neuroscience*. 26:1260-1268.

Jagger, D.J., and A. Forge. 2014. Connexins and gap junctions in the inner ear - it's not just about K recycling. *Cell and Tissue Research*.

Jagger, D.J., and G.D. Housley. 2003. Membrane properties of type II spiral ganglion neurones identified in a neonatal rat cochlear slice. *Journal of Physiology*. 552:525-533.

Jagger, D.J., R. Nickel, and A. Forge. 2014. Gap Junctional Coupling is Essential for Epithelial Repair in the Avian Cochlea. *Journal of Neuroscience*. 34:15851-15860.

Jagger, D.J., D. Robertson, and G.D. Housley. 2000. A technique for slicing the rat cochlea around the onset of hearing. *Journal of Neuroscience Methods*. 104:77-86.

Jarlebark, L.E., G.D. Housley, N.P. Raybould, S. Vlajkovic, and P.R. Thorne. 2002. ATP-gated ion channels assembled from P2X2 receptor subunits in the mouse cochlea. *Neuroreport*. 13:1979-1984.

Johnson, S.L., T. Eckrich, S. Kuhn, V. Zampini, C. Franz, K.M. Ranatunga, T.P. Roberts, S. Masetto, M. Knipper, C.J. Kros, and W. Marcotti. 2011. Position-dependent patterning of spontaneous action potentials in immature cochlear inner hair cells. *Nature Neuroscience*. 14:711-717.

Kamiya, K., K. Takahashi, K. Kitamura, T. Momoi, and Y. Yoshikawa. 2001. Mitosis and apoptosis in postnatal auditory system of the C3H/He strain. *Brain Research*. 901:296-302.

Kenna, M.A., B.L. Wu, D.A. Cotanche, B.R. Korf, and H.L. Rehm. 2001. Connexin 26 studies in patients with sensorineural hearing loss. *Archives of Otolaryngology - Head and Neck Surgery*. 127:1037-1042.

Khadra, A., Z. Yan, C. Coddou, M. Tomic, A. Sherman, and S.S. Stojilkovic. 2012. Gating properties of the P2X2a and P2X2b receptor channels: experiments and mathematical modeling. *Journal of General Physiology*. 139:333-348.

Khakh, B.S., X.R. Bao, C. Labarca, and H.A. Lester. 1999. Neuronal P2X transmitter-gated cation channels change their ion selectivity in seconds. *Nature Neuroscience*. 2:322-330.

King, M., G.D. Housley, N.P. Raybould, D. Greenwood, and S.G. Salih. 1998. Expression of ATP-gated ion channels by Reissner's membrane epithelial cells. *Neuroreport*. 9:2467-2474.

Kirischuk, S., H. Kettenmann, and A. Verkhratsky. 2007. Membrane currents and cytoplasmic sodium transients generated by glutamate transport in Bergmann glial cells. *Pflügers Archiv. European Journal of Physiology*. 454:245-252.

Kitajiri, S.I., M. Furuse, K. Morita, Y. Saishin-Kiuchi, H. Kido, J. Ito, and S. Tsukita. 2004. Expression patterns of claudins, tight junction adhesion molecules, in the inner ear. *Hearing Research*. 187:25-34.

Knipper, M., L. Gestwa, W.J. Ten Cate, J. Lautermann, H. Brugger, H. Maier, U. Zimmermann, K. Rohbock, I. Kopschall, B. Wiechers, and H.P. Zenner. 1999. Distinct thyroid hormone-dependent expression of TrKB and p75NGFR in nonneuronal cells during the critical TH-dependent period of the cochlea. *Journal of Neurobiology*. 38:338-356.

Kolston, P.J., and J.F. Ashmore. 1996. Finite element micromechanical modeling of the cochlea in three dimensions. *Journal of the Acoustical Society of America*. 99:455-467.

Koshimizu, T., M. Koshimizu, and S.S. Stojilkovic. 1999. Contributions of the C-terminal domain to the control of P2X receptor desensitization. *Journal of Biological Chemistry*. 274:37651-37657.

Koshimizu, T.A., K. Kretschmannova, M.L. He, S. Ueno, A. Tanoue, N. Yanagihara, S.S. Stojilkovic, and G. Tsujimoto. 2006. Carboxyl-terminal splicing enhances physical interactions between the cytoplasmic tails of purinergic P2X receptors. *Molecular Pharmacology*. 69:1588-1598.

Kros, C.J., J.P. Ruppersberg, and A. Rusch. 1998. Expression of a potassium current in inner hair cells during development of hearing in mice. *Nature*. 394:281-284.

Kuhn, B., and M. Vater. 1995. The arrangements of F-actin, tubulin and fodrin in the organ of Corti of the horseshoe bat (Rhinolophus rouxi) and the gerbil (Meriones unguiculatus). *Hearing Research*. 84:139-156.

Kupzig, S., S.A. Walker, and P.J. Cullen. 2005. The frequencies of calcium oscillations are optimized for efficient calcium-mediated activation of Ras and the ERK/MAPK cascade. *Proceedings of the National Academy of Sciences of the United States of America*. 102:7577-7582.

Lagostena, L., J.F. Ashmore, B. Kachar, and F. Mammano. 2001. Purinergic control of intercellular communication between Hensen's cells of the guinea-pig cochlea. *Journal of Physiology*. 531:693-706.

Lagostena, L., and F. Mammano. 2001. Intracellular calcium dynamics and membrane conductance changes evoked by Deiters' cell purinoceptor activation in the organ of Corti. *Cell Calcium*. 29:191-198.

Lahne, M., and J.E. Gale. 2008. Damage-induced activation of ERK1/2 in cochlear supporting cells is a hair cell death-promoting signal that depends on extracellular ATP and calcium. *Journal of Neuroscience*. 28:4918-4928.

Lautermann, J., W.J. ten Cate, P. Altenhoff, R. Grummer, O. Traub, H. Frank, K. Jahnke, and E. Winterhager. 1998. Expression of the gap-junction connexins 26 and 30 in the rat cochlea. *Cell and Tissue Research*. 294:415-420.

Leis, J.A., L.K. Bekar, and W. Walz. 2005. Potassium homeostasis in the ischemic brain. *Glia*. 50:407-416.

Leybaert, L., and M.J. Sanderson. 2012. Intercellular Ca(2+) waves: mechanisms and function. *Physiological Reviews*. 92:1359-1392.

Li, L., G. Nevill, and A. Forge. 1995. Two modes of hair cell loss from the vestibular sensory epithelia of the guinea pig inner ear. *Journal of Comparative Neurology*. 355:405-417.

Liberman, M.C. 1978. Auditory-nerve response from cats raised in a low-noise chamber. *Journal of the Acoustical Society of America*. 63:442-455.

Liberman, M.C., L.W. Dodds, and S. Pierce. 1990. Afferent and efferent innervation of the cat cochlea: quantitative analysis with light and electron microscopy. *Journal of Comparative Neurology*. 301:443-460.

Lim, D.J. 1986. Functional structure of the organ of Corti: a review. *Hearing Research*. 22:117-146.

Lipmann, F. 1941. Metabolic generation and utilization of phosphate bond energy. *Advances in Enzymology and Related Subjects of Biochemistry*. 1:99-162.

Lustig, K.D., A.K. Shiau, A.J. Brake, and D. Julius. 1993. Expression cloning of an ATP receptor from mouse neuroblastoma cells. *Proceedings of the National Academy of Sciences of the United States of America*. 90:5113-5117.

Lynch, K.J., E. Touma, W. Niforatos, K.L. Kage, E.C. Burgard, T. van Biesen, E.A. Kowaluk, and M.F. Jarvis. 1999. Molecular and functional characterization of human P2X(2) receptors. *Molecular Pharmacology*. 56:1171-1181.

Majumder, P., G. Crispino, L. Rodriguez, C.D. Ciubotaru, F. Anselmi, V. Piazza, M. Bortolozzi, and F. Mammano. 2010. ATP-mediated cell-cell signaling in the organ of Corti: the role of connexin channels. *Purinergic Signalling*. 6:167-187.

Mallon, B.S., H.E. Shick, G.J. Kidd, and W.B. Macklin. 2002. Proteolipid promoter activity distinguishes two populations of NG2-positive cells throughout neonatal cortical development. *Journal of Neuroscience*. 22:876-885.

Mamaeva, O.A., J. Kim, G. Feng, and J.M. McDonald. 2009. Calcium/calmodulin-dependent kinase II regulates notch-1 signaling in prostate cancer cells. *Journal of Cellular Biochemistry*. 106:25-32.

Mangiardi, D.A., K. McLaughlin-Williamson, K.E. May, E.P. Messana, D.C. Mountain, and D.A. Cotanche. 2004. Progression of hair cell ejection and molecular markers of apoptosis in the avian cochlea following gentamicin treatment. *Journal of Comparative Neurology*. 475:1-18.

Marcotti, W., S.L. Johnson, M.C. Holley, and C.J. Kros. 2003a. Developmental changes in the expression of potassium currents of embryonic, neonatal and mature mouse inner hair cells. *Journal of Physiology*. 548:383-400.

Marcotti, W., S.L. Johnson, A. Rusch, and C.J. Kros. 2003b. Sodium and calcium currents shape action potentials in immature mouse inner hair cells. *Journal of Physiology*. 552:743-761.

Mellado Lagarde, M.M., G. Wan, L. Zhang, A.R. Gigliello, J.J. McInnis, Y. Zhang, D. Bergles, J. Zuo, and G. Corfas. 2014. Spontaneous regeneration of cochlear supporting cells after neonatal ablation ensures hearing in the adult mouse. *Proceedings of the National Academy of Sciences of the United States of America*.

Merchan, M.A., J.A. Merchan, and M.D. Ludena. 1980. Morphology of Hensen's cells. *Journal of Anatomy*. 131:519-523.

Mese, G., G. Richard, and T.W. White. 2007. Gap junctions: basic structure and function. *Journal of Investigative Dermatology*. 127:2516-2524.

Molotkov, D., S. Zobova, J.M. Arcas, and L. Khiroug. 2013. Calcium-induced outgrowth of astrocytic peripheral processes requires actin binding by Profilin-1. *Cell Calcium*. 53:338-348.

Moser, T., and D. Beutner. 2000. Kinetics of exocytosis and endocytosis at the cochlear inner hair cell afferent synapse of the mouse. *Proceedings of the National Academy of Sciences of the United States of America*. 97:883-888.

Munoz, D.J., I.S. Kendrick, M. Rassam, and P.R. Thorne. 2001. Vesicular storage of adenosine triphosphate in the guinea-pig cochlear lateral wall and concentrations of ATP in the endolymph during sound exposure and hypoxia. *Acta Oto-Laryngologica*. 121:10-15.

Munoz, D.J., P.R. Thorne, G.D. Housley, T.E. Billett, and J.M. Battersby. 1995. Extracellular adenosine 5'-triphosphate (ATP) in the endolymphatic compartment influences cochlear function. *Hearing Research*. 90:106-118.

Nakai, J., M. Ohkura, and K. Imoto. 2001. A high signal-to-noise Ca(2+) probe composed of a single green fluorescent protein. *Nature Biotechnology*. 19:137-141.

Nathanson, M.H., A.D. Burgstahler, A. Mennone, M.B. Fallon, C.B. Gonzalez, and J.C. Saez. 1995. Ca2+ waves are organized among hepatocytes in the intact organ. *American Journal of Physiology*. 269:G167-171.

Navarro, B., K. Miki, and D.E. Clapham. 2011. ATP-activated P2X2 current in mouse spermatozoa. *Proceedings of the National Academy of Sciences of the United States of America*. 108:14342-14347.

Nenov, A.P., C. Chen, and R.P. Bobbin. 1998. Outward rectifying potassium currents are the dominant voltage activated currents present in Deiters' cells. *Hearing Research*. 123:168-182.

Oancea, E., and T. Meyer. 1998. Protein kinase C as a molecular machine for decoding calcium and diacylglycerol signals. *Cell*. 95:307-318.

Oesterle, E.C., and P. Dallos. 1989. Intracellular recordings from supporting cells in the guinea-pig cochlea: AC potentials. *Journal of the Acoustical Society of America*. 86:1013-1032.

Ortolano, S., G. Di Pasquale, G. Crispino, F. Anselmi, F. Mammano, and J.A. Chiorini. 2008. Coordinated control of connexin 26 and connexin 30 at the regulatory and functional level in the inner ear. *Proceedings of the National Academy of Sciences of the United States of America*. 105:18776-18781.

Parekh, A.B. 2011. Decoding cytosolic Ca2+ oscillations. *Trends in Biochemical Sciences*. 36:78-87.

Parker, M.S., N.N. Onyenekwu, and R.P. Bobbin. 2003. Localization of the P2Y4 receptor in the guinea pig organ of Corti. *Journal of the American Academy of Audiology*. 14:286-295.

Patuzzi, R.B., G.K. Yates, and B.M. Johnstone. 1989. The origin of the low-frequency microphonic in the first cochlear turn of guinea-pig. *Hearing Research*. 39:177-188.

Peracchia, C. 2004. Chemical gating of gap junction channels; roles of calcium, pH and calmodulin. *Biochimica et Biophysica Acta*. 1662:61-80.

Pfahnl, A., and G. Dahl. 1999. Gating of cx46 gap junction hemichannels by calcium and voltage. *Pflügers Archiv. European Journal of Physiology*. 437:345-353.

Piazza, V., C.D. Ciubotaru, J.E. Gale, and F. Mammano. 2007. Purinergic signalling and intercellular Ca2+ wave propagation in the organ of Corti. *Cell Calcium*. 41:77-86.

Puel, J.L., C. d'Aldin, J. Ruel, S. Ladrech, and R. Pujol. 1997. Synaptic repair mechanisms responsible for functional recovery in various cochlear pathologies. *Acta Oto-Laryngologica*. 117:214-218.

Pujol, R., and J.L. Puel. 1999. Excitotoxicity, synaptic repair, and functional recovery in the mammalian cochlea: a review of recent findings. *Annals of the New York Academy of Sciences*. 884:249-254.

Pujol, R., G. Rebillard, J.L. Puel, M. Lenoir, M. Eybalin, and M. Recasens. 1990. Glutamate neurotoxicity in the cochlea: a possible consequence of ischaemic or anoxic conditions occurring in ageing. *Acta Oto-Laryngologica. Supplementum*. 476:32-36.

Qu, Z., and H.C. Hartzell. 2000. Anion permeation in Ca(2+)-activated Cl(-) channels. *Journal of General Physiology*. 116:825-844.

Raphael, Y., and R.A. Altschuler. 2003. Structure and innervation of the cochlea. *Brain Research Bulletin*. 60:397-422.

Raybould, N.P., and G.D. Housley. 1997. Variation in expression of the outer hair cell P2X receptor conductance along the guinea-pig cochlea. *Journal of Physiology*. 498 (Pt 3):717-727.

Rebecchi, M.J., and S.N. Pentyala. 2000. Structure, function, and control of phosphoinositide-specific phospholipase C. *Physiological Reviews*. 80:1291-1335.

Richardson, G.P., A.N. Lukashkin, and I.J. Russell. 2008. The tectorial membrane: one slice of a complex cochlear sandwich. *Current Opinion in Otolaryngology & Head and Neck Surgery*. 16:458-464.

Richardson, G.P., I.J. Russell, V.C. Duance, and A.J. Bailey. 1987. Polypeptide composition of the mammalian tectorial membrane. *Hearing Research*. 25:45-60.

Rio, C., P. Dikkes, M.C. Liberman, and G. Corfas. 2002. Glial fibrillary acidic protein expression and promoter activity in the inner ear of developing and adult mice. *Journal of Comparative Neurology*. 442:156-162.

Rose, B., I. Simpson, and W.R. Loewenstein. 1977. Calcium ion produces graded changes in permeability of membrane channels in cell junction. *Nature*. 267:625-627.

Sakmann, B., and E. Neher. 2009. Single-channel recording. Springer, New York, NY.

Salazar, C., A.Z. Politi, and T. Hofer. 2008. Decoding of calcium oscillations by phosphorylation cycles: analytic results. *Biophysical Journal*. 94:1203-1215.

Salt, A.N., and K. Ohyama. 1993. Accumulation of potassium in scala vestibuli perilymph of the mammalian cochlea. *Annals of Otology, Rhinology and Laryngology*. 102:64-70.

Scemes, E., and C. Giaume. 2006. Astrocyte calcium waves: what they are and what they do. *Glia*. 54:716-725.

Schuster, S., M. Marhl, and T. Hofer. 2002. Modelling of simple and complex calcium oscillations. From single-cell responses to intercellular signalling. *European Journal of Biochemistry*. 269:1333-1355.

Schwarzmann, G., H. Wiegandt, B. Rose, A. Zimmerman, D. Ben-Haim, and W.R. Loewenstein. 1981. Diameter of the cell-to-cell junctional membrane channels as probed with neutral molecules. *Science*. 213:551-553.

Singer, W., and H.D. Lux. 1975. Extracellular potassium gradients and visual receptive fields in the cat striate cortex. *Brain Research*. 96:378-383.

Slepecky, N., and S.C. Chamberlain. 1987. Tropomyosin co-localizes with actin microfilaments and microtubules within supporting cells of the inner ear. *Cell and Tissue Research*. 248:63-66.

Smedler, E., and P. Uhlen. 2014. Frequency decoding of calcium oscillations. *Biochimica et Biophysica Acta*. 1840:964-969.

Smith, F.M., P.P. Humphrey, and R.D. Murrell-Lagnado. 1999. Identification of amino acids within the P2X2 receptor C-terminus that regulate desensitization. *Journal of Physiology*. 520 Pt 1:91-99.

Spicer, S.S., and B.A. Schulte. 1998. Evidence for a medial K+ recycling pathway from inner hair cells. *Hearing Research*. 118:1-12.

Steele, C.R., and K.M. Lim. 1999. Cochlear model with three-dimensional fluid, inner sulcus and feed-forward mechanism. *Audiology and Neuro-Otology*. 4:197-203.

Straub, R.W., and L. Bolis. 1978. Cell membrane receptors for drugs and hormones : a multidisciplinary approach. Raven Press, New York.

Suarez-Huerta, N., V. Pouillon, J. Boeynaems, and B. Robaye. 2001. Molecular cloning and characterization of the mouse P2Y4 nucleotide receptor. *European Journal of Pharmacology*. 416:197-202.

Sugasawa, M., C. Erostegui, C. Blanchet, and D. Dulon. 1996a. ATP activates a cation conductance and Ca(2+)-dependent Cl- conductance in Hensen cells of guinea pig cochlea. *American Journal of Physiology*. 271:C1817-1827.

Sugasawa, M., C. Erostegui, C. Blanchet, and D. Dulon. 1996b. ATP activates non-selective cation channels and calcium release in inner hair cells of the guinea-pig cochlea. *Journal of Physiology*. 491 (Pt 3):707-718.

Sung, Y.J., Z. Sung, C.L. Ho, M.T. Lin, J.S. Wang, S.C. Yang, Y.J. Chen, and C.H. Lin. 2003. Intercellular calcium waves mediate preferential cell growth toward the wound edge in polarized hepatic cells. *Experimental Cell Research*. 287:209-218.

Surprenant, A., F. Rassendren, E. Kawashima, R.A. North, and G. Buell. 1996. The cytolytic P2Z receptor for extracellular ATP identified as a P2X receptor (P2X7). *Science*. 272:735-738.

Suzuki, M., K. Ikeda, H. Sunose, K. Hozawa, C. Kusakari, Y. Katori, and T. Takasaka. 1995. ATP-induced increase in intracellular Ca2+ concentration in the cultured marginal cell of the stria vascularis of guinea-pigs. *Hearing Research*. 86:68-76.

Szucs, A., S. Somodi, T.J. Batta, A. Toth, G.P. Szigeti, L. Csernoch, G. Panyi, and I. Sziklai. 2006a. Differential expression of potassium currents in Deiters cells of the guinea pig cochlea. *Pflügers Archiv. European Journal of Physiology*. 452:332-341.

Szucs, A., H. Szappanos, T.J. Batta, A. Toth, G.P. Szigeti, G. Panyi, L. Csernoch, and I. Sziklai. 2006b. Changes in purinoceptor distribution and intracellular calcium levels following noise exposure in the outer hair cells of the guinea pig. *Journal of Membrane Biology*. 213:135-141.

Takumi, Y., E.A. Nagelhus, J. Eidet, A. Matsubara, S. Usami, H. Shinkawa, S. Nielsen, and O.P. Ottersen. 1998. Select types of supporting cell in the inner ear express aquaporin-4 water channel protein. *European Journal of Neuroscience*. 10:3584-3595.

Teubner, B., V. Michel, J. Pesch, J. Lautermann, M. Cohen-Salmon, G. Sohl, K. Jahnke, E. Winterhager, C. Herberhold, J.P. Hardelin, C. Petit, and K. Willecke. 2003. Connexin30 (Gjb6)-deficiency causes severe hearing impairment and lack of endocochlear potential. *Human Molecular Genetics*. 12:13-21.

Thalmann, I., G. Thallinger, T.H. Comegys, and R. Thalmann. 1986. Collagen--the predominant protein of the tectorial membrane. *ORL: Journal of Oto-Rhino-Laryngology and Its Related Specialties*. 48:107-115.

Tompa, P., R. Toth-Boconadi, and P. Friedrich. 2001. Frequency decoding of fast calcium oscillations by calpain. *Cell Calcium*. 29:161-170.

Tremblay, I., E. Pare, D. Arsenault, M. Douziech, and M.J. Boucher. 2013. The MEK/ERK pathway promotes NOTCH signalling in pancreatic cancer cells. *PloS One*. 8:e85502.

Tritsch, N.X., and D.E. Bergles. 2010. Developmental regulation of spontaneous activity in the Mammalian cochlea. *Journal of Neuroscience*. 30:1539-1550.

Tritsch, N.X., A. Rodriguez-Contreras, T.T. Crins, H.C. Wang, J.G. Borst, and D.E. Bergles. 2010a. Calcium action potentials in hair cells pattern auditory neuron activity before hearing onset. *Nature Neuroscience*. 13:1050-1052.

Tritsch, N.X., E. Yi, J.E. Gale, E. Glowatzki, and D.E. Bergles. 2007. The origin of spontaneous activity in the developing auditory system. *Nature*. 450:50-55.

Tritsch, N.X., Y.X. Zhang, G. Ellis-Davies, and D.E. Bergles. 2010b. ATP-induced morphological changes in supporting cells of the developing cochlea. *Purinergic Signalling*. 6:155-166.

Troyanovskaya, M., and P.A. Wackym. 1998. Evidence for three additional P2X2 purinoceptor isoforms produced by alternative splicing in the adult rat vestibular end-organs. *Hearing Research*. 126:201-209.

Uhlen, P., and N. Fritz. 2010. Biochemistry of calcium oscillations. *Biochemical and Biophysical Research Communications*. 396:28-32.

Vicente-Torres, M.A., and J. Schacht. 2006. A BAD link to mitochondrial cell death in the cochlea of mice with noise-induced hearing loss. *Journal of Neuroscience Research*. 83:1564-1572.

Virginio, C., A. MacKenzie, R.A. North, and A. Surprenant. 1999a. Kinetics of cell lysis, dye uptake and permeability changes in cells expressing the rat P2X7 receptor. *Journal of Physiology*. 519 Pt 2:335-346.

Virginio, C., A. MacKenzie, F.A. Rassendren, R.A. North, and A. Surprenant. 1999b. Pore dilation of neuronal P2X receptor channels. *Nature Neuroscience*. 2:315-321.

Wadiche, J.I., S.G. Amara, and M.P. Kavanaugh. 1995. Ion fluxes associated with excitatory amino acid transport. *Neuron*. 15:721-728.

Wallingford, J.B., A.J. Ewald, R.M. Harland, and S.E. Fraser. 2001. Calcium signaling during convergent extension in Xenopus. *Current Biology*. 11:652-661.

Walz, W. 2002. Chloride/anion channels in glial cell membranes. *Glia*. 40:1-10.

Wang, J., T.R. Van De Water, C. Bonny, F. de Ribaupierre, J.L. Puel, and A. Zine. 2003a. A peptide inhibitor of c-Jun N-terminal kinase protects against both aminoglycoside and acoustic trauma-induced auditory hair cell death and hearing loss. *Journal of Neuroscience*. 23:8596-8607.

Wang, J.C., N.P. Raybould, L. Luo, A.F. Ryan, M.B. Cannell, P.R. Thorne, and G.D. Housley. 2003b. Noise induces up-regulation of P2X2 receptor subunit of ATP-gated ion channels in the rat cochlea. *Neuroreport*. 14:817-823.

Wang, Y., K. Hirose, and M.C. Liberman. 2002. Dynamics of noise-induced cellular injury and repair in the mouse cochlea. *Journal of the Association for Research in Otolaryngology*. 3:248-268.

Wangemann, P. 1995. Comparison of ion transport mechanisms between vestibular dark cells and strial marginal cells. *Hearing Research*. 90:149-157.

Wangemann, P., K. Nakaya, T. Wu, R.J. Maganti, E.M. Itza, J.D. Sanneman, D.G. Harbidge, S. Billings, and D.C. Marcus. 2007. Loss of cochlear HCO3- secretion causes deafness via endolymphatic acidification and inhibition of Ca2+ reabsorption in a Pendred syndrome mouse model. *American Journal of Physiology: Renal Physiology*. 292:F1345-1353.

Webb, S.E., and A.L. Miller. 2003. Imaging intercellular calcium waves during late epiboly in intact zebrafish embryos. *Zygote*. 11:175-182.

Webb, S.E., and A.L. Miller. 2006. Ca2+ signaling during vertebrate somitogenesis. *Acta Pharmacologica Sinica*. 27:781-790.

Willecke, K., J. Eiberger, J. Degen, D. Eckardt, A. Romualdi, M. Guldenagel, U. Deutsch, and G. Sohl. 2002. Structural and functional diversity of connexin genes in the mouse and human genome. *Biological Chemistry*. 383:725-737.

Willott, J.F. 2001. Handbook of mouse auditory research : from behavior to molecular biology. CRC Press, Boca Raton.

Woll, E., M. Gschwentner, J. Furst, S. Hofer, G. Buemberger, A. Jungwirth, J. Frick, P. Deetjen, and M. Paulmichl. 1996. Fluorescence-optical measurements of chloride movements in cells using the membrane-permeable dye diH-MEQ. *Pflügers Archiv. European Journal of Physiology*. 432:486-493.

Yan, D., Y. Zhu, T. Walsh, D. Xie, H. Yuan, A. Sirmaci, T. Fujikawa, A.C. Wong, T.L. Loh, L. Du, M. Grati, S.M. Vlajkovic, S. Blanton, A.F. Ryan, Z.Y. Chen, P.R. Thorne, B. Kachar, M. Tekin, H.B. Zhao, G.D. Housley, M.C. King, and X.Z. Liu. 2013. Mutation of the ATP-gated P2X(2) receptor leads to progressive hearing loss and increased susceptibility to noise. *Proceedings of the National Academy of Sciences of the United States of America*. 110:2228-2233.

Yi, E., J. Lee, and C.J. Lee. 2013. Developmental Role of Anoctamin-1/TMEM16A in Ca(2+)-Dependent Volume Change in Supporting Cells of the Mouse Cochlea. *Experimental Neurobiology*. 22:322-329.

Yin, H.L., and T.P. Stossel. 1979. Control of cytoplasmic actin gel-sol transformation by gelsolin, a calcium-dependent regulatory protein. *Nature*. 281:583-586.

Yoo, J.C., H.Y. Kim, K.H. Han, S.H. Oh, S.O. Chang, D.C. Marcus, and J.H. Lee. 2012. Na+ absorption by Claudius' cells is regulated by purinergic signaling in the cochlea. *Acta Oto-Laryngologica*. 132 Suppl 1:S103-108.

Yuan, T., S.S. Gao, P. Saggau, and J.S. Oghalai. 2010. Calcium imaging of inner ear hair cells within the cochlear epithelium of mice using two-photon microscopy. *Journal of Biomedical Optics*. 15:016002.

Zhou, Z., and R.I. Hume. 1998. Two mechanisms for inward rectification of current flow through the purinoceptor P2X2 class of ATP-gated channels. *Journal of Physiology*. 507 (Pt 2):353-364.

Zhu, Y., and H.B. Zhao. 2012. ATP activates P2X receptors to mediate gap junctional coupling in the cochlea. *Biochemical and Biophysical Research Communications*. 426:528-532.

Zidanic, M., and W.E. Brownell. 1990. Fine structure of the intracochlear potential field. I. The silent current. *Biophysical Journal*. 57:1253-1268.

Zuccotti, A., S. Kuhn, S.L. Johnson, C. Franz, W. Singer, D. Hecker, H.S. Geisler, I. Kopschall, K. Rohbock, K. Gutsche, J. Dlugaiczyk, B. Schick, W. Marcotti, L. Ruttiger, T. Schimmang, and M. Knipper. 2012. Lack of brain-derived neurotrophic factor hampers inner hair cell synapse physiology, but protects against noise-induced hearing loss. *Journal of Neuroscience*. 32:8545-8553.